VILNIUS UNIVERSITY

CENTER FOR PHYSICAL SCIENCES AND TECHNOLOGY

YURY MALEVICH

TRANSIENT ANISOTROPIC PHOTOCONDUCTIVITY AND
TERAHERTZ PULSE GENERATION FROM SEMICONDUCTORS

Doctoral Dissertation

Physical Sciences, Physics (02 P)

Vilnius 2016

Doctoral dissertation was prepared during 2011 – 2016 at Center for Physical Sciences and Technology, Vilnius, Lithuania.

Dissertation is defended extramurally.

Scientific adviser – dr. Ramūnas Adomavičius (Center for Physical Sciences and Technology, Physical Sciences, Physics – 02P)

VILNIAUS UNIVERSITETAS

FIZINIŲ IR TECHNOLOGIJOS MOKSLŲ CENTRAS

YURY MALEVICH

FOTOLAIDUMO ANIZOTROPIJOS IR TERAHERCINIŲ IMPULSŲ
GENERAVIMO PUSLAIDININKIUOSE DINAMIKA

Daktaro disertacija

Fiziniai mokslai, fizika (02 P)

Vilnius 2016

Disertacija rengta 2011 – 2016 metais Fizinių ir technologijos mokslų centre, Vilniuje, Lietuvoje.

Disertacija ginama eksternu.

Mokslinis konsultantas – dr. Ramūnas Adomavičius (Fizinių ir technologijos mokslų centras, fiziniai mokslai, fizika – 02P).

ABSTRACT

The study of transient photoconductivity in semiconductors excited by femtosecond laser pulses is of fundamental importance for understanding of photocarrier dynamics on a subpicosecond time scale. These investigations are of great practical interest because the ultrafast electronic processes have a profound impact on operation of semiconductor devices operating on a subpicosecond time scale.

The purpose of this work has been to study the influence of the optical alignment of photocarriers over momenta on the transient photoconductivity in cubic semiconductors excited by femtosecond laser pulses and to investigate how this effect is manifested in emission of THz radiation from the semiconductor surface.

The transient photoconductivity in InAs excited by ultrashort laser pulses with different photon energy has been calculated with use of the transport equation for photocarriers in collisionless approximation. It has been found that the nonparabolicity of the electron dispersion law as well as the optical alignment of the photoexcited carrier momenta result in anisotropic photocurrent with a component perpendicular to the dc electric field even in semiconductors with a cubic symmetry. This component of the photocurrent is profoundly revealed on a ballistic stage of photocarrier movement that is during the first few hundreds of femtoseconds after the photoexcitation and causes the emission of terahertz radiation pulses with an amplitude dependent on the angle between the optical field and the crystallographic axes. In the case of InAs the contribution of this component in terahertz emission can be comparable to the contribution of the photocurrent component directed perpendicular to the crystal surface and explains experimental results of both the azimuthal anisotropy of the emitted terahertz pulse amplitude and its dependence on the exciting photon energy.

Monte Carlo simulations of the anisotropic transient photoconductivity in cubic semiconductors InGaAs and InAs excited by a femtosecond laser pulse have been performed. Calculations show that the degree of anisotropy of the transient photocurrent reaches its peak when the excess energy of the optically excited electrons approaches the threshold for the intervalley transfer. It has been also found that when the electrons are excited near the threshold energy for the intervalley transfer, the component of the transient photocurrent directed along dc field can become negative for a short time after photoexcitation. The anisotropy of the transient photoconductivity has been observed experimentally on (001) InGaAs sample by optical pump - terahertz-probe technique. It has been found that in the first few picoseconds after excitation the optically induced change of THz transmission depends on the direction of THz field relative to polarization of the optical pump pulse and crystallographic axes of the semiconductor. On rotation of the sample around normal to the excited semiconductor surface the fourfold symmetry of THz transmission is observed. It has been established experimentally that the degree of photoconductivity anisotropy depends nonmonotonically on the exciting photon energy that is consistent with the results of the Monte Carlo simulation.

ACKNOWLEDGMENTS

I am very grateful to Ramūnas Adomavičius for continuing support and inestimable help in planning and performing the experiments.

I would like to thank Arūnas Krotkus whose ideas and expertise significantly influenced the direction of my research.

I would also like to thank Vitaly Malevich from Institute of Physics National Academy of Sciences of Belarus (Minsk) for help with the Monte Carlo simulation and for the fruitful discussions.

It is a great pleasure to acknowledge continuous support of Vaidas Pačebutas, who helped me a lot with experiment automation and shared a great experience of dealing with equipment.

I have to thank Renata Butkutė, Jan Devenson and Vaidas Pačebutas for MBE fabrication of the semiconductor samples.

I am also indebted to Vytautas Karpus, from whom I learned a great deal about solid state physics and physics of low-dimensional semiconductor structures.

Many thanks to Juozas Adamonis, Andrius Bičiūnas, Andrius Arlauskas, Andžej Urbanovič, Polina Svidovsky, Gediminas Molis, Anton Koroliov and Andrejus Geižutis for continuous help and support. I would also like to thank all students and staff of Center for Physical Sciences and Technology, who helped me during my work.

TABLE OF CONTENTS

INTRODUCTION

Motivation

As it is generally known, the main feature of semiconductors distinguishing them from metals is that the concentration of charge carriers in them can be changed by means of doping or under an external impact such as temperature, lighting, electric and magnetic field, etc. It is precisely the possibility to control the concentration of electrons and holes, and therefore, electric conductivity, that lies in the base of most of semiconductor technical applications.

One of the most remarkable properties of semiconductors is the photoconductivity effect, i.e. its ability to change electrical conductivity under exposure to light. This phenomenon is always accompanied by absorption of radiation which leads to generation of additional electrons and holes in the bands or redistribution of the equilibrium carriers over the electronic states. Depending on the semiconductor type and its parameters (band gap, impurity ionization energy, etc.) this effect can be observed in the infrared, visible or ultraviolet range of the electromagnetic spectrum. The phenomenon of photoconductivity as well as closely related to it photoelectric effects have been studied for quite a long time and find application in semiconductor optoelectronics, laser technology, fiber-optic communication systems et al. Nevertheless, the interest in investigating these effects is not diminishing. First of all, there appear new objects of research, such as wide-band-gap semiconductors, quantum-well structures, graphene, etc. Besides, the availability of femtosecond laser systems has opened possibilities to investigate the dynamics of photoconductivity on a subpicosecond time scale. Such a research conduces to deeper understanding of physical mechanisms of the photoconductivity and stimulates development of new semiconductor optoelectronic devices.

The availability of femtosecond lasers has stimulated investigation of transient response of semiconductor conductivity and closely related to it phenomena, such as the electron velocity overshoot effect [1, 2], the picosecond photoconductivity [3-8], the electric field collapse due to a spatial separation of photoexcited electrons and holes [9-13], and the terahertz (THz) pulse emission [14-17]. With femtosecond optical pulses one can generate nonequilibrium electrons and holes, and investigate their transport and relaxation to a steady state on a subpicosecond time scale [18-20]. A fundamental understanding of the transient electrical response of semiconductors excited by femtosecond laser pulses is important for modern electronic devices because their operation is governed by the ultrafast carrier transport phenomena.

The transient photoconductivity of semiconductors excited by subpicosecond laser pulses is determined by a microscopic dynamics of photoexcited carriers under dc electric field and their relaxation toward the steady state. These effects have been investigated experimentally with use of the optical femtosecond and THz spectroscopy methods. Theoretical investigations of electron transport in semiconductors are predominately based on the kinetic equation. This equation can be solved analytically for simple cases. However, the semiconductor excited by femtosecond optical pulses is not a simple system since the realistic band structure, variety of carrier scattering mechanisms, electron heating, photocarrier-induced screening, and other effects should be taken into account. Therefore, Monte Carlo technique [21] capable of taking into account these effects was advanced for numerical simulation of the transient electronic transport on a subpicosecond time scale. This simulation method allows to clear up the features of photocarrier transport within the first few hundreds of femtoseconds after photoexcitation and to carry out comprehensive analysis of the experimental data. The Monte Carlo technique was, e.g., applied for simulation of picosecond electrical response of photoexcited GaAs in uniform dc electric field [2, 5-6], and the ultrafast energy relaxation and dephasing of the photoexcited carriers [18-20]. It has been

11

established that the character of the transient response in semiconductors depends on the applied dc electric field and the initial photoelectron energy immediately after excitation which is determined by the photon energy of the exciting laser radiation and semiconductor band gap.

In spite of the intensive study there remain a number of effects which have been ignored on consideration of the picosecond transient photoconductivity. One such effect is the optical alignment of photocarriers over momenta which results in the anisotropic distribution of photocarriers in momentum space. This anisotropy decays within a time scale of several hundreds of femtoseconds and therefore it is commonly supposed that the optical alignment affect slightly influences on the steady-state transport of photocarriers. However, one would expect that the anisotropy of the photocarrier momentum distribution will have an appreciable effect on the transient transport of photocarriers in semiconductors excited by femtosecond laser pulses. The transient photocurrent excited in semiconductors by femtosecond laser radiation results in generation of THz pulses. The principal part of THz pulse emerges immediately after photoexcitation within the period of time compared with relaxation time of the anisotropic distribution of photocarriers over momenta arising due to the optical alignment effect. Because of this it is of interest to clear up how this anisotropy impacts on THz generation mechanism caused by the transient photoconductivity induced in semiconductors under femtosecond laser irradiation.

Objective and tasks of this work

The objective of this work has been to study the influence of the optical alignment of photocarriers over momenta on the transient photoconductivity in cubic semiconductors excited by femtosecond laser pulses and to investigate how this effect is manifested in emission of THz radiation from the semiconductor surface.

In correspondence with this objective, the following tasks were set:

1. To build optical pump – THz probe experimental setup with tunable wavelength of excitation femtosecond radiation for the investigation of anisotropy of photoconductivity.
2. To investigate the contribution of anisotropic photoconductivity to azimuthal anisotropy of THz generation.
3. To study the anisotropy of optically induced change of THz transmission through the sample using optical pump – THz probe technique.
4. To investigate spectral dependence of the anisotropy of picosecond photoconductivity.

Novelty and importance of this work

This thesis focuses on investigation of anisotropic transient photoconductivity and THz generation in cubic semiconductor excited by femtosecond laser pulses. The dynamics of the transient photocurrent on a subpicosecond time scale, and its dependences on orientation and photon energy of the exciting femtosecond radiation were studied with use of THz spectroscopy methods and Monte Carlo simulation technique.

Investigation of anisotropic picosecond photoconductivity in cubic semiconductors excited by femtosecond laser pulses caused by optical alignment of photocarriers over momenta was carried out for the first time.

It has been shown that the anisotropic photoconductivity makes a significant contribution to azimuthal anisotropy of THz generation in narrow-gap semiconductors.

Spectral dependence of the anisotropy of picosecond photoconductivity was investigated with use of optical pump – THz probe technique for the first time.

The study of transient photoconductivity in semiconductors excited by femtosecond laser pulses is of fundamental importance for understanding of photocarrier dynamics on a subpicosecond time scale. These investigations are of great practical interest because the ultrafast electronic processes have a

profound impact on operation of semiconductor devices operating on a subpicosecond time scale.

Statements for defence

1. In cubic semiconductors excited by linearly polarized femtosecond laser radiation optical alignment of photoexcited electrons over momenta and nonparabolicity of the electron dispersion law result in anisotropic picosecond photoconductivity manifested in arising of the lateral photocurrent component.

2. The lateral photocurrent component results in emission of THz pulses with the amplitude depending on the angle between the optical polarization vector and the crystallographic axes of the semiconductor and explains experimental results of both the azimuthal anisotropy of the emitted terahertz pulse amplitude and its dependence on the exciting photon energy.

3. The anisotropy of picosecond photoconductivity depends nonmonotonically on the wavelength of the exciting femtosecond radiation and attains a maximum when the photoelectrons are excited in the states of conduction band with the energies near the threshold for the onset of their transitions to the subsidiary valleys.

Dissertation layout

The thesis consists of four chapters.

In Chapter 1 the physical mechanisms of photoconductivity in semiconductors are considered. The origin of the anisotropic photocurrent in cubic semiconductors and direct relationship of this effect to the nonlinear character of the photoconductivity are discussed from a phenomenological point of view. The several microscopic mechanisms of the anisotropic photoconductivity in semiconductor under steady-state photoexcitation are

considered. Then the optical alignment effect and associated anisotropic photoconductivity are described in more detail. The current state of research on the transient photoconductivity in semiconductors excited by ultrashort laser pulses is reviewed. The experimental methods and theoretical approach used for studies of subpicosecond dynamics of photocarriers under electric field and their interband and intraband relaxation are presented.

Currently THz spectroscopy methods have been widely used for studying the carrier transport with a subpicosecond time resolution. Chapter 2 describes in detail the mechanisms of THz pulse generation in semiconductors excited by femtosecond laser radiation. The methods of THz coherent detection based on photoconductive antenna and electro-optic sampling are considered. The principles of the THz time-domain spectroscopy and its application for studies of the ultrafast photocarrier transport in semiconductors under femtosecond laser excitation are described.

In Chapter 3 the anisotropic photoconductivity in semiconductor excited by an ultrashort laser pulse is calculated with the use of the kinetic transport equation in collisionless approximation. The anisotropy photocurrent in cubic semiconductor arises due to nonparabolicity and nonsphericity of electron and hole dispersion laws, and anisotropic distribution of the photocarriers in momentum space caused by the optical alignment effect. The semiconductor band structure and the initial distribution of photoexcited carriers over momenta at the instant of their emergence in the band are calculated on the basis of *kp*-method. Azimuthal anisotropy of THz emission from InAs and InSb surfaces excited by femtosecond laser radiation of three different wavelengths is experimentally measured. The contribution of the anisotropic transient photocurrent into THz emission from semiconductor surfaces and its role in the azimuthal anisotropy are studied by comparing the obtained experimental data with the results of calculation.

In Chapter 4 the transient anisotropic photoconductivity in narrow-gap semiconductors (InAs and InGaAs) excited by femtosecond laser pulses is simulated by using an ensemble Monte Carlo method taking into account the

optical alignment of photocarriers over momenta, high-field effects, and semiconductor band structure calculated by *kp*-method. The dependencies of the transient photocurrent on polarization direction and photon energy of the exciting femtosecond radiation are calculated and investigated experimentally by the optical pump – THz probe technique.

In Summary the results obtained during this work are summarized and some suggestions for future research on the picosecond transient photoconductivity in semiconductors are presented.

Contribution of the author

While working on this thesis I assembled all experimental setups, performed all measurements and data processing. I took part in experimental data analysis, writing of scientific publications and presenting the results at conferences. Monte Carlo simulations were performed with use of program kindly provided by V. Malevich. First measurements of excitation wavelength dependences of THz emission from semiconductor surfaces were performed by A. Bičiūnas from Center for Physical Sciences and Technology in Vilnius.

CHAPTER 1
PICOSECOND PHOTOCONDUCTIVITY IN SEMICONDUCTORS

In this chapter the main ideas on the photoconductivity of semiconductors are set forth, the peculiarities of the photocurrent formation dynamics at excitation of semiconductors by femtosecond laser pulses are considered, the main methods used for studying the processes of generation, relaxation and transition of photoexcited charge carriers on a subpicosecond time scale are reviewed.

1.1 Mechanisms of photoconductivity in semiconductors

When a semiconductor is illuminated by light with quantum energy exceeding the band gap, the nonequilibrium electrons and holes are generated which are able to carry charge and, consequently, to contribute into electrical conductivity [22-24]. In this case, the change in the electrical conductivity can exceed the value of dark conductivity (in the absence of light) by many orders of magnitude. This phenomenon, known as the intrinsic photoconductivity, is determined by interband optical transitions when both the electrons and holes contribute to the change in conductivity. In the spectral range corresponding to the photons energy lower than the semiconductor band gap, the impurity photoconductivity is observed. Depending on the impurity type, the contribution to the photoconductivity comes from either electrons or holes generated due to impurity-band transitions.

Charge carries mobility in semiconductors depends on their energy. This effect is determined by nonparabolicity of the electron and hole dispersion laws as well as by the energy dependence of their momentum relaxation times. That is why, in the general case, the contribution to the semiconductor photoconductivity comes from the change both in concentration of electrons and holes and in their mobility's. The contribution of the latter effect into the

photoconductivity is determined by the fact that the electron and hole generated as a result of absorption of a photon with energy $\hbar\omega$ possess the total energy $\left(\hbar\omega - \varepsilon_g\right)$ (where ε_g is the semiconductor band gap). As a result, the energy and, correspondingly, mobility of photoexcited and equilibrium carriers can differ significantly. Photoexcited electrons relax to the bottom of the conduction band and thermalize within a time comparable to the energy relaxation time τ_e. That is why if the life time of nonequilibrium electrons in the band $\tau_r \gg \tau_e$, then the photoelectrons manage to thermalize, i.e. attain the steady state in the conduction band which is characterized by the same distribution over energies and momenta as for the equilibrium electrons. In this case the relative contribution of the change in mobility into the photoconductivity will be minor ($\sim \tau_e/\tau_r \ll 1$) and the photoconductivity will be mainly determined by changing the concentration of electrons and holes. On the other hand, at low temperatures or in specially grown semiconductors the condition $\tau_r \leq \tau_e$ can be fulfilled. In this case, the contribution into the photoconductivity of the changes in both the concentration and mobility of the carriers should be taken into account.

When a semiconductor is irradiated with far infrared radiation, a so-called intraband or μ-photoconductivity can be observed which is determined only by the change in the carriers mobility owing to their redistribution over electronic states at the intraband absorption of radiation [25-27]. It should be noted that the intraband photoconductivity can be both positive and negative depending on whether the carrier mobility increases or decreases with increase of its energy.

Therefore, there are several mechanisms responsible for the photoconductivity in semiconductors. However, further we will confine ourselves to considering only the intrinsic photoconductivity determined by the interband optical transitions of electrons from the valence band to the conduction band.

At a quasistationary lighting (lighting duration is significantly longer than the characteristic time for intraband relaxation of photoexcited electrons) the intrinsic photoconductivity $\delta\sigma$ is determined mainly by the change in the concentration of electrons δn and holes δp and equals to $\delta\sigma = e(\mu_n \delta n + \mu_p \delta p)$ (where μ_n and μ_p are electron and hole mobility). The kinetics of photoconductivity is usually described within the frames of diffusion-drift approximation using the continuity equations for electrons and holes taking into account the optical generation processes, the Poisson equation for the electric field and expressions for the drift and diffusion current of the electrons and holes. Under the conditions of uniform generation of electron-hole pairs the following equation describing the kinetics of the intrinsic photoconductivity can be obtained [22]:

$$\frac{d\delta\sigma}{dt} = e(\mu_n + \mu_p)g - \frac{\delta\sigma}{\tau_{ph}}, \qquad (1.1)$$

where τ_{ph} is the photoconductivity relaxation time depending on the life time, concentration and mobility of electrons and holes, $g = \kappa\nu I$ is the charge carrier optical generation rate, κ is the coefficient of interband optical absorption, ν is the quantum yield of intrinsic photoeffect, I is the photon flux density.

The simulation of the photoconductivity kinetics basing on Eq. (1.1) with the unified relaxation time τ_{ph} is quite a rough approximation as a recombination of nonequilibrium carriers occurs through the several channels with different relaxation times. However, when considering time τ_{ph} as an adjustable parameter, equation (1.1) can be used for obtaining semi-quantitative estimations.

It follows from Eq. (1.1) that in the constant relaxation time approximation the photoconductivity growth is described by the following expression

$$\delta\sigma(t) = \delta\sigma_s \left[1 - \exp\left(-t/\tau_{ph} \right) \right], \tag{1.2}$$

where $\delta\sigma_s = e(\mu_n + \mu_p)g\tau_{ph}$ is the photoconductivity value in the steady state. After the illumination is turned off, the photoconductivity decreases exponentially

$$\delta\sigma(t) = \delta\sigma_s \exp\left(-t/\tau_{ph} \right). \tag{1.3}$$

It follows from Eqs. (1.2) and (1.3) that under quasistationary excitation the photoconductivity and, consequently, the photoconductor sensitivity are proportional to the relaxation time τ_{ph}. However, the response time of the photoconductor will increase with increase of the time τ_{ph}.

1.2 Anisotropy of photoconductivity in cubic semiconductors

In a homogeneous semiconductor the photocurrent is linear in the dc electric field and quadratic with respect to the amplitude of the electric field radiation. Therefore, the photoconductivity can be considered as a third order non-linear effect and the photocurrent density **j** can be presented as follows [28, 29]

$$j_i = \sigma_{ijkl}F_jE_kE_l, \tag{1.4}$$

where F_i and E_i are the components of the dc electric field and the electric field of the light, σ_{ijkl} is the photoconductivity tensor. It follows from Eq. (1.4) that this tensor is symmetrical with respect to the two last indexes.

Further we will consider the anisotropic effect in cubic crystals for which the electrical conductivity and linear optical properties are isotropic. In this

case, σ_{xxxx}, σ_{xxyy}, and σ_{xyxy} will be the nonvanishing photoconductivity tensor components. Besides, in an isotropic medium the condition $\sigma_{xxxx} - \sigma_{xxyy} - 2\sigma_{xyxy} = 0$ should be fulfilled.

If follows from Eq. (1.4) that in the general case the photocurrent and dc electric field do not necessarily coincide in directions. In the samples opened in the transverse direction (perpendicular to the dc field) this will result in the transverse photovoltage. Another effect occurring due to anisotropy of the photoconductivity is the dependence of the photocurrent along the dc field on the polarization direction of the electromagnetic wave field relative to the dc field and the semiconductor crystallographic axes.

There are several known physical mechanisms of anisotropic photoconductivity in cubic semiconductors. One of them is realized in many-valley semiconductors and is determined by a non-uniform population of the valleys by electrons excited from the impurity levels by polarized light [28]. The anisotropy of electron mobility in an individual ellipsoidal valley results in anisotropic contribution of photoelectrons from all the valleys into the electrical conductivity. In this case, non-uniform distribution of electrons between the valleys is caused by the dependence of the probability of an electron optical transfer from the impurity level to the valley on the orientation of the latter relative to the radiation polarization vector. The calculations show [28] that in this case the transverse photovoltage is proportional to the small parameter τ_{iv}/τ_r (where τ_{iv} is the time of the intervalley transfers of electrons) and can be observed only at low temperatures.

It is known that at photoionization of an impurity center, the electrons are mainly emitted in the direction of the light wave electric field and as a result their momentum distribution in the conduction band becomes anisotropic. The electrons, the momentum of which constitutes an acute angle with the dc electric field direction will slow down and lose their energy under this field whereas the electrons with the opposite momenta will accelerate and their energy will grow. In Ref. [29] it was shown that under such conditions the

21

energy dependence of the momentum relaxation time of electrons results in the appearance of a photocurrent component transversal to the dc field.

The photoconductivity anisotropy can also result from the anisotropy of momentum distribution of electrons and holes generated by interband optical transitions [30]. In this case, the reason for the anisotropic distribution is a tight relation between the angular moment and momentum of carriers in the valence band as well as the selection rules for interband optical transitions. This phenomenon, named as the optical alignment of electrons over momenta, leads to polarized hot-electron photoluminescence in semiconductors [31, 32].

We will consider the case of the optical transitions of electrons from the heavy hole subband to the conduction band under exposure to linearly polarized electromagnetic radiation. For heavy holes the projection of the total angular momentum on the momentum direction can take the value of $M = \pm 3/2$. In the coordinate system with z-axis directed along the momentum, these two states correspond to the Bloch functions $(X + iY)\uparrow$ and $(X - iY)\downarrow$, where X and Y are the functions transforming as the corresponding coordinates, the arrows characterize the spin direction. Probability W of the direct optical transition of an electron to the conduction band with the momentum along z-axis is proportional to the square of the dipole moment matrix element

$$ W \sim \left| \left\langle (X \pm iY) \left| \mathbf{d}\mathbf{e} \right| S \right\rangle \right|^2, \tag{1.5} $$

where S is the Bloch function of electrons in the conduction band, $\mathbf{e}$ is the polarization vector of radiation, $\mathbf{d}$ is the dipole moment operator. In the dipole approximation it is apparent that only matrix elements $\left\langle X \left| d_x \right| S \right\rangle = \left\langle Y \left| d_y \right| S \right\rangle = \left\langle Z \left| d_z \right| S \right\rangle$ are nonvanishing. So, as follows from Eq. (1.5), the probability of excitation of an electron with the momentum parallel to the radiation polarization vector (along z-axis) vanishes. On the other hand, the probability of excitation of electrons with the momenta lying in the plane

22

perpendicular to the radiation electric field will be maximum. Similarly, it can be shown that for transition from the light hole subband the momenta of the generated electrons and holes are directed predominantly along vector **e**.

In the general case, with the use of the wave functions of the states with arbitrary direction of momentum **p** (they are connected by the finite rotation matrices with functions for the states with $\mathbf{p} \parallel oz$), it can be shown that at interband absorption of linearly polarized radiation the electrons distribution function at the instant of generation takes the form of [31, 32]

$$f(\mathbf{p}) \sim 1 + \alpha_0 P_2(\cos\theta), \qquad (1.6)$$

where θ is the angle between the radiation electric field vector and the electron momentum, $P_2(x) = (3x^2 - 1)/2$ is the second order Legendre polynomial. Parameter $\alpha_0 = -1$, $+1$ and 0 correspond to the transitions from the heavy, light and spin-orbit split-off holes subbands. Eq. (1.6) describes the electron distribution in the spherical approximation when the corrugation of constant-energy surfaces of the valence band is neglected. Fig. 1.1 illustrates the pattern of Eq. (1.6) for transitions from the heavy- and light-hole subbands. In Ref. [30] it was shown that the optical alignment of photoexcited electrons over their momenta and the energy dependence of their momentum relaxation time results in the anisotropic photoconductivity. The mechanism of the anisotropy at interband transitions does not fundamentally differ from the mechanism suggested in Ref. [29]. Just as in the case of impurity-band transitions, the electrons having at the instance of generation the momentum component directed along and opposite to the dc field will lose and, correspondingly, gain energy. As the photoelectrons have the velocity component perpendicular to the dc electric field, it is apparent that due to the energy dependence of the electron scattering rate the contributions of these two groups of electrons into the current are no longer compensating each other. As a result the photocurrent component perpendicular to the field **F** will appear.
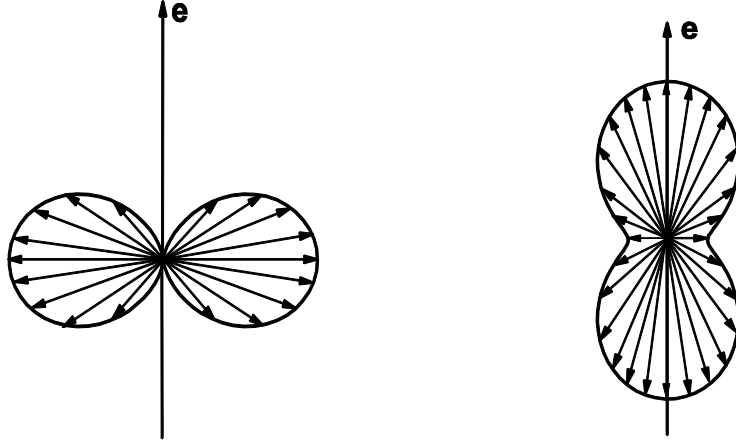
Fig. 1.1. Distribution over the momentum directions of photoelectrons excited from the heavy- (a) and light- (b) hole subbands by radiation linearly polarized along vector **e**. The population of state with the corresponding momentum direction is proportional to the length of the vector. Spatial distribution is obtained as a result of rotation of the shown distribution around the polarization vector.

In the isotropic case the photocurrent can be expressed as

$$\mathbf{j}_{ph} = \alpha \mathbf{F}(\mathbf{E}\mathbf{E}) + \beta \mathbf{E}(\mathbf{F}\mathbf{E}),\qquad(1.7)$$

where **E** is an amplitude of the light wave electric field, coefficients α and β can be expressed in terms of the photoconductivity tensor components σ_{ijkl}. It follows from Eq. (1.7) that the transverse component of the photocurrent which is perpendicular to field **F** is proportional to $\beta \sin 2\vartheta$ (where ϑ is the angle between vectors **F** and **E**) and reaches its maximum at $\vartheta = 45°$. At stationary photoexcitation the following expression was obtained for coefficient β determining the anisotropic part of the photocurrent [30]

$$\beta \sim \frac{e^2 \tau_p \tau_2 \kappa c}{m\hbar\omega} \frac{d\ln\tau_p(\varepsilon)}{d\ln\varepsilon}\bigg|_{\varepsilon=\varepsilon_0},\qquad(1.8)$$

24

where m is the effective mass of the electron in the conduction band, κ is the absorption coefficient of optical radiation with frequency ω, τ_p and τ_2 are the relaxation times of the first and the second spherical harmonics of the electron distribution function depending on its energy ε, $\varepsilon_0 = \hbar\omega - \varepsilon_g$ is the photoelectron kinetic energy at the instance of generation. As it follows from Eq. (1.8) the ratio of the anisotropic part of the conductivity to the ordinary photoconductivity is determined by parameter τ_2/τ_r. The relaxation time τ_2 of anisotropic part of the distribution function (1.6), as a rule, is considerably smaller than the carrier life time in the conduction band. That is why under stationary excitation and at room temperatures the anisotropic photoconductivity is usually minor.
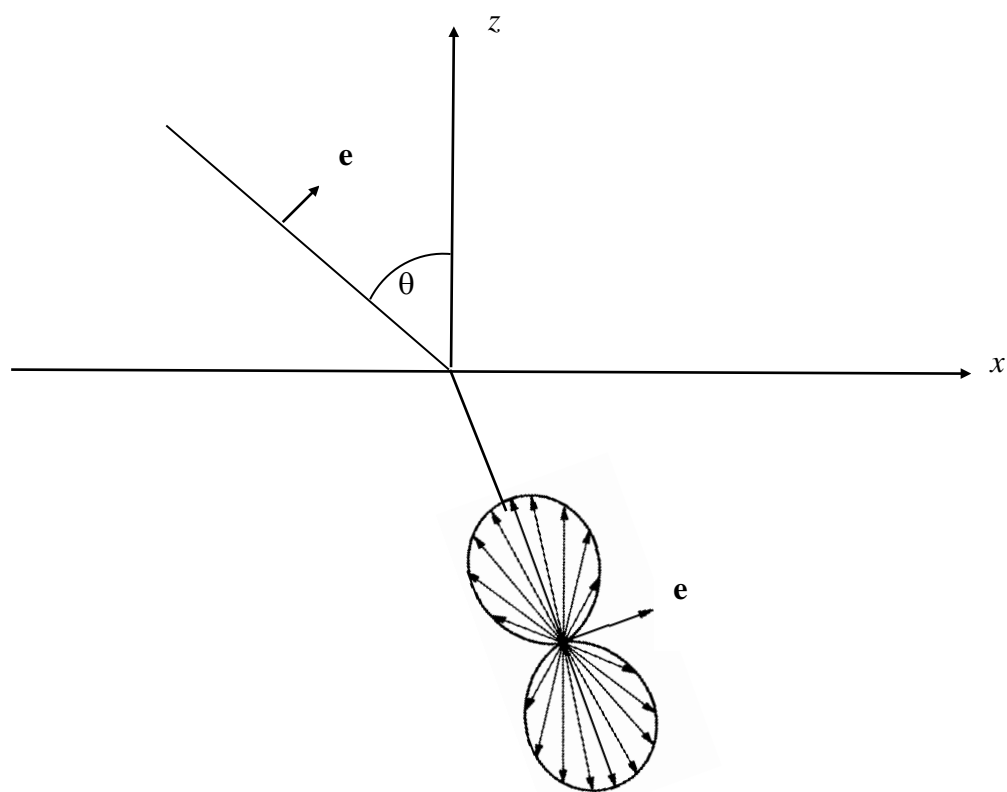

Fig. 1.2. The mechanism of the surface ballistic photoeffect caused by the optical alignment of the photoexcited electrons over momenta and their diffuse surface scattering.

Optical alignment of photoexcited carriers over momenta can also result in a so-called surface ballistic photoeffect [33] which manifests itself in the appearance (under no dc electric field) of the lateral photocurrent parallel to the illuminated semiconductor surface. The mechanism of this effect is illustrated in Fig. 1.2. Let the radiation linearly polarized in the plane of incidence with quantum energy exceeding the band gap impinges on the semiconductor surface (z=0) at angle θ. As a result of interband optical transitions, the electrons with anisotropic momentum distribution are generated (Fig. 1.2. illustrates only the distribution for transitions from the heavy-hole subband).

Electrons from the upper lobe moving towards the surface will experience the surface scattering in contrast to the electrons from the lower lobe. If the scattering at the surface is partially diffuse, the electrons flowing to the left will lose their momentum more intensively than the electrons flowing to the right. In this case the electrons flows to the left and to the right will no longer compensate each other and the resulting lateral flow of electrons to the right will appear. It is not difficult to understand that the contribution to the lateral photocurrent will mainly come from the photoelectrons that reached the surface without experiencing volume scattering. That is why the value of the surface photocurrent to a great extent depends on the relation between the mean free path of electrons in volume Λ and the length of optical absorption κ^{-1}. Under the condition $\Lambda \kappa \gg 1$ the surface photocurrent is proportional to $P\eta\Lambda\left(eI/\hbar\omega\right)$, where $\eta = \left[1 - \left(\mathbf{n}\mathbf{e}\right)^2\right]\left(\mathbf{n}\mathbf{e}\right)$, $\mathbf{n}$ is the normal vector to the surface, P is the diffuse reflection factor for electron surface scattering. At a normal incidence the surface photocurrent vanishes.

1.3 Photoconductivity excited by ultrashort laser pulses

The kinetics of intrinsic photoconductivity is determined by the processes of intraband and interband relaxation of nonequilibrium electrons and holes excited in the course of direct interband optical transitions. The processes of the electron-electron scattering as well as interaction of electrons with the

lattice result in momentum relaxation of nonequilibrium carriers that manifests itself in decay of the anisotropic momentum distribution of photoelectrons. The typical time of the intraband momentum relaxation of electrons usually constitutes several hundreds of femtoseconds and depends on the density and energy of electrons, temperature and the semiconductor parameters. Intraband energy relaxation of photoexcited electrons resulting in their losing the excessive energy when interacting with the lattice and gaining the same distribution over energy as the equilibrium ones, occurs a little slower than the momentum relaxation. The point is that an electron momentum relaxation usually occurs within one scattering act whereas as a rule several such acts are needed for thermalization of photoelectrons. Intraband electron relaxation over energy usually occurs as a result of their interaction with optical phonons. Certainly, the total time of photoelectrons thermalization will depend on their initial energy which is determined by the band structure of the semiconductor and the photon energy of the exciting optical radiation.

At stationary irradiation, part of the photocarriers of the order τ_p / τ_r is anisotropically distributed over their momenta, whereas the fraction of the hot photocarriers distributed isotropically in a momentum space but having nonequilibrium energy distribution is proportional to parameter τ_e / τ_r. At room temperature the typical intraband relaxation times of the carriers are usually considerably smaller than their life time, and hence the influence of the nonequilibrium energy and momentum distribution of photocarriers on the photoconductivity are minor. Thus, such effects, like, for example, anisotropic photoconductivity, can be observed only at low temperatures.

Appearance of laser systems generating femtosecond optical pulses allows to investigate the dynamics of intraband relaxation of photoexcited carriers and the photocurrent in semiconductors with subpicosecond time resolution. Ultrafast relaxation of the distribution function of charge carriers generated by a femtosecond pulse is usually studied by probing the semiconductor with a probe wide-band femtosecond pulse and by measuring

the dependence of the transmittance spectrum change on the delay time of the probe pulse relative to the pump pulse [34-37]. In this case, the change in the optical transmittance of the probe radiation is connected with the effect of population of the states in the conduction band and valence band by photoexcited carriers, transfers between which result in absorption of the probe optical radiation.

For investigation of intraband relaxation of photoexcited carriers the hot photoluminescence spectroscopy technique [31, 38-39] is applied. This effect manifests itself in the presence of high-frequency tail of the edge luminescence and is determined by the contribution into luminescence of photoexcited carriers which recombine before they manage to thermalize. The hot luminescence spectrum gives a kind of a time scan of the process of the carrier intraband relaxation over energy. The studies of the hot luminescence polarization determined by the effect of optical alignment of photocarriers over momenta as well as of depolarization of recombined radiation in the magnetic field allow measuring both the time of energy relaxation and the time of momentum anisotropy relaxation. In Ref. [40] the method of photoluminescence with subpicosecond time resolution was applied for investigating the dynamics of hot photocarriers relaxation.

In the general case, the electrons can be excited from three valence subbands, including the subbands of the heavy, light and spin-split-off holes. Therefore, if the photon energy exceeds the threshold energy for transition from the spin-orbit split-off subband, at the instant of photoexcitation the energy distribution of electrons in the conduction band takes the form of three peaks. Initial width of these peaks is determined by the spectral width of the pump femtosecond pulse as well as by the bands corrugation. If the energy of the photons is smaller than the threshold value, two peaks will be observed in the distribution of photoelectrons which correspond to the transitions from the heavy and light-hole subbands.

At direct optical transitions, the energies of the states being populated with photoexcited carriers, are almost uniquely determined by the exciting

photon energy. Therefore, the evolution of the distribution of photoexcited carriers over energy can be defined out of the measurement of the spectral dependence of the probe radiation transmittance change on the delay time. For interpretation and analysis of results of the measurements the Monte Carlo simulation is usually used
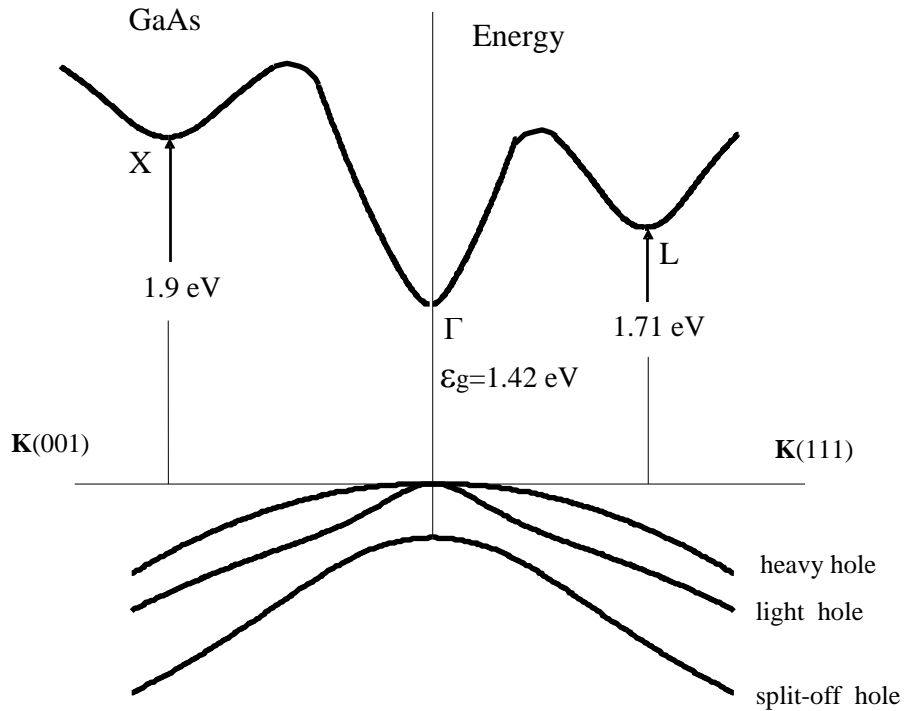

Fig. 1.3. GaAs band structure.

[37, 19] which allows to take into account the actual band spectrum, the variety of carrier scattering mechanisms and other effects which are difficult to take into account within the frames of an analytical approach. The authors of Ref. [37] with the use of the femtosecond pump-continuum-probe method and the Monte Carlo simulation have studied the subpicosecond dynamics of photocarriers in the $Al_{0.1}Ga_{0.9}As$ semiconductor. It was shown that considerable impact on dynamics of intraband photocarrier relaxation comes from the intervalley transfers of photoelectrons which occur when they are excited towards the conduction band states with the energy higher than the bottom of the lateral valleys. In this case, the intraband relaxation process occurs in the following way. Photoexcited electrons being excited by light

from the valence band towards the states of the central Γ-valley, very quickly (within less than 100 fs) are scattered to the lateral L- and X-valleys where they relax to their bottom. Then within approximately several picoseconds they return back to the central valley and then, by scattering predominantly on the optical phonons, go down to the bottom of this valley where they reach the state of local intraband equilibrium state. Comparatively long time of the electrons transfer from the lateral valleys to the central valley results from high density of the electron states in the lateral valleys comparing to the central valley.

The dynamics of the intervalley transfers of electrons was studied in GaAs with the use of the optical pump – terahertz probe method. The dependence of the reflection [3] and transmittance [41] of a probing THz pulse on the delay time of this pulse relative to the optical pump pulse was measured. The time dependence of mobility of photoexcited electrons and the time of intervalley L-Γ transfers were calculated out of the transmittance and reflection spectra on the basis of the Drude model.

In Ref. [40] the dynamics of intervalley transfers in GaAs was investigated using the photoluminescence method with subpicosecond time resolution. It was found that the photoluminescence signal was considerably delayed relative to the pump pulse and reached its maximum only in 10 ps after the pump pulse. Such a long delay time is explained by the low rate of photoelectron transfer from the L-valley to the central Γ-valley.

At the initial stage when the interband recombination processes are still minor the distribution function of photoexcited electrons and holes is usually formed as a result of the generation and intraband relaxation processes. The dynamics of these processes is usually described using the semiclassical approach wherein the Boltzmann equations for electron and hole distribution function are solved. This approximation, however, does not take into account the phase coherence between photoexcited electrons and holes and hence it is justified when the pump optical pulse duration is longer than the phase coherence relaxation time. For shorter pulses the semiconductor excitation

should be analyzed on the basis of the system of semiconductor Bloch equations [42] containing the equations both for the distribution function of the carries within the bands and the interband polarization induced by an optical pulse. In this case the photoexcitation process occurs in two stages: first, under the exposure to the optical pulse the coherent interband polarization is excited, then, as a result of interaction of this polarization with the electric field of the pulse the electrons and holes are generated. In a number of Refs. it was shown theoretically [20, 43-45] and experimentally [39] that the coherence effects become essential at pulse durations less than 100 fs and result in faster energy relaxation of photoexcited carriers.

Relaxation of anisotropy of photocarrier momentum distribution occurs within one or two collisions. It is evident that particularly this time will determine the time of the phase coherence relaxation of photoexcited electrons and holes. For the first time the decay dynamics of anisotropy of photoelectron momentum distribution was studied in Ge [46] using the technique of the probe optical pulse diffraction on the lattice of the electrons anisotropically distributed in a momentum space. Such a lattice was formed by an optical field with polarization periodically changing in space. The anisotropy of absorption saturation of a probe optical pulse in GaAs pre-excited by an intensive linearly polarized laser pulse was studied in Ref. [47]. The quantum energy of the exciting radiation was chosen so that the excessive energy of photoelectrons in the band was lower than the threshold of the optical phonon emission and the main contribution into the momentum relaxation would come from the electron-electron interaction. The dependence of absorption anisotropy on the delay time between the probe and pump pulses was measured. It was found that at the density of electron-hole pairs of $6 \cdot 10^{17}$ cm^{-3}, the decay time of momentum distribution anisotropy was about 190 fs.

The intraband relaxation time of photoexcited carriers depends on the band structure of the semiconductor, photon energy of the exciting radiation, dc electric field strength and density of the electron-hole plasma. At the intraband relaxation stage which usually ranges from several hundreds of

31

femtoseconds to several tens of picoseconds, the effects connected with ballistic transport, heating and intervalley transfers of electrons can emerge. Peculiarities of the hot carriers dynamics in the electric field connected with these effects manifest themselves on subpicosecond and picosecond time scales and lead to the so-called transient photoconductivity.

In a weak electric field not resulting in the charge carrier heating, the transient photoconductivity is defined by the dynamics of the photoexcited carrier intraband relaxation depending on the initial energy of photoelectrons in the conduction band, which, in turn, is defined by the photon energy of the exciting radiation and the semiconductor band structure parameters. At room temperatures the main mechanism of energy relaxation of hot photoelectrons is the emission and absorption of optical phonons. In the low temperature region $T < \hbar \omega_0 / k_B$ (where ω_0 is the frequency of optical phonons, k_B is the Boltzmann constant) the main relaxation process is the spontaneous emission of optical phonons. When an electron reaches the passive region where its energy ε becomes lower than $\hbar \omega_0$, this process is prohibited and the acoustic phonon scattering can contribute into the energy relaxation. The total time of energy relaxation of photoelectrons to the bottom of the conduction band increases with growth of the photoelectron initial energy and in $A_3 B_5$ semiconductors usually constitutes from several hundreds of femtoseconds to several picoseconds [48]. Electron-electron scattering can also impact on the energy relaxation of photoexcited electrons. Though these processes do not result in the change of the total energy of the electron subsystem they may cause re-distribution of electrons over their energies so that some electrons from the passive region can jump to the active region ($\varepsilon > \hbar \omega_0$) and pass the energy to the lattice by emitting an optical phonon.

Under the condition when the main mechanism of energy relaxation of photoexcited electrons is the cascade emission of polar optical phonons, the transient photoconductivity can manifest a nontrivial dependence on time in the first few picoseconds after excitation by a subpicosecond laser pulse [7, 49-

50]. Thus, if the initial energy of photoexcited electrons counted from the bottom of the conduction band is close to a multiple of the polar optical phonon energy, the photoconductivity on a picosecond timescale can become negative. This effect was theoretically considered in GaAs on the basis of the transport Boltzman equation [7, 49-50]. The analysis was made on the assumption that the density of the electron-hole plasma is low and the impact of the carrier-carrier interaction on the energy relaxation of electrons can be neglected. It was also assumed that photoelectrons were excited towards the states lying lower than the bottom of overlying subsidiary valleys and so their intervalley scattering can be neglected. Here it should be noted that such a mechanism of absolute negative photoconductivity under stationary photoexcitation was for the first time considered in Refs. [51, 52].

In Ref. [53] the linear high-frequency conductivity of hot electrons in GaAs was theoretically studied. It was shown that in the first few picoseconds after subpicosecond excitation the conductivity behaves in a non-trivial way and cannot be described using the Drude expression. When the initial energy of photoelectrons is a multiple of the polar optical phonon energy, the real part of the high-frequency transient conductivity manifests a peak in the terahertz frequency range which shifts to the low-frequency region with time increase. The imaginary part of the photoconductivity in this case shows an oscillating dependence on the frequency.

When the initial energy of photoelectrons is close to or higher than the threshold energy of intervalley transfers, the energy relaxation time can considerably increase. Slowing-down of relaxation rate is connected here with longer time of photoelectron scattering from the lateral valleys to the central valley. This effect was observed in GaAs [3] in which the dynamics of transient mobility of electrons excited by femtosecond pulses with the photon energy of 2 eV was measured with subpicosecond time resolution.

Ballistic lateral transport of photoexcited electrons in the electric field was experimentally studied in GaAs quantum well structure [54, 10]. Femtosecond laser radiation excites electrons in the states close to the bottom

of the conduction band. The distribution function of the excited photoelectrons and its evolution over time were found basing on the dependence of the change in transmittance spectrum of a probe femtosecond pulse on the delay time of this pulse relative to the pump pulse. It was shown that in the structure under investigation the photoexcited electrons are ballistically accelerated by the field within approximately 150 fs.

When the electric field is strong enough to result in heating of photoexcited electrons, a so-called velocity overshoot effect can appear [55]. This effect lies in the fact that in the first several hundreds of femtoseconds after photoexcitation, so far the photoelectrons still move in the quasi-ballistic mode, their drift velocity can several times exceed the value of the stationary velocity. In semiconductors like GaAs the velocity overshoot effect results from the intervalley transfer of hot photoelectrons from the central valley to the lateral valleys characterized by a larger effective mass. The electrons excited by optical radiation to the central valley accelerate in electric field F and within time t that is of the order of their momentum relaxation time achieve velocity $v(t) = eFt/m$ and energy $\varepsilon(t) = \varepsilon_i + e^2 F^2 t^2 / 2m$ (where m is the effective mass of the electrons in the central valley, ε_i is the initial energy of a photoelectron). When the electrons reach the threshold energy they are transferred to the lateral heavy valleys of the conduction band where they slow down. If the electric field is strong enough, the velocity of electrons in the central valley $v(t)$ can reach the value exceeding the average stationary velocity which is determined by the electron velocities in the central and lateral valleys and the population degree of the latter.

In Ref. [1] it was experimentally established that in the first several picoseconds after the femtosecond optical excitation the drift velocity of photoelectrons in GaAs is approximately twofold bigger than the value of the steady velocity. The velocity of electrons was found basing on the dynamics of the electric field change owing to the screening effect determined by spatial separation of photoexcited electrons and holes. The electric field was measured

from the change in absorption of the probe radiation in the spectral range near the band gap edge which was determined by the transient Franz-Keldysh electro-optical effect.

The transient carrier response in electric fields with strengths up to 130 V/cm was studied in GaAs and InP by the use of the THz emission spectroscopy technique with time resolution of 20 fs [56, 16]. The contributions of coherent lattice oscillations and of the free charge carriers into THz generation were investigated separately. It was found that as a consequence of the velocity overshoot effect the peak velocity of electrons reached $8 \cdot 10^7$ cm/s in InP and $6 \cdot 10^7$ cm/s in GaAs.

The transient electrical response of GaAs, excited by a subpicosecond laser pulse, in a homogeneous electric field has been simulated by using the ensemble Monte Carlo method [5]. For calculation of the band structure and matrix elements of direct optical transitions of electrons from three valence subbands to the conduction band, the *kp*-method was used. In the Monte Carlo simulation of the electron transport a three-valley conduction band model was used. The electrons scattering by acoustic, optical and intervalley phonons was taken into account. On calculating the initial distribution function of the photoelectrons over energies the broadening of the electron states due to the electron scattering and their drift in the electric field was taken into account. The results of the simulation show that the threshold strength of the electric field resulting in the velocity overshoot effect increases with increase of the exciting photon energy. For example, in the electric field of 5 kV/cm the effect occurs under excitation by photons with 1.5 eV energy but is absent under excitation by 1.7 eV photons. It has been shown that the velocity overshoot effect appears under the condition that the average steady energy of photoelectrons in the electric field exceeds their energy at the instant of excitation.

As the Monte Carlo simulations show [5], at excitation of GaAs by femtosecond radiation with the photon energy of 2 eV, the velocity overshoot effect is absent in the electric field with strength less than 20 kV/cm. However,

this conclusion contradicts to the experimental results, as this effect was observed at lower fields [57]. Besides, it was determined that the measured duration of the photocurrent surge several-fold exceeded the calculated value. The authors of Ref. [9] assumed that the experimentally observed photocurrent surge in GaAs at 2 eV femtosecond excitation is conditioned not by the velocity overshoot effect but occurs as a result of screening of the applied electric field due to a spatial separation of photoexcited electrons and holes. To confirm this conclusion the Monte Carlo simulation of photocarriers transport taking into account the electric field screening effect was carried out. The calculations show that at 2 eV excitation the effect of the electric field collapse due to the screening results in the photocurrent surge in GaAs with a characteristic decay time determined by the dielectric relaxation time depending on the density of the photoexcited electron-hole plasma. When the density of the photoexcited plasma is of 10^{17} cm^{-3} the threshold value of the electric field strength resulting in this effect constitutes about 3 kV/cm whereas the duration of the photocurrent pulse is of several picoseconds. Decrease of the excitation intensity results in increase of the photocurrent pulse duration and threshold value of the electric field.

The peculiarities of the transient photoresponse of GaAs excited by a subpicosecond laser pulse with quantum energy of 2 eV have been studied with the use of the electro-optical method and Monte Carlo simulation [6, 58]. The calculations show that on exciting the electrons towards the states of the conduction band lying above the bottom of the lateral L-valley, the major contribution into the velocity overshoot effect comes from the electrons which at the instant of excitation have a velocity component along the electric field. Under the electric field these electrons slow down and their energy becomes lower than the threshold energy of transfer to the lateral valleys. As a result, particularly these electrons remain in the central valley and result in the velocity overshoot effect. It is noted that the photocurrent growth begins not immediately after the pump pulse but within some time delay depending on the electric field strength. This delay is defined by the time required to accelerate

the electrons moving at the instant of photoexcitation along the field and transfer them in the states with the velocity component directed against the electric field. The velocity overshoot effect and the delay depending on the electric field strength were observed in GaAs at 2 eV photoexcitation. The threshold electric field for the velocity overshoot effect considerably depends on the deformation potential constant for the Γ-L intervalley transfers. In Ref. [6] it is shown that the value of this constant can be defined by comparing the calculated and experimentally measured values of the threshold electric field resulting in the velocity overshoot effect.

At high intensities of optical excitation when the density of photoexcited electron-hole pairs exceeds 10^{17} cm^{-3} it is necessary to take into account the impact of the electron-hole interaction on the picosecond photoresponse. In Ref. [2] the photoresponse of GaAs excited by 1.55 eV femtosecond pulse in a strong electric field was simulated by Monte Carlo method taking into account the electron-hole scattering. It has been found that at the excitation intensity corresponding to the density of electron-hole pairs of 10^{18} cm^{-3}, the energy and momentum transfer from the electron- to the hole-subsystem due to the electron-hole interaction results in the decrease of fraction of electrons in the lateral valleys and of the average electron velocity.

As a result of the carriers capture by the surface states a space charge region can be formed in a semiconductor near its surface. For typical semiconductors the thickness of this region depends on the doping level and constitutes from 10^{-6} to 10^{-3} cm, i.e. it can be comparable with the absorption depth of light. In highly doped semiconductors the strength of electric field induced by such a space charge can achieve the value of several megavolts per centimeter. When a semiconductor surface is excited by femtosecond laser radiation, the photoexcited electrons and holes are spatially separated by the space charge field. The occurring polarization results in the screening of the surface electric field, the dynamics of which is determined by the photocarrier transport. Therefore, by means of exciting the electrons and holes close to the

semiconductor surface by femtosecond laser pulses it is possible to investigate subpicosecond dynamics of the electric field and photocarriers.

In Ref. [11] the subpicosecond dynamics of screening of the built-in surface field close to a GaAs surface excited by femtosecond laser pulses was experimentally and theoretically studied. The field dynamics was defined from the change of the reflectivity from the photoexcited semiconductor surface which is caused by the electro-optical effect in the space charge field. The dependence of the reflection coefficient of the probe femtosecond pulse on its delay time relative to the pump pulse generating electrons and holes was measured. The dynamics of the charge carriers and surface electric field screening was calculated self-consistently with the use of the diffuse-drift approximation. The time of the built-in electric field screening which was measured using the electro-optic method was consistent with the calculation results and ranged from several hundreds of femtoseconds at high density of electron-hole pairs ($\sim 5 \cdot 10^{18}$ cm^{-3}) to several picoseconds at low density ($\sim 5 \cdot 10^{16}$ cm^{-3}).

The subpicosecond dynamics of the surface electric field screening in GaAs was also studied using the time-resolved photoluminescence method [12]. As in the previous work [11] the analysis and interpretation of the measured kinetics of photoluminescence decay was carried out by comparing experimental data with the results of simulation of the electric field and photocarrier dynamics which were obtained as a result of self-consistent solution of the continuity equations for electrons and holes and the Poisson equation for the electric field.

The steady-state photoconductivity is usually analyzed within the frames of a simplified model when the processes of the carrier generation by light and their intraband transport under dc electric field are considered separately, i.e. not taking into account the quantum coherence effects determined by the interference of intraband and interband electron transitions in dc and light wave electric fields. Such a semi-classical approach, however, can be unjust when considering the subpicosecond photoconductivity dynamics. That is why

the rigorous theory of photoresponse of semiconductors excited by femtosecond laser pulses should be developed basing on the quantum-mechanical approach. The most general expression of the third order nonlinear conductivity tensor σ_{ijkl} (see (1.4)) determining photoconductivity was obtained by Genkin and Mednis [59]. The obtained expression describes the photoresponse of a semiconductor excited by optical radiation with photons energy both higher and lower than the band gap. In the former case the radiation generates real carriers which contribute into the photocurrent. In the latter case, when the photon energy is lower than the fundamental absorption edge of semiconductor, the expression for the non-linear conductivity describes the so-called virtual photoconductivity [60-65]. This effect implies that the low-frequency polarization occurs and it can be considered as the inverse Franz-Keldysh effect. Contrary to the real photoconductivity, the virtual photoconductivity is almost instantaneous as in this case there is no generation of real electrons and holes in the bands.

CHAPTER 2
TERAHERTZ SPECTROSCOPY OF SEMICONDICTORS

In this chapter the mechanisms of generation of terahertz electromagnetic pulses in semiconductors excited by femtosecond laser radiation are considered. The methods of coherent detection of terahertz radiation using photoconducting antennas and the electro-optical effect are described. The basic principles of terahertz spectroscopy and peculiarities of its application for investigation of ultrafast electron transport in semiconductors excited by ultrashort laser pulses are presented.

2.1 Generation of terahertz electromagnetic pulses in semiconductors

A photocurrent surge excited in a semiconductor by femtosecond laser radiation can be a source of terahertz electromagnetic radiation. This phenomenon in the basis of the operation of photoconductive semiconductor antennas used for generation of wide-band pulses of terahertz radiation [66-68]. The radiating antenna represents a stripline, formed at the surface of a photosensitive semiconductor material, to which the constant bias is applied (Fig. 2.1). When the gap between the stripline electrodes is irradiated by an ultrafast laser pulse, in the semiconductor a photocurrent surge is generated which excites the antenna. The amplitude of the THz electric field in the far field region is determined by acceleration of photocarriers, i.e. it is proportional to the derivative of the photocurrent with respect to time. When the excitation level is low the amplitude of a terahertz pulse is proportional to the energy of the pump laser pulse and the strength of the bias. In a real situation the energy of a terahertz pulse experiences saturation with increase of the laser pulse energy. It is related to the screening of the interstrip electric field by photoexcited carriers and the reaction of the generated terahertz radiation. Increase of the bias field also encounters limitations related to the

possible electric breakdown of the substrate. A possible thermal breakdown caused by decrease of the semiconductor resistance owing to its heating under photocurrent and laser radiation also restricts the amplitude of generated THz field. That is why for obtaining efficient THz generation in a photoantenna it is necessary to use semiconductor materials with high enough photocarrier mobility and high breakdown voltage.

At present the highest efficiency of THz generation is achieved at GaAs photoconductive antennas excited by the radiation of femtosecond titanium-sapphire lasers. At the best samples of such antennas the conversion efficiency (over energy) is achieved at a level of 10^{-4}. In such antennas layers of so-called LTG-GaAs (gallium arsenide obtained by the method of molecular beam epitaxy to a cold substrate) are usually used as a photoconductive material.
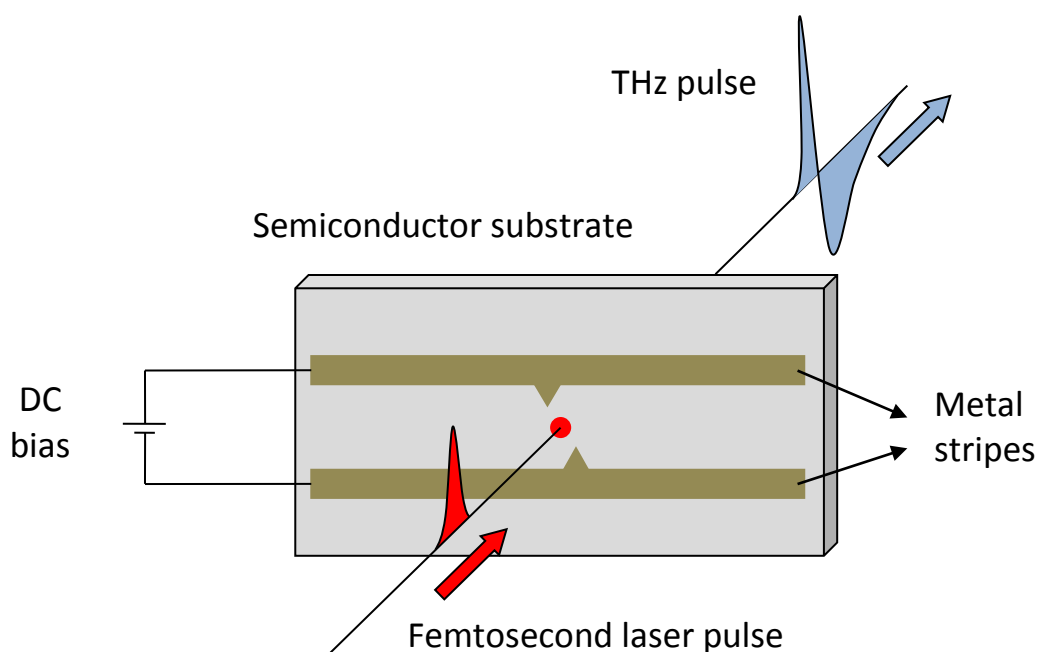

Fig. 2.1. THz pulses emission with a photoconductive antenna.

This semiconductor material is characterized by a high enough breakdown voltage and high mobility of the current carriers. However, its main peculiarity is the very short life time of nonequilibrium photocarriers which allows to use it in photoconductive antennas intended for coherent detection of THz pulses. At present the layers of LTG-GaAs with life time of nonequilibrium carriers of

less than 200fs have been obtained using the method of low-temperature molecular beam epitaxy; the photoconductive antennas made from this semiconductor are able to generate and detect THz radiation within the frequency range of 0.1 – 5THz.

Recently relatively cheap and compact femtosecond laser systems generating radiation within the range of 1 – 1.5µm have been developed. In this spectral range the GaAs-based photoconductive antennas prove to be inefficient as the photosensitivity of this semiconductor is very low. Therefore photoconductive antennas based on more narrow-gap InGaAs [69, 70] and GaBiAs [71] semiconductors which can be excited in the wavelength range of 1 – 1.5µm were developed and made.

Recently it has been shown that under excitation of a semiconductor surface with femtosecond laser pulses a large enough THz radiation can be generated [14-15, 72]. This effect was observed at femtosecond irradiation of different semiconductor materials, including those having quite long photocarriers life time. It was shown that the highest efficiency of THz generation was achieved in narrow-gap semiconductors, like InAs, which had the optical absorption edge in the middle infrared spectrum range.

The effect of THz generation by surfaces of semiconductors irradiated by femtosecond laser pulses has quite a universal character and can be of interest for THz spectroscopy of semiconductors. It should be noted that in comparison with a photoconductive antenna the irradiated surface of a semiconductor generates a wider and less divergent far field THz beam which might appear significant for applications in THz imaging systems. The ease of making the surface THz emitters is also an important advantage. Unlike photoconductive antennas, their fabrication does not require expensive technological techniques like, for example, molecular beam epitaxy or ion implantation. In this case, the requirements to the semiconductor material parameters, in particular to the life time of nonequilibrium carriers, are not that strict as in the case of THz emitters based on the photoconductive antennas.

We will consider in more detail the main mechanisms of THz pulses generation by the surfaces of semiconductors excited by femtosecond laser radiation. THz radiation from a photoexcited surface of a semiconductor is caused by a dynamic dipole which is induced near its surface when excited by a femtosecond laser pulses. The contributions to the formation of this dipole come from a photocurrent surge and non-linear polarization at the frequency of the envelope of the pump laser pulse. Relative contributions of these mechanisms to THz pulses generation depends on the type and parameters of the semiconductor as well as on the intensity of the exciting optical radiation.

In the dipole approximation the electric field of THz radiation in the far field region can be expressed in the following form [72, 73]:

$$E_{THz} = -\frac{S}{c^2 R} \int_0^\infty \left(\frac{\partial j}{\partial t} + \frac{\partial^2 P}{\partial t^2} \right) dz , \qquad (2.1)$$

where c is the speed of light in vacuum, R is the distance from the observation point to the emitting region, S is area of the illuminated zone at the semiconductor surface, j and P are the projections of the photocurrent density and non-linear polarization on the polarization direction of THz field.

Integration in expression (2.1) is performed over the sample depth, the z-axis is directed into the bulk of the semiconductor. Expression (2.1) is non-applicable when the diameter of the illuminated area becomes larger than the wavelength of the generated THz radiation. In this case the THz field should be calculated taking into account the diffraction effect, i.e. by adding up the contributions of the separate emitting regions to the field taking into account the phase shift between them.

In semiconductors with strong surface band bending, such as, for example, GaAs and InP [14, 74-76], THz radiation is induced by a subpicosecond photocurrent $j(t)$ appearing as a result of the interband

excitation of electrons and holes under femtosecond laser radiation and their following spatial separation in the built-in electric field (Figure 2.2). The opposite polarity of the THz field generated in GaAs with *n*- and *p*-type of conductivity that is explained by different polarity of the depletion electric field in these samples [74] also counts in favor of this mechanism. The photocarrier transport in the depletion layer is accompanied by the spatial redistribution of charge and the electric field screening effect. When the photoexcitation level is low and the concentration of photocarriers is quite small, the screening effect can be neglected. However, since the intensive laser radiation is usually used to excite THz radiation, the photocarrier density can considerably exceeds the concentration of the equilibrium carriers. Therefore, when investigating the dynamics of photocurrent surge and emitted THz electric field in photoexcited semiconductors, the photocarrier transport and the dynamics of the built-in field screening should be considered self-consistently.
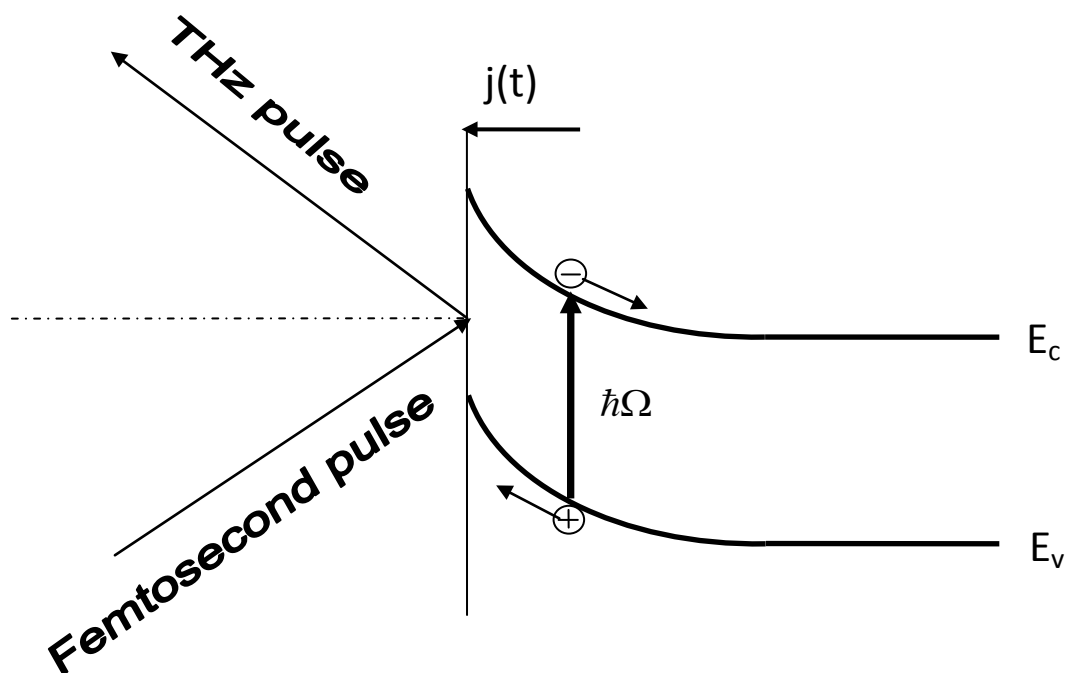

Fig. 2.2. THz pulse generation from semiconductor surface under femtosecond laser radiation.

The dynamics of photocarriers and depletion electric field was analyzed basing on self-consistent solution of the transport equations for electrons and holes in the diffusion-drift approximation and Poisson's equation for the field [11]. However, the diffusion-drift approximation does not take into account a wide range of effects such as the carrier heating by the depletion field and radiation, velocity overshoot effect, reactive current component, etc. Strictly speaking, this approximation is not quite correct when considering THz generation because the processes determining the dynamics of this effect occur at the times of $\sim 10^{-13}$ s which are comparable with the momentum relaxation time of the carriers in the semiconductor.

For the most complete description of subpicosecond dynamics of the photocurrent surge and THz field emitted from the semiconductor surface the ensemble Monte Carlo method [77] should be used, wherein the carrier motion in a fast-varying non-uniform electric field calculated self-consistently from Poisson's equation is scholastically simulated. Using this approach it is possible to take into account the influence of ballistic and heating effects on the photocarrier transport as well as variety of carrier scattering mechanisms, and real electronic structure of semiconductor considering such effects as corrugation of the valence band, nonparabolicity and multi-valley character of the electron spectrum, and et al.

As follows from the experimental data, the shape of a THz pulse can be both bipolar and oscillating. In Refs. [78, 79] the oscillating waveform of the THz field generated in the *p-i-n* structures and at the GaAs surface when excited by femtosecond radiation was associated with plasma oscillations of electrons. This mechanism of THz generation is usually considered as an independent one. However, in the reality it does not fundamentally differ from the mechanism caused by the photocurrent surge, because the plasma oscillations appear as a result of collisionless transport of carriers in a self-consistent electric field. In Ref. [77] on the basis of the ensemble Monte Carlo method the self-consistent dynamics of the depletion electric field and photoexcited carriers was simulated and the THz pulses generation from GaAs

surface was investigated. It was shown that in the hydrodynamic regime wherein the scattering rate of electrons exceeds the plasma frequency, the THz pulse has a bipolar shape. In the collisionless mode wherein the plasma frequency exceeds the frequency of electrons scattering , screening of the surface field is accompanied by plasma oscillations which results in the oscillating shape of a THz pulse.

Recently, the THz pulses emission from the surfaces of narrow-band semiconductors, like InAs and InSb excited by femtosecond laser radiation have been intensively studied. In these semiconductors the surface band bending is small and so the mechanism of THz generation realized in them differs from that in GaAs and InP. The photocurrent surge generating THz radiation in narrow-gap semiconductors appears as a result of the Dember effect [22-24], which is caused by the spatial separation of photoexcited electrons and holes generated near the irradiated surface and moving with different velocities inward the sample. This mechanism of THz generation is supported by the experimental data from which it follows that in narrow-band semiconductors the polarity of a THz signal does not depend on the type of conductivity [80-82].

The Dember effect was investigated at quasistationary photoexcitation and was analyzed using mainly the diffusion-drift approximation. However, this approach is quite rough as it does not take into account the effects of ballistic transport and carrier heating by light. The dynamics of photo-emf at the initial time after photoexcitation was considered basing on the kinetic approach [83, 84]. It was determined that in this case the photo-emf and photocurrent reach maximum values at the ballistic stage of movement of photoexcited electrons and holes reflected from the irradiated surface and moving with different velocities inward the semiconductor. The Monte Carlo simulation shows [84] that in InAs excited by femtosecond pulses the photo-emf in the maximum reaches 1 V and the photocurrent surge resulting from the spatial separation of electrons and holes makes a considerable contribution to the generation of THz pulses.

46

The dependences of amplitudes of THz field generated from InAs and InSb surfaces on the quantum energy of the exciting femtosecond laser radiation were studied [85, 86]. It was found that the efficiency of THz generation nonmonotonically depends on the quantum energy of the exciting radiation. At first, it grows with increasing the photon energy and reaches the maximum in the vicinity of the threshold for photoelectron transfers to the lateral valleys. At higher photon energy the intervalley transfers result in a considerable reduction of generated THz field. In InAs the maximal efficiency of THz generation is reached at excitation by 800nm radiation of titanium-sapphire lasers. Under excitation by a fiber erbium lasers generating at 1560nm wavelength high efficiency of THz generation can be obtained in InSb.

Efficiency of THz generation in some semiconductors can be significantly increased by applying magnetic field in parallel to the irradiated surface [87-92]. The magnetic field leads to appearance of the photocurrent Hall component generating radiation in the direction perpendicular to the semiconductor surface. This radiation does not essentially undergo total internal reflection and hence it can efficiently escape from the semiconductor. Increase of THz generation efficiency approximately by one order of magnitude was observed in GaAs and InAs under exposure to a magnetic field.

In semiconductors excited by femtosecond laser radiation the non-linear polarization can be generated at the frequency of the laser pulse envelope. This effect, known as a non-linear optical rectification, can substantially contribute into generation of THz pulses [93-100] (Figure 2.3). In cubic crystals without the inversion center (including the semiconductors of group A_3B_5) both the second and the third order optical nonlinearities can contribute into the low-frequency non-linear polarization; in so doing the third order contribution is proportional to the strength of the surface electric field. The most important peculiarity of THz generation caused by the effect of optical rectification is its azimuthal anisotropy, i.e. dependence of efficiency of THz generation on orientation of the polarization vector of the exciting radiation relative to crystallographic axes of the semiconductor. The type of the azimuthal

47

anisotropy depends on the crystallographic orientation of the semiconductor surface plane; nonlinearities of the second and the third orders can result in different azimuthal dependences of the THz signal. It allows to separate the contributions of the volume and electric field induced mechanisms to the optical rectification effect and THz generation [99]. The experimental and theoretical investigations [99] of the azimuthal anisotropy of THz generation from different crystallographic planes in InAs show that the volume contribution is negligible while the mechanism of THz generation caused by the third order optical rectification effect prevails.
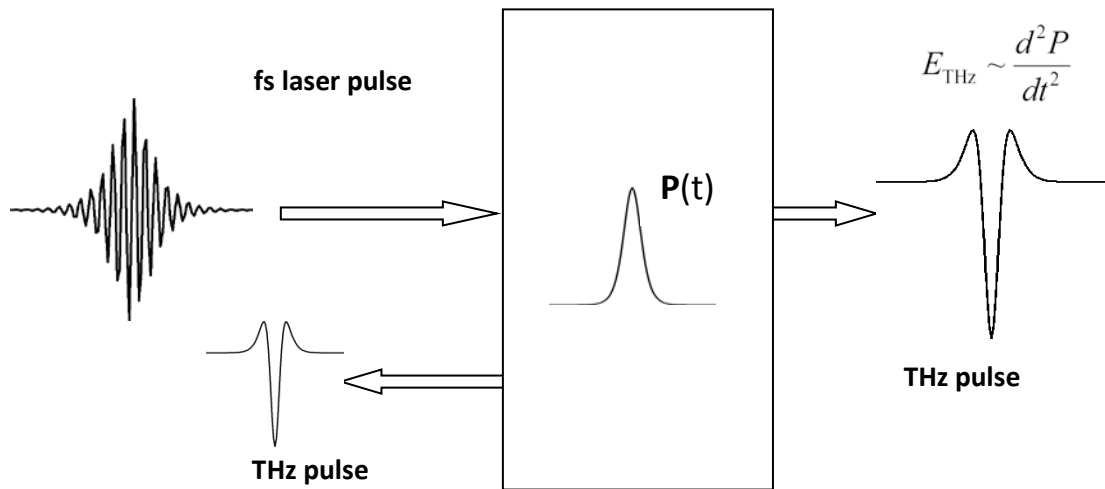

Fig. 2.3. THz pulse generation due to optical rectification effect.

At present the highest efficiency of THz generation is obtained at excitation of (111) surface of p-InAs by femtosecond laser radiation of a titanium-sapphire laser [98]. Usually it is assumed that the main contribution to generation of THz pulses in this semiconductor comes from the Dember effect [80-82]. However, experimentally observed azimuthal dependence of THz generation [98, 101] witnesses that in this semiconductor a considerable contribution to THz generation is made by the optical rectification effect. At

48

high excitation level when the Dember effect is saturated the contribution of the optical rectification effect to THz generation can become dominant.

The mechanism of THz generation in InAs stems from the third order non-linear optical rectification effect in the electric field induced by the spatial separation of photoexcited electrons and holes moving in the quasiballistic mode from the illuminated surface into the bulk of the semiconductor [102]. This mechanism allows to explain the main peculiarities of THz generation in this material, including azimuthal anisotropy as well as dependence of the THz field on the magnetic field and quantum energy of the exciting radiation.

Polarization induced by polar optical phonons generated at femtosecond laser excitation of some semiconductors can also be the source of THz radiation. This mechanism of THz emission is presumably realized at femtosecond excitation of Te surface [103]. In this semiconductor the coherent generation of optical phonons results from interaction of the Dember electric field caused by a spatial separation of photogenerated electrons and holes with the lattice polarization.

It should be noted that in the spectral range higher than the fundamental absorption edge of semiconductor the photoconductivity can be considered in terms of a non-linear third order optical rectification effect and so the difference between the mechanisms of THz generation caused by the third order optical rectification effect and photoconductivity is conditional enough. Azimuthal anisotropy of THz generation and presence of the *s*-polarized component in the THz field, the effects which usually serve as an evidence of contribution of the third order optical rectification effect to THz generation, can also be explained in terms of the anisotropic picosecond photoconductivity. The effect of THz field enhancement in the magnetic field [104] as well as its non-monotonic dependence on the quantum energy of the exciting radiation [85] witness in favor of the fact that the considerable contribution to THz generation from semiconductor surfaces is made by the real electrons and holes in the bands. The latter effect is related to intervalley scattering of photoexcited electrons.

It should be noted that studying THz emission by the semiconductors surface allows to investigate photoconductivity, ballistic transport, dynamics of electric fields screening by photocarriers on a subpicosecond time scale, and to get information about the band structure of semiconductors, carrier scattering mechanisms, etc.

2.2 Methods of THz radiation detection

There exist two fundamentally different methods of THz radiation detection – the coherent and non-coherent ones. The coherent method of detection implies obtaining temporal profile of the electric field of THz pulse while the basis of the non-coherent method is the measurement of the absolute value of this pulse energy. For non-coherent registration of THz radiation the IR radiation detectors are used such as bolometers cooled down to the temperature of liquid helium, pyroelectric detectors, Golay cells, etc. The principal advantage of this method is the possibility to register radiation within a wide frequency range – from far IR to visible spectrum. But, unfortunately, this detection technique is not free from shortcomings. One of them is the low signal/noise ratio constituting about 300:1 (50dB) [105]. On the contrary, when using the coherent detection method the signal/noise ratio can reach the values of about 10000:1 (100dB), though the spectral range of the detector sensitivity is limited only to the far IR [105].

The coherent methods of THz detection is based on the optical gating technique [66-67, 106]. The essence of this method is that the electric field of a THz pulse is measured at the instance of arrival of the sample optical femtosecond pulse at the detector. The temporal profile of the electric field of the THz pulse can be obtained by shifting the time of the sample pulse arrival at the THz detector. Thus, this method provides information on the amplitude and phase of the THz pulse. Moreover, the coherent detection method allows to suppress background noise and to considerably increase the signal/noise ratio

(up to 10^5). Unfortunately, this method has shortcomings as well, in particular the spectral range of sensitivity is limited from the side of higher frequencies and usually does not exceed 10THz.

In THz time-domain spectroscopy two detection techniques are generally used – free space electro-optic sampling and photoconductive antenna detection. The main idea of the electro-optic sampling lies in registration of the change of polarization ellipticity of the probe femtosecond beam going through an electro-optical crystal. The change of ellipticity stems here from the birefringence caused by the electric field of THz pulse. The typical scheme realizing the electro-optic sampling technique is shown in Figure 2.4. The probe pulse of laser radiation having passed the polarizer P and having been reflected from the beam splitter BS hits the ZnTe electro-optical crystal. The phase shift is usually registered with the use of the balanced detection method. For this purpose a quarter-wave plate changing the state of probe beam polarization to circular is installed after the electro-optic crystal. Then an analyzer (usually a Wollaston prism WP is used) splits the probe beam into two orthogonal components whose intensities are measured using two low-noise photodiodes PD1 and PD2. The difference in the photodiode currents is registered by a synchronous detector C. If the THz field is absent both the polarizations have the same intensity and the signal at the balance detector equals zero. In the presence of the THz field, the birefringence is induced in the electro optic crystal and the optical pulse becomes elliptically polarized. In this case photodiodes PD1 and PD2 measure the intensity difference between the two orthogonal components of the probe pulse, which is proportional to the applied THz field amplitude. The balance detection method allows to suppress laser noise and therefore the detecting capability of this method is mainly limited by the photodiode noise.

Zinc-blende semiconductors are usually used as electro optic crystals for electro-optic sampling since they possess strong electro-optic nonlinearity and weak absorption at the wavelength of probe radiation and in the THz range. The phase matching condition determines the frequency band in which the

51

electric field of THz pulses can be coherently registered. It means that those spectral components of the THz pulse will be detected for which the phase velocity is close to the group velocity of the sample pulse. The presence of phonon resonances in electro-optic crystals considerably limits the operating frequency range of detectors. In electro-optical THz detectors two crystals are most often used– ZnTe and GaP. The former crystal provides the phase matching condition for laser radiation at wavelength of 800nm while the latter – for ytterbium-based lasers generating near 1030 nm. The most optimum configuration is realized when (110) cut crystal is used, the THz electric field is directed along axis [001] and the probe pulse is polarized perpendicularly to this axis. It should also be noted that the [110] oriented plates of the electro-optic crystals can be comparatively easily produced because the (110) crystal plane is the cleavage plane of ZnTe and GaP.
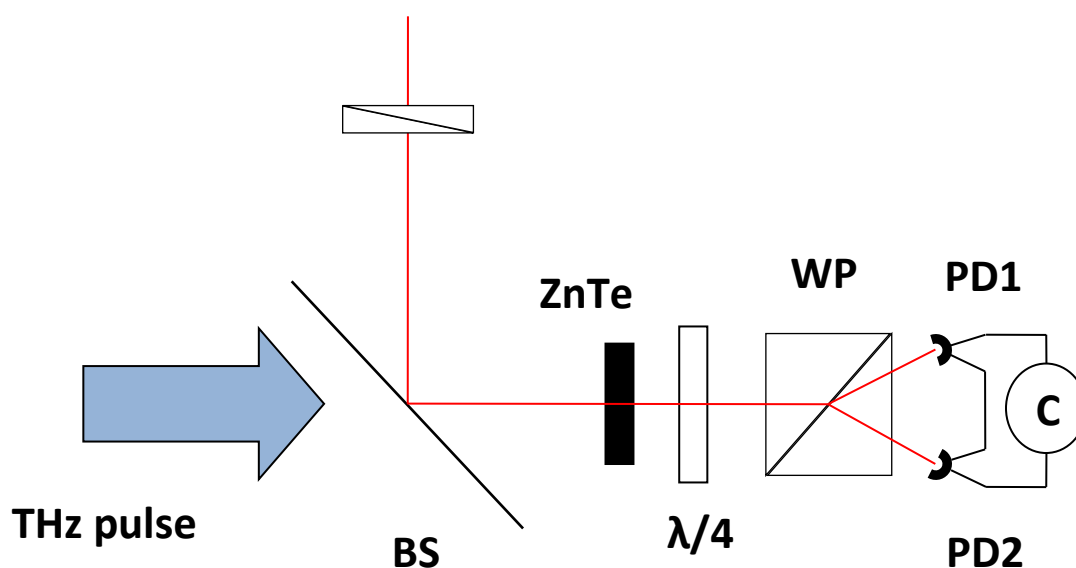

Fig. 2.4. Scheme of the electro-optic sampling technique.

The design of a dipole photoconductive antenna intended for coherent detection of THz radiation is shown in Fig. 2.5. In contrast to the generating antenna for which the bias is applied, in this case the detector electrodes are

connected to the lock-in amplifier which measures the current excited in antenna.
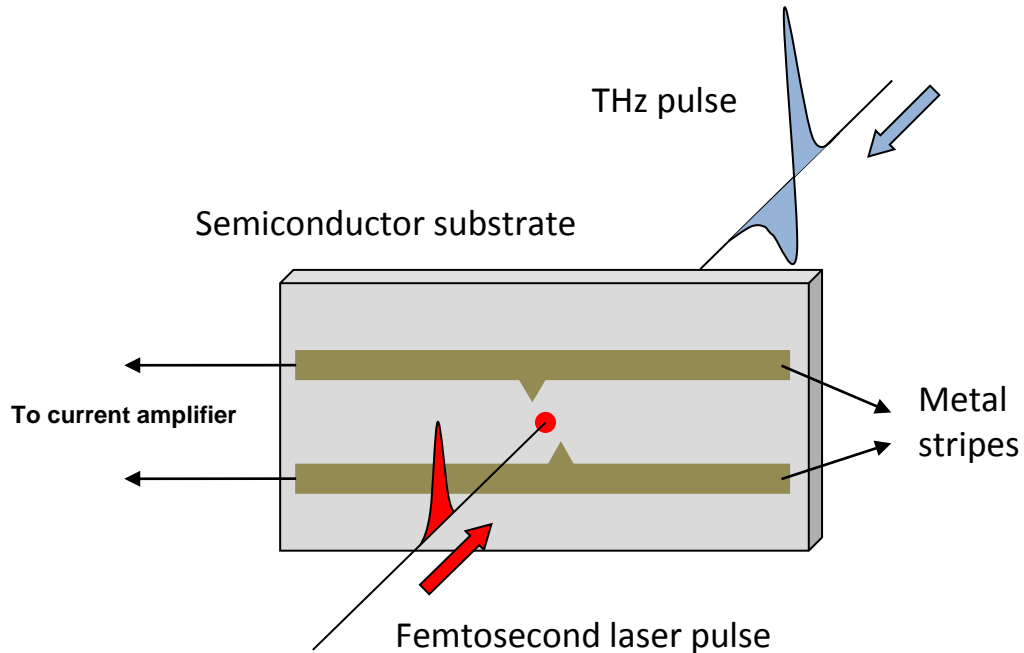

Fig. 2.5. THz pulse detection with a photoconductive antenna.

The principle of operation of the photoconductive antenna as THz detector is as follows. A femtosecond pulse with quantum energy exceeding the semiconductor band gap is focused into the gap between the stripline electrodes at the photoconductor surface. Under exposure to light nonequilibrium carriers are generated in the photoconductive layer which make contribution to the photocurrent proportional to the THz electric field at the instance of the excitation of photoconductive antenna by the sample femtosecond optical pulse. Successively varying the delay time of femtosecond pulse relative to the THz pulse by means of the optical delay line allows to measure the temporal dependence of the THz field with subpicosecond time resolution (see Figure 2.6). It is very substantial that this detection method is sensitive to the polarity of the THz electric field and, consequently, allows phase measurement. The spectrum of THz radiation is obtained as a result of

Fourier transformation of the registered temporal dependence of the photocurrent.

The highest possible frequency of the registered THz radiation is determined by the response time of the photoconductive antenna which is limited by the life time of photocarriers in the semiconductor. That is why for producing the photoconductive antennas capable of detecting THz radiation it is necessary to use specially grown semiconductor layers having subpicosecond life times of photocarriers.
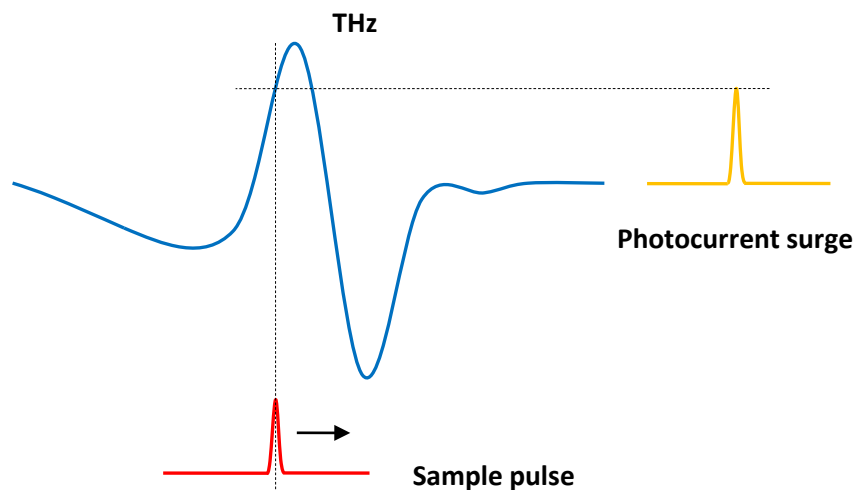

Fig. 2.6. Schematic representation of gaiting method during THz pulse detection using photoconductive antenna.

2.3 Principles of Terahertz Spectroscopy

The THz time-domain spectroscopy method is based on measuring the time dependence of the electric field of THz radiation $E(t)$ passing through the sample investigated [66, 106]. Fourier transform of the temporal shape allows to obtain the spectrum $E(\omega)$ of the THz electric field:

$$E(\omega) = A(\omega)e^{i\varphi(\omega)} = \int_{-\infty}^{\infty} E(t)e^{i\omega t}dt, \qquad (2.2)$$

where $A(\omega)$ and $\varphi(\omega)$ correspond to the amplitude and the phase spectra of the pulse.

THz pulse usually contains barely several field oscillations, and hence its spectral width is comparable to the center frequency of the pulse and usually lies within the range from 0.1THz to 10THz. By measuring the THz pulse shape with high time resolution and by calculating its spectrum it is possible to find spectral characteristics of the object within a wide frequencies range. Accuracy of the spectrum reconstruction, i.e. the spectral resolution of the spectrometer δv, is determined by the scanning interval T as $\delta v = T^{-1}$. Thus, to increase the spectral resolution it is necessary to use the delay lines with as large scanning length as possible.

For measuring the spectral characteristics of the investigated sample it is necessary to register the temporal shape of the pulse that have passed through the medium with known spectral characteristics and then to measure the shape of the pulse that have passed through the investigated object. The absorption coefficient α and the refraction index n of the sample are calculated as follows:

$$\alpha(\omega) = d^{-1}\ln\frac{A_0(\omega)}{A(\omega)}, \quad n(\omega) = 1 + \frac{c}{\omega d}\left[\varphi(\omega) - \varphi_0(\omega)\right], \qquad (2.3)$$

where d is the thickness of the sample, c is the speed of light in vacuum. The amplitude $A(\omega)$ and the phase $\varphi(\omega)$ correspond to the signal that has passed through the sample; these values for the reference signal are marked with the index 0. To avoid influence of the Fresnel reflection at the edges for obtaining

the reference signal, the same sample but having a different thickness is usually used.

Thus, in the THz time-domain spectroscopy the dependence of the electric field of the THz pulse on time is measured giving the information both on the amplitude and phase. Using these data the spectral dependences of the refractive index and absorption coefficient can be determined in a wide frequency range without using the Kramers-Kronig relations. It should be noted that the Fourier transform of the detector signal is the product of the Fourier transform of three functions: the shape of the sample pulse envelope, the instrument function of the detector determining its response to the δ-pulse, and the shape of the THz pulse $E(t)$. The form of the first two functions is insignificant as they are cancelled and will not be included into expressions (2.3) determining the spectral characteristics of the investigated specimen.

THz spectroscopy can be used for measuring kinetic and relaxation characteristics of different media and objects. For these purposes the so-called optical pump-THz probe method is widely used [66]. In this method the transmission (and/or reflection) of the probe THz pulse through the investigated object which has been preliminarily excited by an ultrashort optical pulse is measured. By varying the delay time between the optical and THz pulses, the dynamics of change in the properties of the photoexcited object can be measured with subpicosecond time resolution. The typical scheme of the experimental setup is shown in Figure 2.7. Femtosecond laser beam is divided into three, one of which being more powerful excites the sample while the remaining two are used for exciting the emitter of THz pulses and sampling the THz detector. In the setup two delay lines are used, one of which changes the delay time of the probe THz pulse relative to the pump optical pulse while the other one changes the arrival time of the optical pulse exciting the THz emitter. To provide a homogeneous optical excitation across the THz beam cross-section the diameter of the excited area at the sample shall be at least twice as large as the diameter of the probe THz beam. By using THz optical elements, the THz radiation can be focused into a spot with the

56

characteristic size of about several millimeters and, consequently, the optical excitation spot size of about 0.5–1cm is desirable. Therefore the setups for optical pump-THz probe spectroscopy usually use femtosecond laser systems with regenerative amplifier which provides sufficiently high energy density of radiation in order to observe the change in the sample properties within THz frequencies range.

In semiconductors the THz radiation efficiently interacts with the plasma of free charge carriers. That is why the optical pump-THz probe method is very efficient for studying a subpicosecond dynamics of photoexcited electrons and holes. The thickness of photoexcited electron-hole plasma layer is determined by the absorption length of the exciting optical radiation and usually is several orders of magnitude less than the wavelength of THz radiation. For interpretation of the experimental results of THz pulses interaction with photocarriers, the approximation of thin layer electrodynamics is usually used. In this approach the photoexcited electron-hole plasma is considered as a two-dimensional layer. The optical pump-THz probe method was used for measuring subpicosecond life times of nonequilibrium carriers in semiconductors. Using this method the dynamics of intervalley transfers and interband relaxation of photoexcited charge carriers in GaAs [8] and Ge [107] was studied.

Femtosecond laser radiation with the photon energy exceeding the semiconductor band gap excites a picosecond photocurrent pulse which can be a source of THz radiation. As is known, in the far field region the THz electric field is proportional to the derivative of the photocurrent over time, i.e. essentially is determined by acceleration of charge carriers. Thus, the dynamics of electrons and holes in semiconductors on a subpicosecond time scale can be investigated by analyzing the temporal shape of the generated THz pulse and its dependence on parameters of semiconductor and exciting radiation. This principle lies in the base of the method of the so-called terahertz emission spectroscopy.
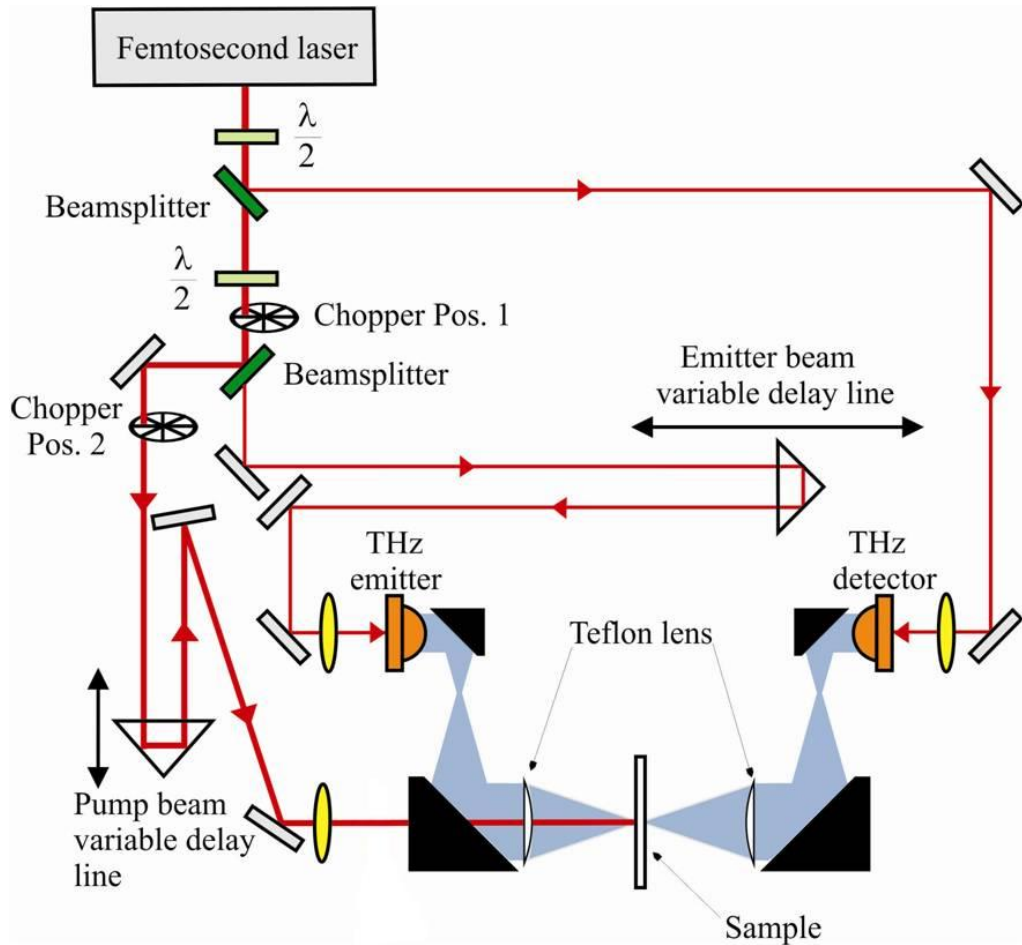
Fig. 2.7. Typical scheme of optical pump – THz probe experimental setup.

The dynamics of the photocurrent generating THz radiation in semiconductors under femtosecond laser excitation is determined by acceleration of the photoexcited carriers in the electric field and their scattering by phonons, impurities and due to the carrier-carrier interaction. Therefore the THz emission spectroscopy method turns to be useful for studying the carrier transport (including ballistic phenomena) with a subpicosecond time resolution, electronic band structure and carrier scattering mechanisms in semiconductors. It is significant that this method enables to study the dynamics of hot photocarriers with energy considerably exceeding the thermal one. In particular, by using THz emission spectroscopy method the dynamics of intervalley transfers of photoelectrons in GaAs and Ge was studied [8, 107]. The energy gaps between the lateral valleys and the central valley of the conduction band in InAs, InGaAs and InSb were estimated from the measured

dependencies of the efficiency of THz pulse emission on the photon energy of the femtosecond radiation [85, 108]. The screening of the electric field caused by a spatial separation of photoexcited electrons and holes substantially impacts on the photocurrent dynamics and hence the data obtained by THz emission spectroscopy method should be analyzed taking into account the dynamics of screening the electric field by photocarriers.

In some semiconductors considerable contribution to generation of THz pulses comes from polarization appearing as a result of non-linear optical rectification of femtosecond laser radiation. In this case the efficiency of THz generation considerably depends on the orientation of polarization of the exciting radiation relative to crystallographic axes of the non-linear crystal. By studying the polarization and orientation dependences of THz radiation one can establish the peculiarities of the optical rectification effect and separate its contribution to the THz emission from the contribution of the photocurrent surge.

Using THz emission spectroscopy the dependences of picosecond photoconductivity in GaAs [56, 16, 109, 110] on temperature, electric field, wavelength and power of femtosecond optical radiation were investigated; the influence of the magnetic field on this effect was also studied. By analyzing the temporal shape of THz pulses emitted from the narrow-band A_3B_5 semiconductors it was found that in these semiconductors the ballistic stage of the photocarrier transport is crucial in Dember effect at femtosecond laser excitation [84]. Investigation of the temperature dependence of the shape and polarity of THz pulses generated by the surface of InP allowed to separate the contributions to THz emission of the photocurrents caused by Dember effect and by built-in electric field of depletion surface layer [111, 112]. Using THz emission spectroscopy the coherent plasma oscillations in GaAs excited by femtosecond laser radiation were also investigated [78].

Recently THz pump-THz probe spectroscopy method has been offered. In contrast to the optical pump-THz probe spectroscopy in this case for excitation of the investigated sample a high-power THz pulses with the electric field

amplitude reaching up to 0.1–1 MV/cm is used. At such a high field the changes in the sample properties occur which can be registered by probing it with a weaker probe THz pulse. Using this method the dynamics of energy relaxation of electrons in GaAs [113], impact ionization in InSb [113] were studied. In contrast to the optical pump-THz probe spectroscopy in this method there is no interband generation of nonequilibrium carriers which can complicate interpretation of the experimental data on carrier transport.

CHAPTER 3

TERAHERTZ PULSES EMISSION FROM CUBIC SEMICONDUCTOR INDUCED BY A TRANSIENT ANISOTROPIC PHOTOCURRENT

Transient photoconductivity can contribute significantly to emission of THz radiation from semiconductor surfaces excited by femtosecond laser pulses. Since the amplitude of generated THz electric field depends on the photocurrent direction it would appear reasonable that the anisotropy of the photocurrent will impact on THz emission. By this means the transient anisotropic photoconductivity in semiconductors can be investigated on a subpicosecond time scale using THz emission spectroscopy method.

In this chapter we present a calculation of the anisotropic photoconductivity caused by optical alignment of photocarriers momenta in cubic semiconductor excited by an ultrashort laser pulse. We assume that the effect considered is caused by nonparabolicity and nonsphericity of electron and hole dispersion laws rather than by the energy dependence of carrier momentum relaxation time [30]. Specific numerical calculations will be performed for InAs – narrow gap semiconductor that is the most effective THz emitter at 800 nm laser excitation. The band structure and the anisotropic initial momentum distribution of photoexcited carriers calculated on the basis of *kp*-method were used. The contribution of the lateral photocurrent component to the THz pulse generation in this semiconductor is considered. Azimuthal anisotropy of THz signals generated from InAs and InSb surfaces excited by femtosecond laser radiation of three different wavelengths is studied experimentally. Finally, we compare the obtained experimental data with the results of calculation. Our results demonstrate that the anisotropic photoconductivity effect should be taken into account when considering the THz emission from semiconductor surfaces and that experimentally observed

azimuthal anisotropy of this emission [80, 98-100, 114] might, at least in part, be ascribed to this effect.

3.1 Mechanisms of transient anisotropic photoconductivity

Excitation of semiconductors by light with the photon energy exceeding forbidden band gap leads to the appearance of nonequilibrium electrons and holes, which can create a dc current. This phenomenon known as photoconductivity has been studied for a long time and finds applications in a variety of areas [24]. Commonly at not too high excitation levels the photocurrent is linear in dc bias electric field and quadratic with respect to the electric field of the light wave, thus basically the photoconductivity can be conceived as a nonlinear effect of the third order [59]. Consequently, the photocurrent density **j** in a homogeneous semiconductor can be represented as $j_i = \sigma_{ijkl} F_j E_k E_l$, where E_i and F_i are the components of the electric field of the light with the frequency Ω and the dc electric field, respectively. Symmetrical over two last indexes tensor σ_{ijkl} can be, in general, associated with the third order optical nonlinear susceptibility $\chi_{ijkl}(0;0,\Omega,-\Omega)$, which determines the so-called electric field induced optical rectification effect (EFIOR) implying that electromagnetic field generates in the semiconductor a low-frequency nonlinear polarization proportional to the applied dc electric field [115]. If semiconductor is optically excited below the fundamental absorption edge, no real photocarriers appear, and in this case EFIOR effect can be considered in terms of "virtual photoconductivity" implying that the virtual electron-hole pairs are polarized under dc electric field and, as a result, displacement photocurrent arises [60-62, 64]. Here it is important to note that in zinc-blend semiconductors excited above the band gap the quadratic in light field photocurrent can arise even without dc electric field. This effect results in the second order optical rectification effect that, in the case when femtosecond optical pulses are used for the excitation, gives rise to THz emission from semiconductor surface. The second order nonlinear susceptibility determining

this effect was calculated [116-118] and it was shown that it was resonantly enhanced over two orders of magnitude when the semiconductor was excited above the band gap.

From the symmetry reasons the photocurrent in cubic semiconductors like A^3B^5 can be represented in the coordinate system of the crystal as follows

$$\mathbf{j} = \alpha \mathbf{F} E^2 + \beta \mathbf{E}(\mathbf{FE}) + \gamma\left(F_x E_x^2 \hat{\mathbf{x}} + F_y E_y^2 \hat{\mathbf{y}} + F_z E_z^2 \hat{\mathbf{z}}\right), \qquad (3.1)$$

where $\hat{\mathbf{x}}$, $\hat{\mathbf{y}}$ and $\hat{\mathbf{z}}$ are the basic vectors directed along the principal crystallographic axes and the coefficients α, β, and γ are expressed in terms of three nonvanishing tensor components σ_{zzzz}, σ_{zzxx}, σ_{zxxz} as $\alpha = \sigma_{zzxx}$, $\beta = 2\sigma_{zxxz}$, $\gamma = \sigma_{zzzz} - \sigma_{zzxx} - 2\sigma_{zxxz}$. In the case of isotropic symmetry the condition $\gamma = 0$ is fulfilled and the photocurrent depends on the angle between dc and light wave electric fields while not depending on the orientation of these fields with respect to the crystallographic axes. As it follows from Eq. (3.1), even in the isotropic case the photocurrent and dc electric field do not necessarily coincide in directions and hence the photocurrent component perpendicular to the dc electric field can appear. It means that, in general, the photoconductivity by being inherently nonlinear effect is anisotropic and is characterized by the same dependence on the electric field orientation as the EFIOR effect.

Several microscopic mechanisms responsible for anisotropy of photoconductivity were suggested. It has been known that anisotropic photoconductivity can be caused by the hot carrier effect. In many-valley semiconductors this could happen due to the effective mass anisotropy and different populations of separate conduction band valleys oriented at different angles with respect to the bias electric field [28].

Peculiar mechanism of anisotropic photoconductivity can originate from the optical alignment of photoexcited electron momenta [119, 120]. The optical momentum alignment effect in semiconductors results from the selection rules

for interband electron transitions and manifests itself in the anisotropic momentum distribution of photocarriers excited by linearly polarized light. For example, in cubic semiconductors an absorption of linearly polarized radiation with the photon energy near the band gap results in the momenta of electrons excited from the heavy hole valence subband lie mainly in the plane perpendicular to the electric field of light wave, while the momenta of electrons excited from the light hole subband are predominantly aligned along the vector of polarization. The effect of optical alignment of electron momenta can cause such effects as polarized hot-electron photoluminescence [119] and surface ballistic photogalvanic effect [33]. It was also shown that, if the momentum relaxation time of carriers depends on their energy, optical alignment of photocarriers over momenta can result in the anisotropic photoconductivity [30]. For a stationary excitation this effect is small because the anisotropic part of the photocarrier distribution function over momenta is damped on a short time scale (at about 10^{-12} - 10^{-13} s) determined by the carrier momentum relaxation rate. Because of this, in order to suppress the carrier momenta disorientation polarized hot-electron photoluminescence and surface ballistic photogalvanic effect have been usually observed at cryogenic temperatures. However in semiconductors excited by femtosecond laser pulses photocurrent achieves peak value on a time scale smaller or comparable to the carrier momentum relaxation time, and hence the optical momentum alignment effect will be more noticeable and will result in anisotropy of the transient photoconductivity even at the room temperature.

As it is well-known, the transient photocurrent arising near semiconductor surface illuminated with femtosecond laser pulses can generate terahertz radiation [14]. When analysing this effect it is generally assumed that the transient photocurrent is directed perpendicular to the illuminated semiconductor surface, along the direction of surface electric field that is built in [15] or can be induced by a spatial separation of photoexcited electrons and holes [17, 82]. However, from what was said above it follows that the optical alignment of electron momenta can result also in the appearance of a lateral

(parallel to the illuminated semiconductor surface) component of the transient photocurrent. THz radiation induced by this photocurrent component is predominantly directed perpendicular to the illuminated surface and hence it will be more efficiently out-coupled from the semiconductor.

The main part of the THz pulse is generated during the first 100 – 200 fs after the photoexcitation, that is at the ballistic stage of photocarriers movement. At this stage the dependence of the carrier relaxation time on energy will most probably be of minor importance for the magnitude of the anisotropic photocurrent. Thus, it may be assumed that the energy dependence of carrier effective masses caused by the nonparabolicity and nonsphericity of conduction and valence bands will be of a considerable importance to the anisotropy of the transient photocurrent. The mechanism of the transverse photocurrent component can be explained in the following manner. Photoexcited electrons having momenta **p** aligned mainly along the dc electric field (right petal) will slow down and lose their energy, whereas the energy of photoelectrons with the opposite momenta (left petal) will grow (Fig. 3.1). Due to the nonparabolicity of electron dispersion law the effective masses of these two groups of photoelectrons will become different. As a result, the flows of photoelectrons aligned along *x*-axis and opposite to it are no longer compensating each other resulting in the appearance of the net photocurrent component in the direction perpendicular to the dc electric field.

3.2 Model and calculation

We consider a direct band gap cubic semiconductor excited by ultrashort laser pulses with quantum energies exceeding the forbidden gap. Interband optical transitions will give rise to nonequilibrium carriers that are accelerated by a homogeneous dc electric field. The coefficients α, β, γ in Eq. (3.1) determining the photocurrent value are calculated by using the Boltzmann transport equations for distribution functions of optically generated electrons

$f_c(\mathbf{p},t)$ and holes $f_v^i(\mathbf{p},t)$ in three valence subbands ($i=1,2,3$ correspond to the heavy (1), light (2), and spin-orbit split-off holes (3)):

$$\frac{\partial f_c(\mathbf{p},t)}{\partial t} - e\mathbf{F}\frac{\partial f_c(\mathbf{p},t)}{\partial \mathbf{p}} = \sum_{i=1}^{3} G_{i,\mathbf{p}}\delta(t), \qquad (3.2)$$

$$\frac{\partial f_v^i(\mathbf{p},t)}{\partial t} + e\mathbf{F}\frac{\partial f_v^i(\mathbf{p},t)}{\partial \mathbf{p}} = G_{i,\mathbf{p}}\delta(t), \quad i=1,2,3, \qquad (3.3)$$

where $-e$ is the electron charge, $\mathbf{p}$ is the carrier momentum, the terms in the right side of Eqs. (3.2) and (3.3) determine the rate of photocarrier generation by laser pulse the temporal shape of which is approximated by a delta-function.
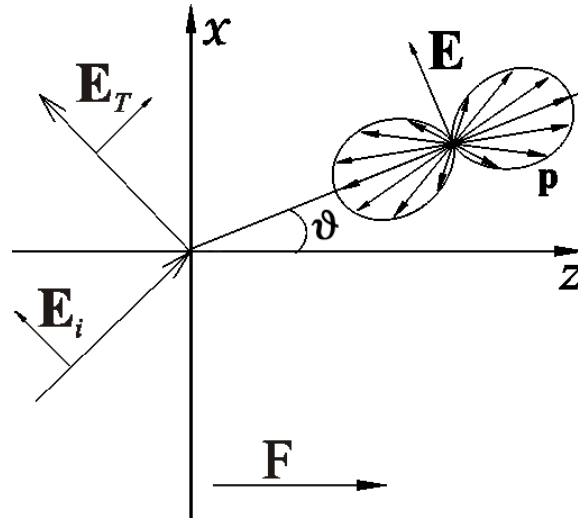

Fig. 3.1. The optical momentum alignment of electrons excited from the heavy hole subband by linearly polarized light with electric field $\mathbf{E}_i$ impinging on semiconductor ($z>0$); ϑ is the refraction angle, $\mathbf{E}$ is the light electrical field in the semiconductor, $\mathbf{E}_T$ is THz electric field radiated in the quasi-reflection direction.

Since the generation of THz pulses is mainly determined by the movement of photocarriers on an early ballistic stage, we shall restrict ourselves to the simplest approximation and neglect the relaxation terms in Eqs. (3.2) and (3.3).

The terms $G_{i,\mathbf{p}}$ determining the rate of photocarrier generation are defined by the matrix elements for direct optical transitions of electrons from the valence subbands to the conduction band.

By solving Eqs. (3.2) and (3.3), one can obtain the electron and hole distribution functions at $t > 0$:

$$f_c(\mathbf{p},t) = \sum_{i=1}^{3} G_{i,\mathbf{p}+e\mathbf{F}t} \, , \quad f_v^i(\mathbf{p},t) = G_{i,\mathbf{p}-e\mathbf{F}t} \, . \tag{3.4}$$

The density of photocurrent can be written as

$$\mathbf{j}(t) = \frac{-e}{4\pi^3 \hbar^3} \int d^3\mathbf{p} \left[\frac{\partial \varepsilon_{c,\mathbf{p}}}{\partial \mathbf{p}} f_c(\mathbf{p},t) - \sum_{i=1}^{3} \frac{\partial \varepsilon_{v,\mathbf{p}}^i}{\partial \mathbf{p}} f_v^i(\mathbf{p},t) \right], \tag{3.5}$$

where $\varepsilon_{c,\mathbf{p}}$ and $\varepsilon_{v,\mathbf{p}}^i$ are the electron and hole dispersion laws.

After substituting the distribution functions given by expressions (3.4) into Eq. (3.5), the photocurrent density can be represented as

$$\mathbf{j}(t) = \frac{-e}{4\pi^3 \hbar^3} \sum_{i=1}^{3} \int d^3\mathbf{p} \, G_{i,\mathbf{p}} \frac{\partial \left(\varepsilon_{c,\mathbf{p}-e\mathbf{F}t} - \varepsilon_{v,\mathbf{p}+e\mathbf{F}t}^i \right)}{\partial \mathbf{p}} \, . \tag{3.6}$$

The rates of photocarrier generation are obtained in the dipole approximation by using Fermi's golden rule as

$$G_{i,\mathbf{p}} = \frac{16\pi^2 e^2 W}{c\bar{n} \hbar m_0^2 \Omega^2} \left| M_{c,v}^i(\mathbf{p}) \right|^2 \delta(\varepsilon_{c,\mathbf{p}} + \varepsilon_{v,\mathbf{p}}^i - \hbar\Omega), \tag{3.7}$$

where W is the laser pulse fluence, c is the light velocity, $\bar{n}$ is the refractive index, $M_{c,v}^i(\mathbf{p})$ are the momentum matrix elements for interband transitions of

electrons, m_0 is the free electron mass, and Ω is the center frequency of the laser pulse.

By substituting (3.7) in (3.6) one obtains

$$
\mathbf{j}(t) = \frac{-4e^3 W}{\pi \hbar^4 c \bar{n} m_0^2 \Omega^2} \sum_{i=1}^{3} \int d^3 \mathbf{p} \left| M_{c,v}^{i}(\mathbf{p}) \right|^2 \times
$$
$$
\times \frac{\partial \left(\varepsilon_{c,\mathbf{p}-e\mathbf{F}t} - \varepsilon_{v,\mathbf{p}+e\mathbf{F}t}^{i} \right)}{\partial \mathbf{p}} \delta(\varepsilon_{c,\mathbf{p}} + \varepsilon_{v,\mathbf{p}}^{i} - \hbar\Omega) \qquad (3.8)
$$

After integration in spherical coordinate system over p in expression (3.8) we get

$$
\mathbf{j}(t) = \frac{-4e^3 W}{\pi \hbar^4 c \bar{n} m_0^2 \Omega^2} \times
$$
$$
\times \sum_{i=1}^{3} \int_{-1}^{1} d\theta \, \sin\theta \int_{0}^{2\pi} d\varphi \frac{\left| M_{c,v}^{i}(\mathbf{p}_*) \right|^2 p_*^2}{\left| \mathbf{v}_{i,\mathbf{p}_*} \right|} \left. \frac{\partial \left(\varepsilon_{c,\mathbf{p}-e\mathbf{F}t} - \varepsilon_{v,\mathbf{p}+e\mathbf{F}t}^{i} \right)}{\partial \mathbf{p}} \right|_{\mathbf{p}=\mathbf{p}_*} , \quad (3.9)
$$

where the direction of the vector $\mathbf{p}_*$ in a spherical coordinate system is determined by the angles θ and φ. For orientation specified by the angles θ and φ the length of vector $\mathbf{p}_*$ depends on the valence subband number and is determined as the root of the equation $\varepsilon_{c,\mathbf{p}} + \varepsilon_{v,\mathbf{p}}^{i} - \hbar\Omega = 0$. The velocity $\mathbf{v}_{i,\mathbf{p}_*}$ appearing in Eq. (3.9) is given by

$$
\mathbf{v}_{i,\mathbf{p}_*} = \left. \frac{\partial(\varepsilon_{c,\mathbf{p}} + \varepsilon_{v,\mathbf{p}}^{i})}{\partial \mathbf{p}} \right|_{\mathbf{p}=\mathbf{p}_*} . \qquad (3.10)
$$

In a linear approach with respect to $\mathbf{F}$ from Eq. (3.9) one can obtain

$$\mathbf{j}(t) = \frac{4e^4 Wt}{\pi\hbar^4 c\bar{n}m_0^2\Omega^2} \sum_{i=1}^{3} \int_{-1}^{1} d\theta \; \sin\theta \int_{0}^{2\pi} d\varphi \left[\frac{\left| M_{c,v}^{i}(\mathbf{p}) \right|^2 p^2}{\left| \mathbf{v}_{i,\mathbf{p}} \right|} \times \right.$$

$$\left. \times \left(\mathbf{F}\frac{\partial}{\partial\mathbf{p}} \right) \frac{\partial\left(\varepsilon_{c,\mathbf{p}} + \varepsilon_{v,\mathbf{p}}^{i} \right)}{\partial\mathbf{p}} \right]_{\mathbf{p}=\mathbf{p}_*} \qquad . \quad (3.11)$$

The optical transition matrix elements, electron and hole velocities entering in (3.11) are calculated by the eight-band *kp* method [122]. In this approximation four double degenerate bands including conduction band and three valence subbands are taken into account. The Hamiltonian-matrix in Luttinger representation was diagonalized by Jacobi method. Previously the Hermitian matrix is represented as a real matrix with format 16x16. The eigenvalues resulting from diagonalization of this matrix are fourfold degenerate due to spin degeneracy and time-reversal symmetry.

The coefficients α, β, and γ are found by numerical integration in (3.11) for two orientations of the electric field of laser radiation $\mathbf{E}$ with respect to the semiconductor crystallographic axes. At first, z-component of the photocurrent is calculated in the case when the vectors $\mathbf{F}$ and $\mathbf{E}$ are aligned parallel to oz-axis directed along crystallographic axis [001]. As it follows from Eq. (3.1), in this case $j_z = (\alpha + \beta + \gamma)FE^2$. Then x-and z-components of the photocurrent are calculated for the fields oriented as $\mathbf{F} \parallel oz \parallel [001]$, $\mathbf{E} \parallel [101]$. From Eq. (3.1) it follows that in this case $j_z = [\alpha + (\beta + \gamma)/2]FE^2$, $j_x = \beta FE^2/2$. A comparison of the obtained relations with the corresponding photocurrent components resulting by numerical integration in Eq. (3.11) gives the values of the coefficients α, β, and γ As it follows from (3.11) in the framework of the used collisionless approximation the photocurrent grows linearly with time. It is clear that the inclusion of photocarrier relaxation will result in the exponential decay of the photocurrent after reaching its peak value at times defined by the momentum relaxation time.

Numerical calculations were performed for InAs excited by laser pulses with four different photon energies: 1.55, 1.2, 0.8 and 0.4 eV. Parameters of InAs given in Ref. 121 were used.

3.3 THz emission: experiment

Terahertz pulse emission was investigated experimentally by photoexciting (111) crystallographic planes of p-type InAs ($p=2 \cdot 10^{16}$ cm^{-3}) and InSb (intrinsic conductivity at the room temperature) single crystals. The first and second harmonics pulses of femtosecond Er-doped fiber laser (Toptica) with the wave-lengths of 1560 nm and 780 nm and the pulse durations of 80 fs and 88 fs, respectively, were used for the sample excitation. *P*-polarized optical beams were impinging on the crystal surfaces at the angle of 45° (see Fig. 3.1); the radiated in the quasi-reflection direction *p*-polarized THz signal was separated by a polyethylene polarizer and its power was measured by a Golay cell (Tydex) (Fig. 3.2).

Fig. 3.3 shows the radiated THz power dependences on the azimuthal angle ϕ for both crystals excited by femtosecond pulses at 1560-nm wavelength demon- strating clear cos(3ϕ) type periodicity. Fig. 3.4 (a) presents the dependences of average radiated THz power on the average optical power at this wavelength. Over the most of the investigated optical power range these dependences are quadratic, which allowed us to compare the efficiencies of the optical-to-THz power conversion in both crystals at different laser wavelengths (Fig. 3.4 (b)). Although at 1560 nm wavelength the average THz power radiated at p-InAs and InSb surfaces is of a similar order of magnitude, at shorter laser wavelengths the emission from InSb becomes much weaker than that from p-type InAs. Hereafter we will present only the results of the experimental investigation of the later semiconductor.
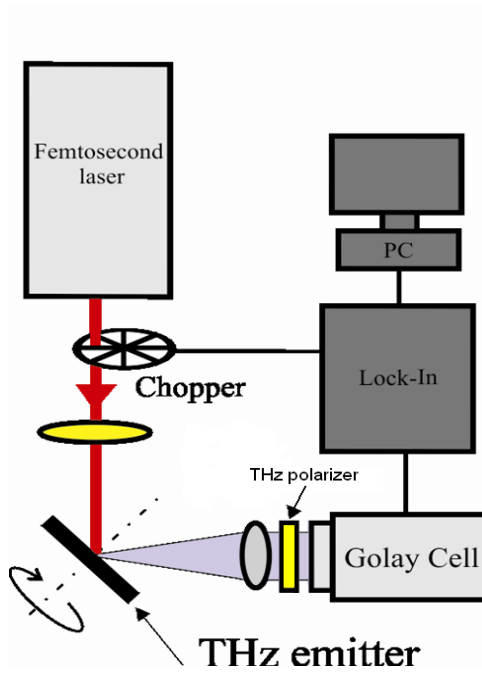
Fig. 3.2. Experimental setup for investigation of azimuthal dependencies of THz pulses generation from semiconductor surfaces.
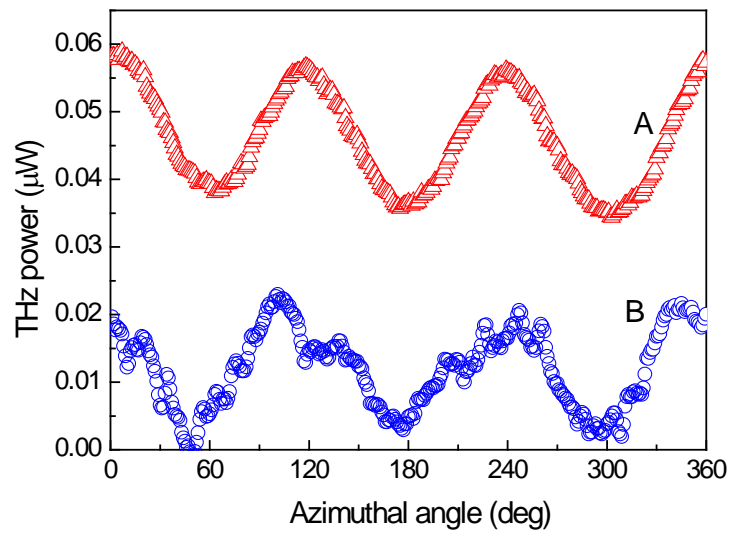

Fig. 3.3. Dependences of average p-polarized THz power on the azimuthal angle for p-InAs (A) and InSb (B) crystals excited by femtosecond pulses with 1560 nm central wavelength.
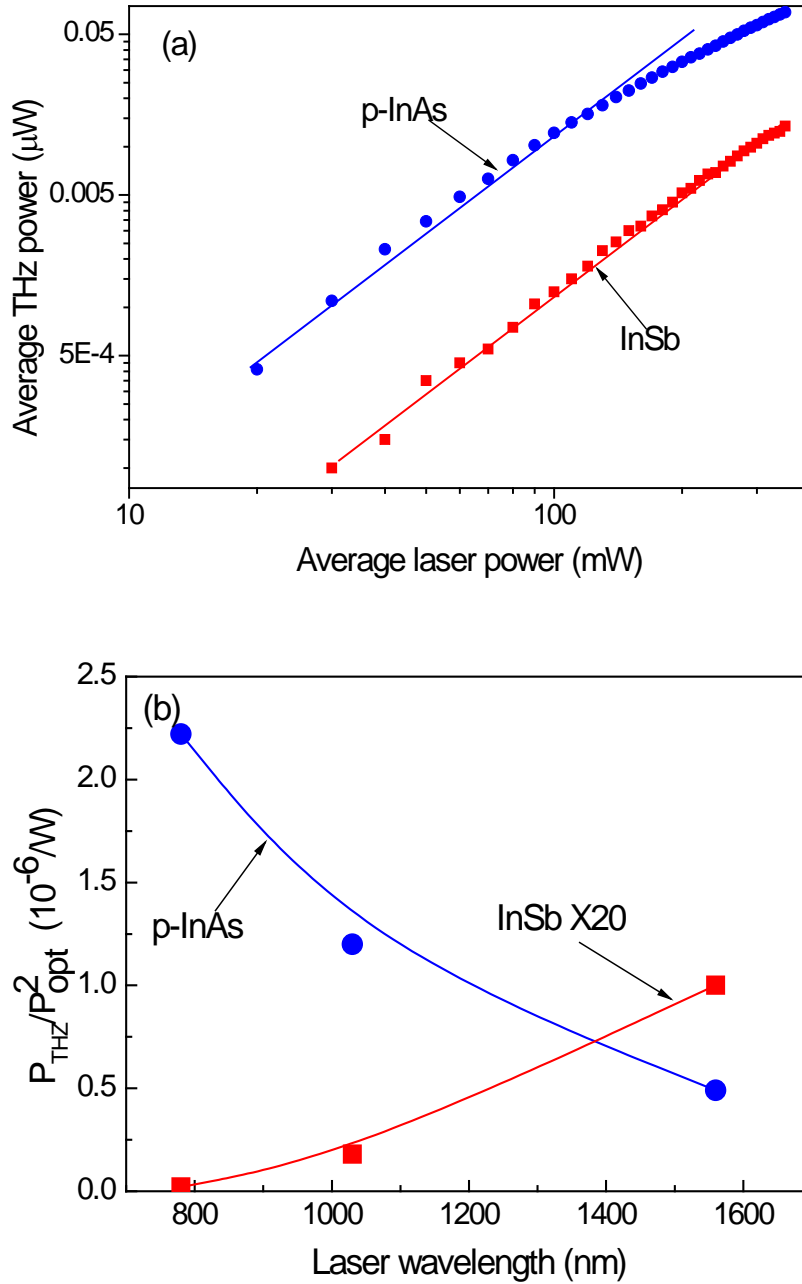
Fig. 3.4. (a) Dependences of radiated average THz power (P_{THz}) on the average optical power (P_{opt}) at 1560nm wavelength; the straight lines correspond to quadratic slope. (b) Efficiencies of the optical-to-THz power conversion in both crystals at different laser wavelengths.

Azimuthal angle dependences of *p*-polarized THz power emitted from p-type InAs surface illuminated by femtosecond laser pulses having two different central wavelengths are presented on Fig. 3.5. THz power values in this graph are normalized to the number of light quanta absorbed in the semiconductor. It

is seen from Fig. 3.5 that the increase of wavelength in the exciting laser pulses leads to a significant reduction of the angle dependent component in the radiated THz pulse power. In the following, this effect will serve as the main proof of the physical model proposed in this work.
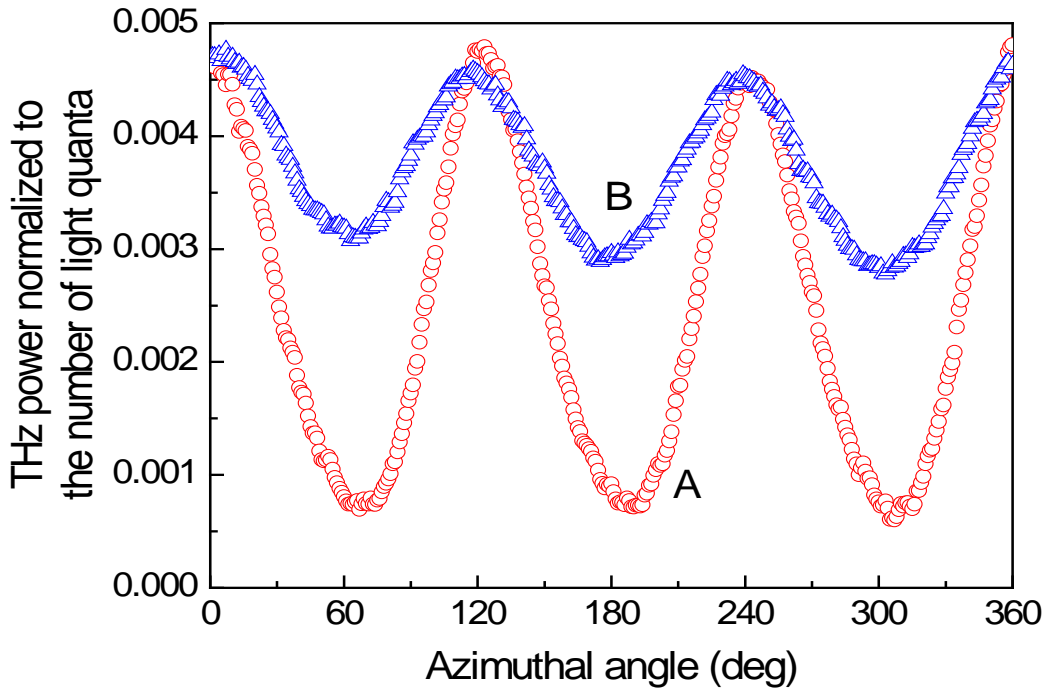

Fig. 3.5. Azimuthal angle dependences of *p*-polarized THz power emitted from p-type InAs surface illuminated by femtosecond laser pulses with 780nm (A) and 1560nm (B) central wavelengths. THz power values are normalized to the number of light quanta absorbed in the semiconductor.

3.4 Results and discussion

The calculated dependences of the probabilities for optical transitions of electrons from the heavy and light hole subbands to the conduction band on the direction of electron momentum are shown in Figs. 3.6 and 3.7 for two photon energies. The polar and azimuthal angles θ and ϕ specify the directions of the electron momentum in a spherical coordinate system with polar axis directed

73

along the electric field of radiation. It can be seen from Fig. 3.6 that at the excitation near the semiconductor band gap ($\hbar\Omega = 0.4$ eV) the momenta of
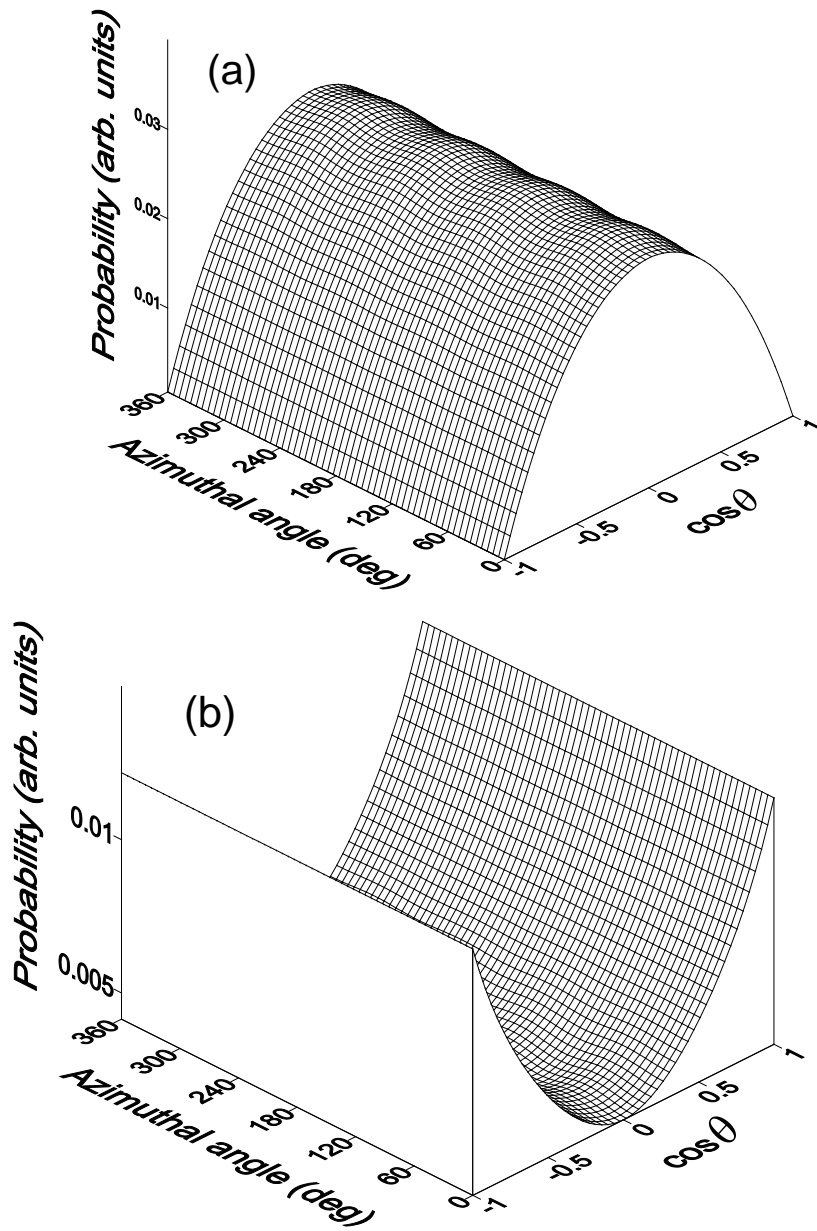

Fig. 3.6. Calculated distributions over momenta directions of photoelectrons excited by linearly polarized light with the photon energy 0.4 eV from the heavy (a) and light (b) hole valence subbands in InAs. The angles θ and φ determine the direction of electron momentum in spherical coordinate system with polar axis along (001) crystallographic direction, azimuthal angle φ are measured from axis (100). The light wave electric field is directed along (001) axis ($\theta = 0$).

electrons generated from the heavy and light hole subbands are oriented differently - mainly normally, for the heavy-hole band excitation, and in parallel to the radiation electric field, for the light-hole band excitation.
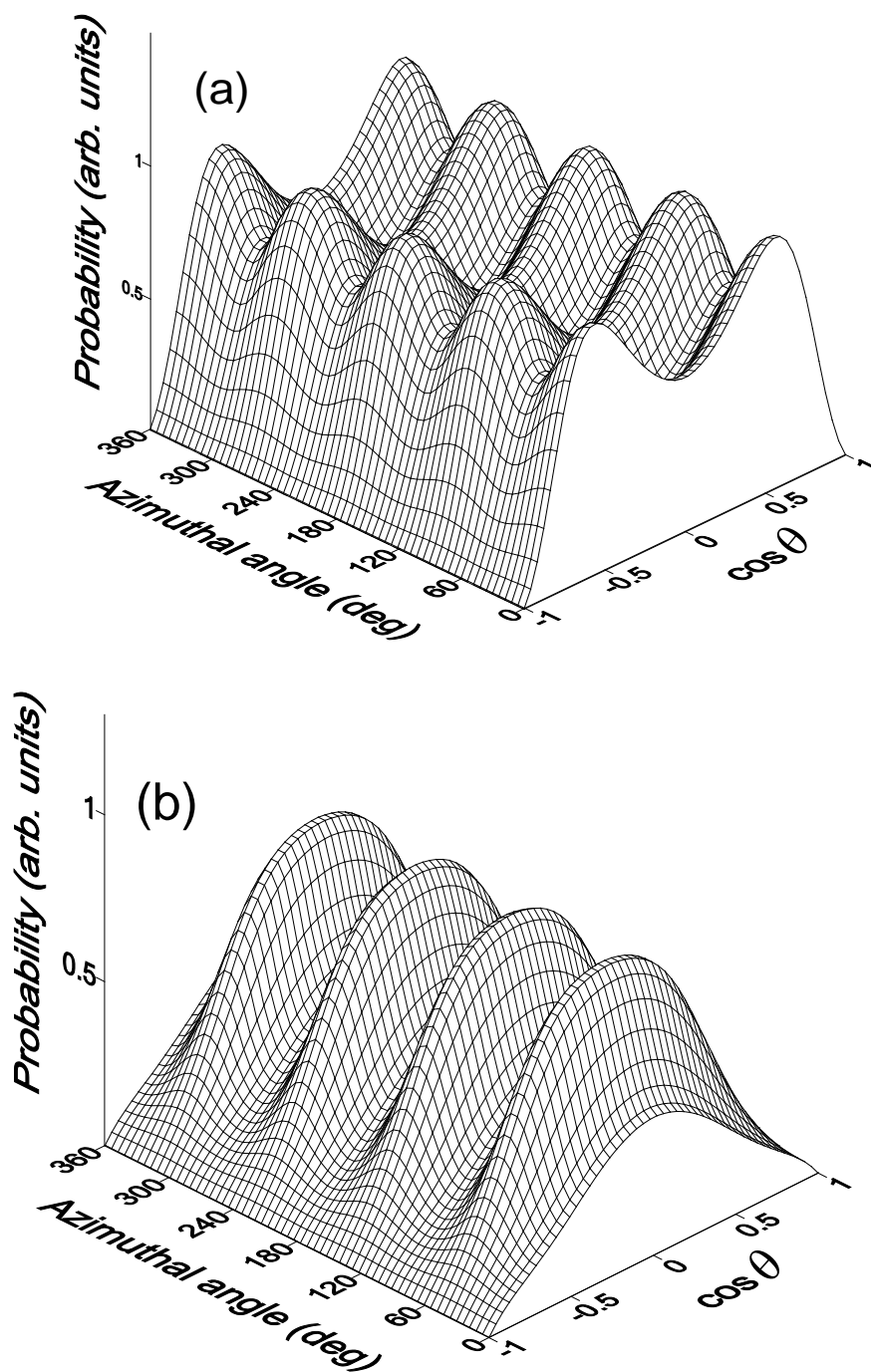

Fig. 3.7. Calculated distributions of photoelectrons over momenta directions as described in Fig. 3.6, for excitation with the photon energy 1.55 eV.

The different orientation of photocarriers excited from two valence subbands results in opposite signs of their contributions to the transverse photocurrent. On the other hand, when the photon energy $(\hbar\Omega = 1.55\text{ eV})$ significantly exceeds the energy gap of InAs the interband kp-interaction becomes essential. As a result, the wave functions of photoelectrons are modified in such a way that the momenta of those carriers excited from the both valence subbands are aligned much the same – in the plane that is perpendicular to the light polarization vector (Fig. 3.7). Also, it is following from these calculations that the anisotropy of the optical transition probabilities becomes larger with increasing photon energy.

The calculated contributions of electrons and holes excited from three valence subbands to coefficients α, β and γ are listed separately in Table I; in the lowest row of this table the total values of these coefficients obtained by summing up the partial contributions are presented. As it follows from calculations (see Table I) at the photon energy slightly exceeding the energy gap of semiconductor dimensional-less parameters β/α and γ/α determining the extent of the anisotropic photoconductivity is small. However with the increase of the light frequency these parameters grow substantially becoming at the photon energy of 1.55 eV more than one order larger than in the case of the excitation near the fundamental absorption edge of semiconductor ($\hbar\Omega = 0.4\text{ eV}$).

The calculated photocurrent components were used for estimation of the azimuthal dependences of THz electric field emitted from (111) and (110) InAs surfaces, which is excited by femtosecond laser pulse polarized in the incident plane and impinging at the angle of 45°. The photocurrent components are initially calculated in the crystallographic coordinate system and then are transformed in the laboratory system with z- and x-axis which for (111) surface are oriented along [111] and [11$\overline{2}$] directions, respectively. THz electric field components E_T^p and E_T^s of p and s polarization are given by projections of the

TABLE I. The partial and total coefficients α, β and γ calculated for three values of the photon energy. The contributions of three types of holes and electrons excited from heavy-hole (hh), light-hole (lh) and spin-orbital split-off (sh) valence subbands are represented separately for electrons and holes. The empty cells denote that the calculated value of the corresponding coefficient is negligible (<0.01). In the bottom line the total values of the coefficients derived as a sum of the partial contributions are presented.

The type of transitions	$\hbar\Omega$=1.55 eV			$\hbar\Omega$=1.2 eV			$\hbar\Omega$=0.8 eV			$\hbar\Omega$=0.4 eV		
	α	β	γ	α	β	γ	α	β	γ	α	β	γ
Electrons (hh)	2.2	1.31	-1.05	1.05	0.52	-0.36	1.14	0.42	-0.21	0.22	0.02	-0.01
Heavy holes	1.13	0.7	-0.87	0.42	0.19	-0.27	0.3	0.09	-0.17	0.02		-0.01
Electrons (lh)	1.11	0.4	-0.16	0.43	0.15	-0.05	0.25	0.05	-0.01	0.04		
Light holes	0.61	0.2	-0.35	0.13	0.01	-0.01	0.05	0.06	-0.01	0.03		
Electrons (sh)	0.05	-0.02	0.01	0.04			0.03					
Spin-orbit split off holes	0.06		-0.01	0.04			0.01					
Total	5.16	2.53	-2.43	2.11	0.87	-0.69	1.78	0.62	-0.4	0.31	0.02	-0.02

photocurrent on the corresponding field direction and after some little manipulations one can obtain for (111) surface

$$
\begin{aligned}
E_T^p \propto \left(\alpha + \frac{\gamma}{3} + \beta \, \sin^2 \vartheta \right) \, \sin \vartheta - \cos^2 \vartheta \times \\
\times \left[\left(\beta + \frac{2}{3}\gamma \right) \, \sin \vartheta + \frac{\gamma}{3\sqrt{2}} \, \cos \vartheta \, \cos 3\phi \right]
\end{aligned}
\tag{3.12}
$$

$$
E_T^s \propto \frac{\gamma}{3\sqrt{2}} \, \cos^2 \vartheta \, \sin 3\phi ,
\tag{3.13}
$$

where ϑ is the angle of refraction for optical radiation, which is determined by the relation $\sin 45° = \bar{n} \sin \vartheta$, ϕ is the azimuthal angle between incidence plane of radiation and $[11\bar{2}]$ axis.

For (110) semiconductor surface THz electric field components are deduced analogously and given by

$$E_T^p \propto \left[\alpha - \beta \, \cos 2\vartheta + \frac{\gamma}{4}\left(2 - 3 \, \cos^2 \vartheta\right) \right] \sin \vartheta -$$
$$-\frac{\gamma}{4} \, \sin \vartheta \, \cos^2 \vartheta \, \cos 2\phi \qquad , \quad (3.14)$$

$$E_T^s \propto -\frac{\gamma}{4} \, \sin 2\vartheta \, \sin 2\phi , \qquad\qquad (3.15)$$

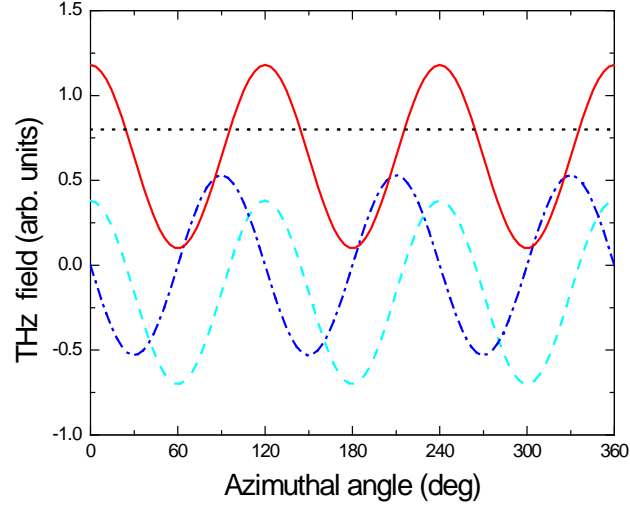where the azimuthal angle is measured from [$\bar{1}$ 10].

Fig. 3.8. Calculated azimuthal angle dependences of *p*-polarized (solid curve) and *s*-polarized (dash-and-dot curve) THz electric fields emitted from InAs (111) surface excited by 1.55 eV energy photons. The dashed and dotted lines correspond to the contributions of the lateral and normal photocurrent components into *p*-polarized THz radiation, respectively.

In derivation of Eqs. (3.12) – (3.15) we neglected the dispersion of refractive index. THz radiation is supposed to be detected in the direction of the reflected optical beam that is at the angle of 45^0. For InAs excited by photons with the energy of 1.55 eV $\bar{n} \simeq 3.9$ and we find $\vartheta \approx 10.4°$, $\cos \vartheta \approx 0.98$, $\sin \vartheta \approx 0.18$. In Fig. 3.8 the calculated contributions of the normal and the lateral photocurrent components into THz electric field are

presented in dependence on the azimuthal angle for (111) surface. It is seen that the lateral photocurrent essentially contributes to p-polarized THz electric field and entirely determines the s-polarized THz emission.

As it follows from (3.12)–(3.15), THz electric fields can be represented as $E_T^p \propto a_1 + b_1 \cos 3\phi$, $E_T^s \propto c_1 \sin 3\phi$ for   (111)   surface   and   as $E_T^p \propto a_2 + b_2 \cos 2\phi$, $E_T^s \propto c_2 \sin 2\phi$ for (110) surface. For InAs surface excited by 1.55 eV radiation using the calculated coefficients presented in Table   I,   one   can   get $a_1 \approx 0.64$, $b_1 \approx 0.54$, $c_1 \approx -0.53$ and $a_2 \approx 0.6$, $b_2 \approx -0.1$, $c_2 \approx -0.19$ for (111) and (110) surfaces, respectively. From the obtained expressions it follows that the depths of azimuthal oscillations of THz field are defined by the relations b_1 / a_1 and b_2 / a_2 and tend to diminish with decreasing the excitation photon energy; at 0.4 eV excitation their values decrease approximately one order as compared with 1.55 eV excitation. This conclusion is confirmed by results of experimental studies of spectral dependence of azimuthal anisotropy of THz generation in InAs (Fig. 3.5).

As can be seen at the excitation of InAs (111) surface with 780 nm laser pulses the quantity of azimuthal anisotropy is about 0.86 that is in a good agreement with our calculated results ($b_1 / a_1 \simeq 0.84$). With twofold increasing the wavelength of excitation (~1560 nm) the quantity describing the anisotropy of the radiated THz field amplitude becomes equal to 0.19 (Fig. 3.5) that is less than the theoretical value (~0.37) by a factor of 2. It is conceivable that this discrepancy results from the decay of anisotropic momentum distribution of photoelectrons due to their scattering. This effect is more noticeable at lower photon energy because the rate of scattering by polar optical phonons grows with decrease of the photoelectron energy.

It is appropriate here to note, that since quasiballistic regime is considered here our main implications are valid if the intervalley electron scattering is not essential. It means that our approach can be used for laser excitation with the photon energy lower than the threshold for transition of photoelectrons into L-valleys of conduction band (the threshold energy for InAs is about 1.6 eV)

[85]. At the higher photon energy (>1.6 eV) the electrons are intensively scattered in the lateral valleys and the optical alignment will slightly affect on photoconductivity and THz generation induced by the transient photocurrent. At high excitation level electron-electron scattering will also essentially reduce the anisotropy of photocurrent. However, since the cross-section of Coulomb scattering drops quadratically with increase of electron energy one would expect that in InAs excited high above forbidden energy gap this scattering mechanism will have a small effect on the lateral photocurrent and its contribution in THz emission at least at the photocarrier density lower than 10^{18} cm^{-3}. At last it should be pointed out that a closer consideration of photocarrier relaxation is unlikely to essentially change the obtained results concerning the contribution of the optical alignment effect in THz emission because the dominant part of THz pulse is mainly generated at the ballistic stage of photocarriers movement when their scattering is not manifested yet.

3.5 Chapter summary

In conclusion, we calculated the photocurrent in InAs excited by ultrashort laser pulse with different photon energy taking into account optical alignment of photoexcited electrons and holes over momenta. At the ballistic stage of photocarrier movement anisotropic momentum distribution of photocarriers results in anisotropy of photoconductivity that is manifested in the appearance of perpendicular to the dc electric field photocurrent component depending on orientation of electric and optical field relative to crystallographic axes of semiconductor. At the excitation of semiconductor surface with femtosecond laser pulses optical alignment of electrons over momenta results in the lateral transient photocurrent which like a normal photocurrent component induces THz emission. The relative contribution of the lateral photocurrent into THz emission from InAs surface grows with increase of the photon energy and at 800 nm excitation it compares with the contribution of the photocurrent directed perpendicular to the irradiated semiconductor surface. Experimentally

observed azimuthal anisotropy of THz signal generated from InAs surface under femtosecond laser excitation may be attributed to anisotropic transient photoconductivity caused by the anisotropic distribution of photocarriers excited by polarized femtosecond radiation over momenta.

CHAPTER 4

ANISOTROPIC PICOSECOND PHOTOCONDUCTIVITY CAUSED BY OPTICAL ALIGNMENT OF ELECTRON MOMENTA IN CUBIC SEMICONDUCTORS

In the preceding chapter the transient anisotropic photoconductivity in cubic semiconductors excited by an ultrashort laser pulse was calculated in the simplified approach based on the Boltzmann transport equations for optically generated electrons and holes in collisionless approximation. It was shown that the transient photocurrent component perpendicular to the dc electric field grows with increase of the photon energy and causes the emission of terahertz radiation pulses from semiconductor surface with amplitude dependent on the angle between the optical field and the crystallographic axes.

In this chapter the transient anisotropic photoconductivity caused by optical alignment of photocarriers momenta in narrow-gap semiconductors (InAs and InGaAs) excited by femtosecond laser pulses is simulated by using an ensemble Monte Carlo method. As compared to the analytical approach Monte Carlo simulation technique allows to take into account the real band structure of semiconductor, various mechanisms of carrier scattering, high-field effects and so to carry out the most comprehensive analysis of transport phenomena. The dynamics of the photocurrent components directed perpendicular and parallel to the dc electric field on a subpicosecond time scale and their dependencies on polarization direction and photon energy of the femtosecond pulse are calculated. The transient anisotropic photoconductivity is also studied experimentally by the optical pump – THz probe technique [8]. By measuring the time-dependent change in the amplitude of THz-probe pulses passing through the semiconductor one can evaluate the contribution of photoexcited carriers in the sample's conductivity. We observed that during the first 1-2 ps after excitation the change of THz absorption induced by optically

generated carriers depends on polarizations of THz and optical fields relative to each other and to the crystallographic axes of semiconductor.

The spectral dependence of anisotropic transient photoconductivity in InGaAs excited by femtosecond laser pulses is measured using the optical pump–terahertz probe technique [8]. The results of Monte Carlo simulation of THz pulse interaction with a photoexcited electron–hole plasma support the obtained experimental data.

4.1 Monte Carlo simulation of the transient anisotropic photoconductivity

We consider a direct band gap cubic semiconductor excited by a linearly polarized ultrashort laser pulse with the electric field amplitude **E** and the photon energy exceeding the energy band gap. Due to the selection rules for optical interband transitions nonequilibrium electrons and holes are distributed anisotropically in a momentum space. For example, in cubic semiconductors excited by radiation with the photon energy near the band gap, the momentum distribution function of the photoelectrons is proportional to $1 + \eta P_2 (\cos\theta)$, where $P_2(x)$ is the second order Legendre polynomial, θ is the angle between the electron momentum and the electric field of the light wave, η is equal to -1, +1, and 0 for the transitions from the heavy-hole, light-hole, and spin-orbit split-off valence subbands, respectively [119]. However, in narrow-gap semiconductors like InAs the preceding expression for the angle distribution of photocarriers becomes improper because electrons can be excited far deep into the central Γ-valley of the conduction band with the energy exceeding in several times the band gap. In this case, when calculating the momentum matrix elements determining the optical transitions and initial distribution of photocarriers the interband kp interaction and corrugation of conduction and valence bands should be taken into account.

The momentum matrix elements, energy dispersion relations for electrons and holes, and their velocities are calculated by the eight-band kp perturbation method [121, 122]. In this approximation four double degenerate bands including conduction band and three valence subbands are taken into account. The Hamiltonian-matrix in Luttinger-Kohn representation was diagonalized by Jacobi method for the range of carrier momenta specified in a spherical coordinate system on a mesh of $100\times100\times180$ points. Previously the Hermitian matrix is represented as real matrix with format 16x16. The eigenvalues obtained by diagonalization of this matrix define the dispersion relations for electrons in the central Γ-valley of conduction band and holes in three valence subbands; due to spin degeneracy and time-reversal symmetry these eigenvalues are fourfold degenerate. The higher energy L- and X-valleys of the conduction band are treated on the basis of isotropic Kane model. The electron and hole wave functions used for calculation of the momentum matrix elements are represented as expansions over Luttinger-Kohn basis states with the coefficients determined by the components of the calculated eigenvectors of the Hamiltonian-matrix. The probabilities of optical transitions of electrons from a valence subband state to a conduction band state were calculated in the dipole approximation with the use of Fermi's golden rule.

For simulation of the transient photocurrent we use an ensemble Monte Carlo method. The dynamics of electrons and holes under dc electric field is treated classically with the use of the calculated dispersion relations; Kane dispersion law is used for electrons in L- and X-valleys. Electron and hole scattering by acoustical and optical (polar and deformational) phonons, and (for the electrons) intervalley phonons were taken into account; the carrier scattering rates were calculated in an isotropic approximation. The role of the carrier-carrier scattering was neglected, because in the situation under investigation the photoexcited electrons have high kinetic energy (~1 eV). As the cross-section of Coulomb interaction drops quadratically with increasing electron energy, one would expect that the carrier-carrier scattering will have a small effect on the optical alignment effect at photocarrier densities lower than

$\sim 10^{18}$ cm^{-3}. When simulating carrier transport, the mean free-flight time, the scattering mechanisms, and the final state of the carrier after scattering are chosen using Monte Carlo procedure.

We used the ensemble of particles, each representing many real carriers. The state of the individual particle is characterized by its momentum and the type of the conduction band valley or valence subband, which the particle represents. The particle's charge is defined by the number of electrons or holes comprised and is found from the charge conservation condition. In the calculations we use approach in which the number of the particles remains unchanged, while the charge of the particle varies in time due to the optical generation of nonequilibrium electrons and holes.

The simulation begins with the calculation of the carrier scattering rates, the band structure, and the tables for electron and hole velocities as well as the probabilities for interband optical transitions at the mesh points in momentum space. We start simulation from the ensemble of particles representing thermally equilibrium electrons and holes. The sampling of the initial momenta of the particles having Maxwell distribution follows the method based on the central limit theorem. Then, after 5 ps (the time it takes for the establishment of the steady-state distribution of carriers in the dc electric field) a femtosecond optical pulse is turned on, and at this stage a part of the equilibrium particles is substituted by the particles representing the photoexcited carriers. The fraction of the photoexcited particles in the ensemble is determined by the ratio of the photocarrier density to the total carrier concentration. It increases with time during the photoexcitation and it achieves a steady state value depending on the excitation intensity after ending of the laser pulse. The momentum distribution of the particles at the instant of their photoexcitation is found by Monte Carlo procedure with the use of the calculated probabilities for the optical transitions of electrons.

Simulations were performed for two n-type semiconductors InAs and In$_{0.53}$Ga$_{0.47}$As excited by femtosecond laser pulse with different photon energies in the vicinity of the threshold energy for intervalley electron transfer

in the conduction band. The density of the photoexcited electrons is taken to be 10^{17} cm^{-3} for both semiconductors. The full width at half maximum (FWHM) of the laser pulse is taken 150 fs. The applied dc electric field is aligned parallel to the z-axis coincident with the [001] crystallographic direction. The electric field of the light wave lies in the plane xz (see Fig. 4.1) and forms the angle Θ with the dc field $\mathbf{F}$. In the calculation we choose $\Theta = 45°$ because that particular angle provides a maximal anisotropy effect. The equilibrium carrier densities for the first and the second materials are assumed to be $1.6 \cdot 10^{16}$ cm^{-3} and 10^{15} cm^{-3}, respectively. We use $\mathrm{sech}^2(t/\tau_0)$ temporal shape of the laser pulse intensity with $\tau_0 = 85$ fs (here FWHM is defined as $1.76\tau_0$).
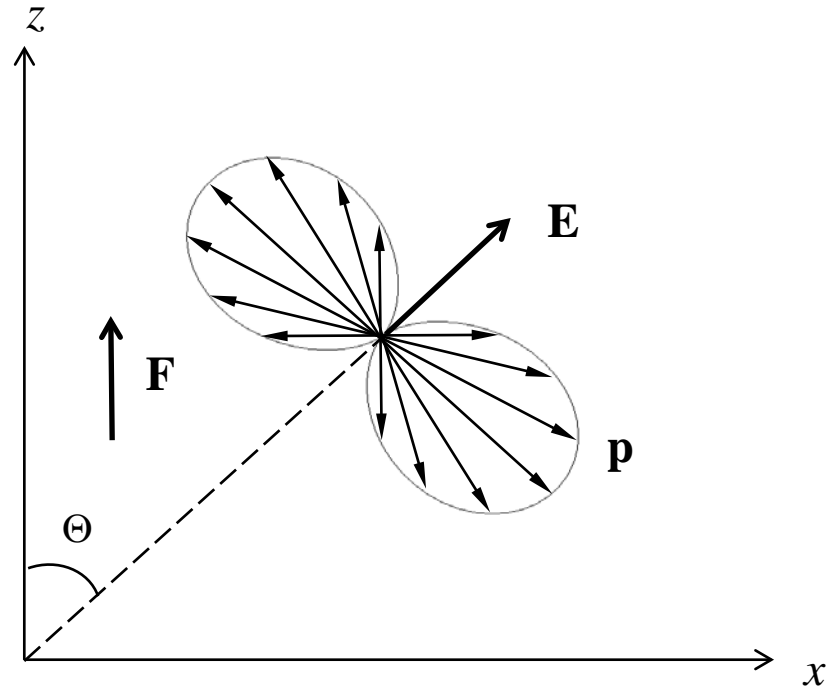

Fig. 4.1. Illustration of the anisotropic photoconductivity appearing due to the optical alignment of electrons excited from the heavy-hole subband.

The parameters used for kp calculation of the semiconductor band structure are presented in Table II. The coefficients for the nonparabolicity and effective masses of electrons in L- and X-valleys of the conduction band,

acoustical and optical deformation potentials, intervalley coupling constants and phonon energies, and other material parameters required for calculation of the carrier scattering rates for both semiconductors were taken from Refs. 121, 123-124. We used the intervalley separation energies in the conduction band which were recently measured by using the THz excitation spectroscopy technique [85, 108].

TABLE II. Band-structure parameters of InAs and $In_{0.53}Ga_{0.47}As$ used for *kp*-calculation and energy separations between conduction band valleys.

Parameter	InAs	$In_{0.53}Ga_{0.47}As$
Band-gap energy (eV)	0.36[a]	0.75[b]
Spin-orbit splitting (eV)	0.41[a]	0.15[b]
Electron effective mass in Γ valley:	$0.023m_0$[a]	$0.041m_0$[b]
Luttinger parameters:		
γ_1	20.0[c]	11.01[c]
γ_2	8.5[c]	4.18[c]
γ_3	9.2[c]	4.84[c]
Subsidiary valleys separations from Γ valley in conduction band (eV):		
L	1.08[d]	0.78[d]
X	1.12[d]	0.83[d]

[a]Ref. 123.
[b]Ref. 124.
[c]Ref. 121
[d]Refs. 85, 108

4.2. Experimental details

The transient anisotropic photoconductivity in $In_{0.53}Ga_{0.47}As$ excited by femtosecond laser pulses has been studied by the optical pump – THz probe technique. Ti:sapphire laser (MIRA Coherent) used in the experiment generates pulses having a central wavelength of 780 nm, the duration of 150 fs, and the repetition rate of 76 MHz. The laser beam is split into three parts, two of which are used for THz probe pulse generation and detection by dipole

LTG-GaAs antennas, and the third part is used for the photocarrier excitation in the sample. The average optical power focused on the gaps of the generating and receiving dipole antennas was about 50 and 30 mW, respectively. The pump beam with a power of about 200 mW was focused on the samples surface in about 2 mm diameter spot. Two Teflon lenses placed before and after the sample were used to collimate the THz probe beam. The direction of pump beam polarization was changed by a half wave plate.

The sample investigated was epitaxial (001) $In_{0.53}Ga_{0.47}As$ film of 1.08 μm thickness grown on InP substrate. The sample surface is irradiated by the optical pump and THz probe beams at normal incidence. The experiment was carried out at room temperature. We measured the dependence of the optically induced change in the amplitude of THz probe pulse transmitted through the sample on its polarization and the time delay of this pulse relative to the pump pulse. The azimuthal symmetry of the optically induced change in THz transmission through InGaAs was also investigated by rotating the sample around its surface normal.

4.3. Results of simulation

On excitation of direct gap semiconductor by femtosecond laser pulses with the photon energy exceeding the band gap in several times the electrons are generated high in the central Γ valley of the conduction band. The wave functions of these electrons are significantly modified due to the interband kp interaction, and as a result their momentum distribution is very different from the distribution of electrons excited near the edge of the conduction band. This is illustrated on Fig. 4.2, where the distribution functions of electrons over the directions of their momenta are presented. The polar and azimuthal angles θ and φ specify the directions of the electron momentum in a spherical coordinate system with the polar axis directed along the electric field of radiation. It is seen from Fig. 4.2 that the momenta of electrons generated from both valence subbands are aligned much the same – in the plane that is

perpendicular to the light polarization vector. Contrary to that, at the excitation with the photon energy close to the semiconductor band gap, the electrons generated from the light-hole subband are aligned mainly along the radiation electric field [120]. Calculations also show that the azimuthal anisotropy of the optical transition probabilities caused by the valence band corrugation becomes larger with increasing the photon energy.

Photocurrent transients calculated for InGaAs excited by femtosecond pulses with the photon energies of 1.5, 1.6, and 1.7 eV for dc fields of 1 and 10 kV/cm are presented in Fig. 4.3 and Fig. 4.4, respectively. In addition to the usual (longitudinal) photocurrent component J_z directed along the dc field, a transversal photocurrent component J_x perpendicular to **F** appears on a picosecond time scale. This photocurrent component reaches its peak immediately after photoexcitation and decays later during 1–2 ps. For F=10 kV/cm within a 0.5 ps wide time window after excitation both photocurrent components are comparable in magnitude. For electric field of 1 kV/cm J_x can even exceed J_z. If the electric field of the optical beam is parallel or perpendicular to the field **F**, the transverse photocurrent vanishes entirely. Note that the amplitude of the photocurrent component J_x nonlinearly depends on the dc field; a tenfold increase of this field enlarges the photocurrent roughly 5 times.

Simulations show that the transversal photocurrent is a nonmonotonic function of the photon energy and reaches its maximum at $h\nu$=1.6 eV which corresponds to the threshold energy for intervalley transfer of the photoexcited electrons. This result is confirmed by theoretical calculations [30], from which it follows that the transverse photocurrent component is proportional to the derivative of the electron mobility with respect to the energy. Near the threshold of intervalley transfer the electron mobility changes sharply, thus this derivative becomes large. From a physical point of view it means that the total
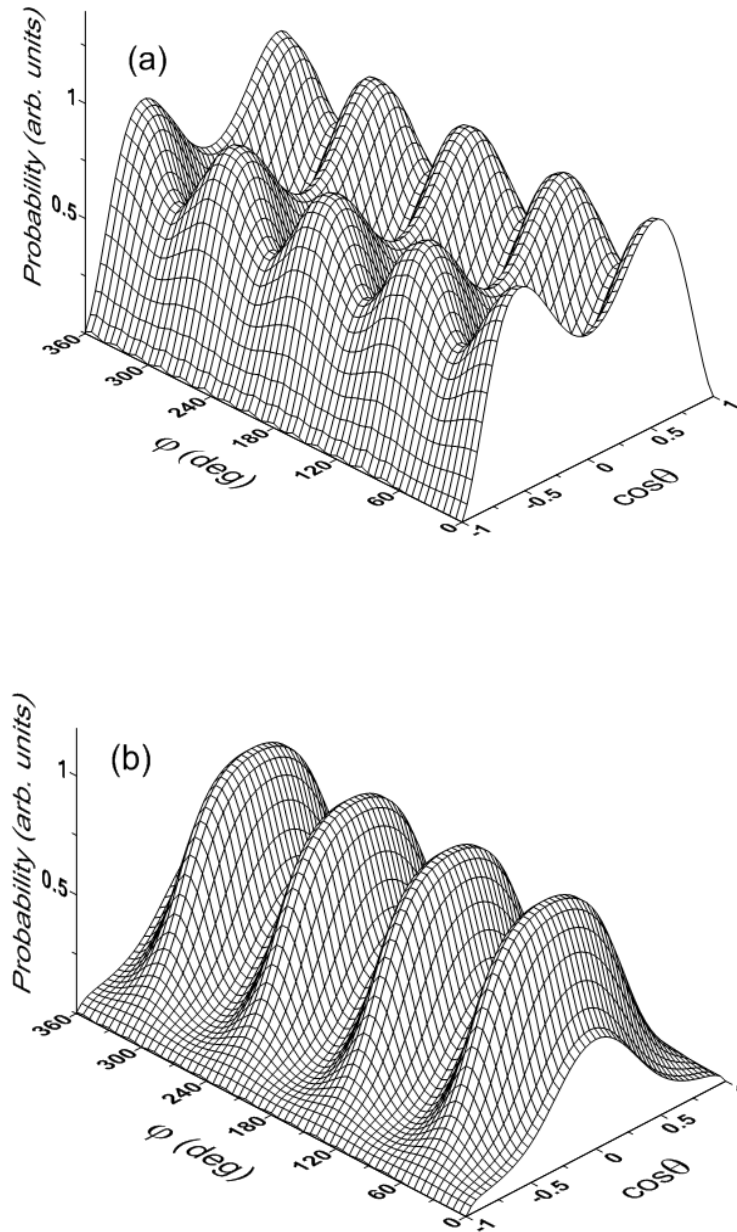
Fig. 4.2. Calculated distributions over momenta directions of photoelectrons excited by linearly polarized light with the photon energy 1.55 eV from the heavy (a) and light (b) hole valence subbands in In$_{0.53}$Ga$_{0.47}$As. The angles θ and φ determine the direction of electron momentum in spherical coordinate system with polar axis along [001] crystallographic direction, azimuthal angle φ are measured from axis [100]. The light wave electric field is directed along [001] axis ($\theta = 0$).

photocurrent component J_x, which is determined by the disbalance of photoelectron flows in both directions of the x-axis significantly increases if

the electrons from the left petal (Fig. 4.1) remain in the central valley, whereas the electrons from the right petal are transferred to the low-mobility *L*- and *X*-valleys. Exactly such a condition is realized in InGaAs under the 1.6 eV excitation.
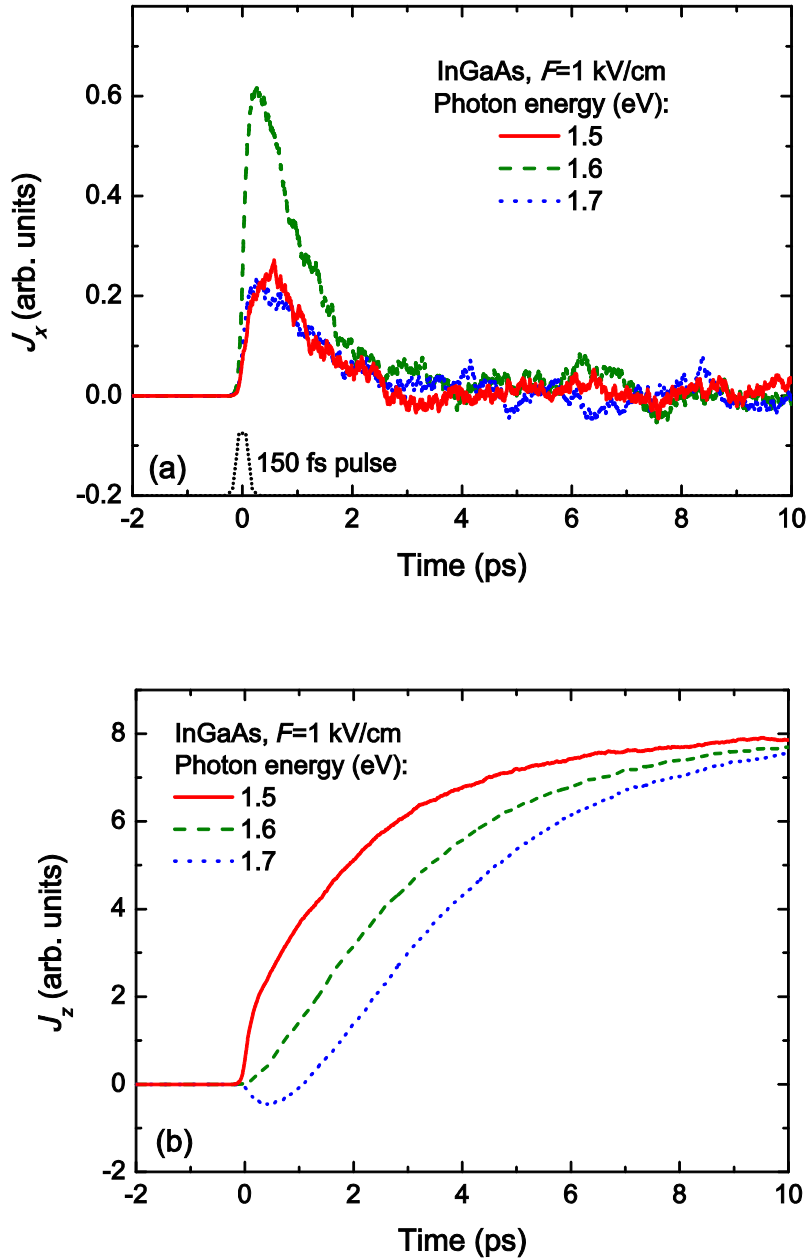

Fig. 4.3. Calculated transversal (a) and longitudinal (b) components of the photocurrent excited in InGaAs by a 150 fs laser pulses with three photon energies at dc field of 1 kV/cm. The shape of 150 fs laser pulse is shown.
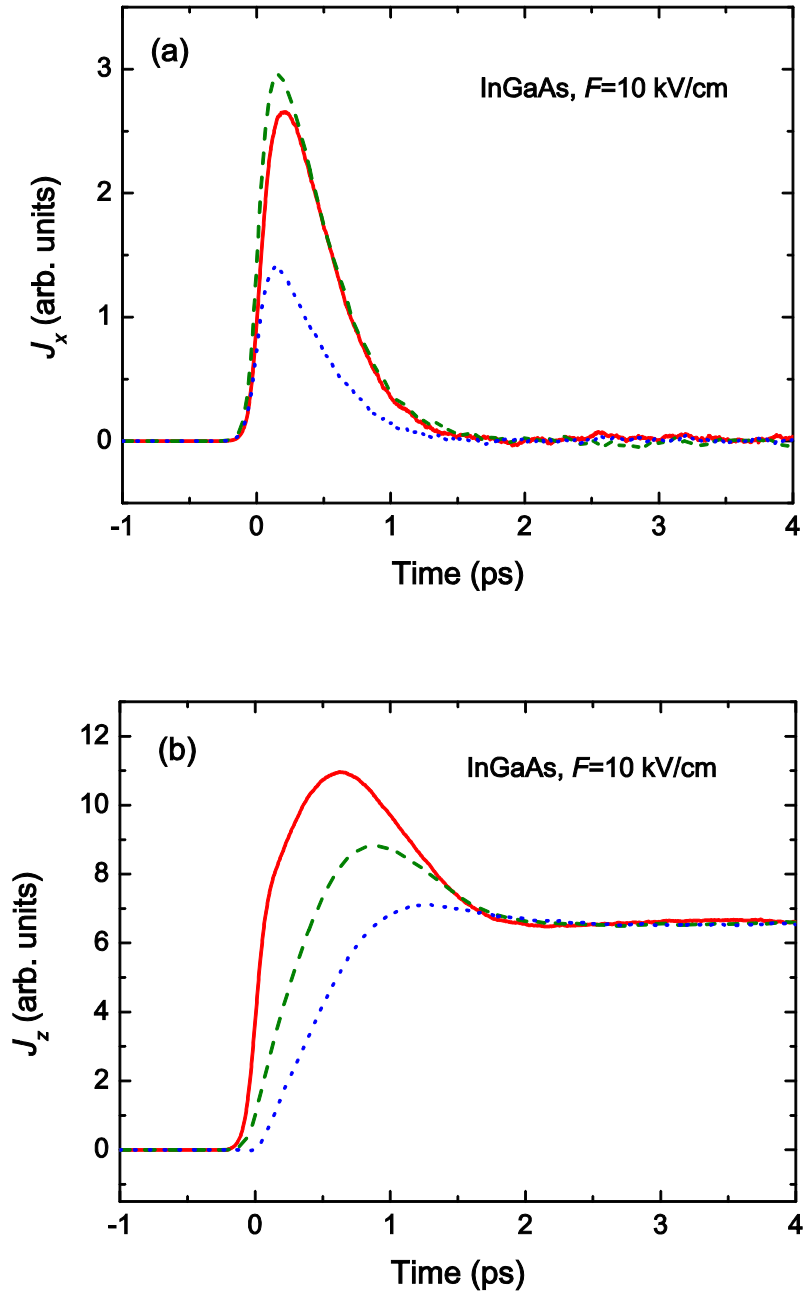
Fig. 4.4. Calculated transversal (a) and longitudinal (b) components of the photocurrent in InGaAs at dc field of 10 kV/cm. The specifications of the curves are the same as in Fig. 4.3.

In Fig. 4.5 the temporal dependencies of the fraction of photoelectrons in the central Γ valley of conduction band are shown. For a field $F=1$ kV/cm the electrons excited at the photon energy in excess of 1.6 eV transfer from the Γ valley to the upper L- and X-valleys for a short time (<100 fs). On the other

hand, electrons return to the central valley time is much longer, of the order of 10 ps. Returned to the Γ valley electrons are cooled down through the cascade emission of polar optical phonons; their mobility increases due to decreasing
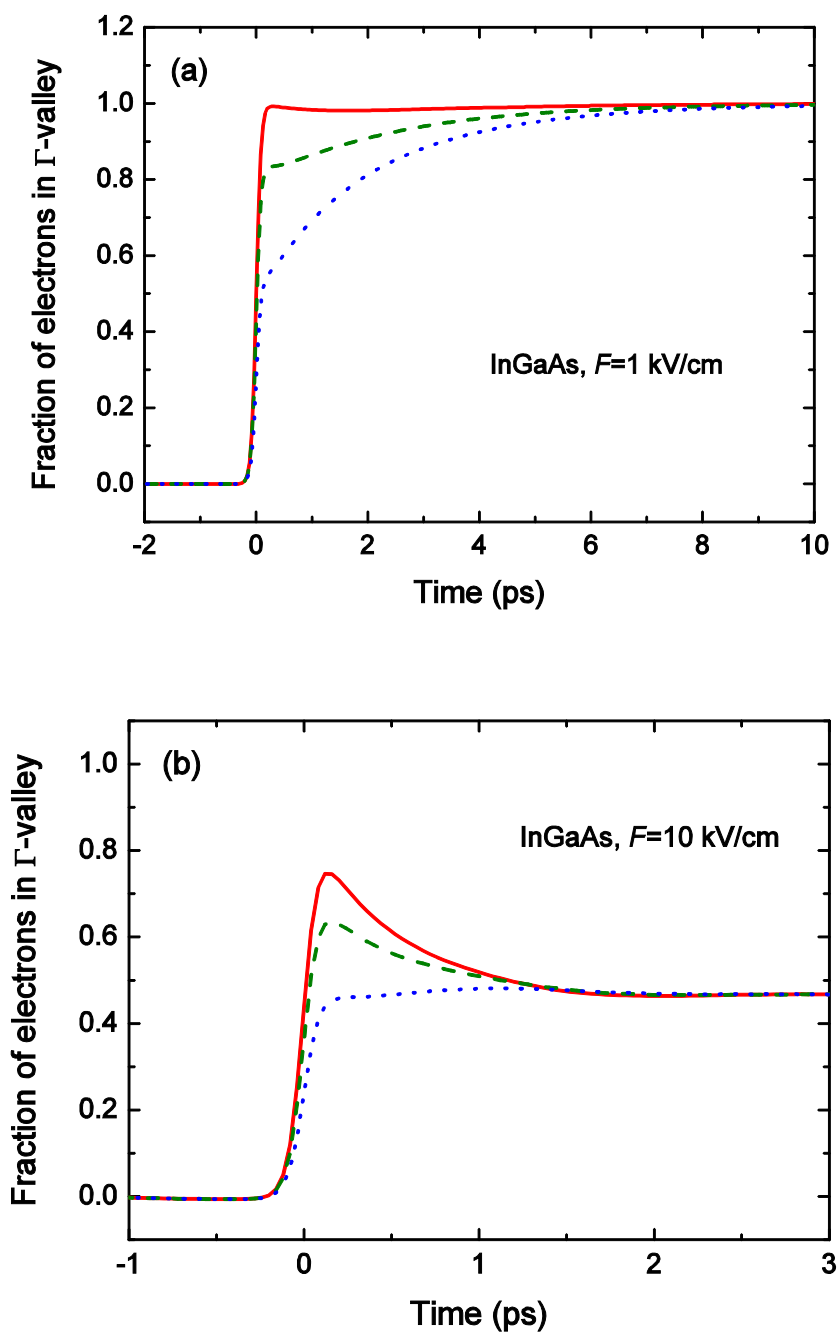

Fig. 4.5. The temporal dependencies of the Γ valley filling with photoexcited electrons in InGaAs for three photon energies and at dc field of 1 kV/cm (a) and 10 kV/cm (b). The specifications of the curves are the same as in Fig. 4.3.

effective mass in the nonparabolic conduction band. As a result (Fig. 4.3) the longitudinal photocurrent component monotonically grows in time and achieves the steady state value in about 10 ps.

For F=10 kV/cm a considerable fraction of the electrons occupies the subsidiary L and X valleys in the conduction band (Fig. 4.5), and clearly defined velocity overshoot effect takes place at the photon energies of 1.5 and 1.6 eV (Fig. 4.4(b)). However, no velocity overshoot effect was observed for 1.7 eV excitation, because in that case the initial energy of the photoexcited electrons is already larger than the threshold for the intervalley transfer.

It can be seen from Figs. 4.3 and 4.4 that the longitudinal photocurrent component J_z decreases with increasing photon energy and at $h\nu$=1.7 eV even becomes negative for a short time. With increasing dc field, this effect becomes smaller. The mechanism of negative photoconductivity can be explained as follows. The electrons moving against dc field acquire more energy from it and start to be transferred to the upper valleys. Due to the intense intervalley scattering these electrons lose almost all their resultant momentum, therefore the main contribution to the photocurrent comes from the electrons remaining in the central valley. It is clear that this contribution will be negative because these electrons move along the electric field. It should be noted that a similar effect can be observed in semiconductors if the initial energy of the photoexcited electrons is close to a multiple of the optical phonon energy [49-52].

The transient photocurrent components calculated for InAs excited by femtosecond laser pulse with different photon energies are shown in Figs. 4.6 and 4.7 for the cases of dc field equal to 1 and 10 kV/cm, respectively. As in the case of InGaAs, the transversal photocurrent reaches its peak value at the photon energy close to the threshold energy for the intervalley transfer of electrons, which is about 1.55 eV for InAs. For the 1.75 eV excitation the longitudinal component of the transient photocurrent becomes negative for about 1 ps long time window after the laser pulse.
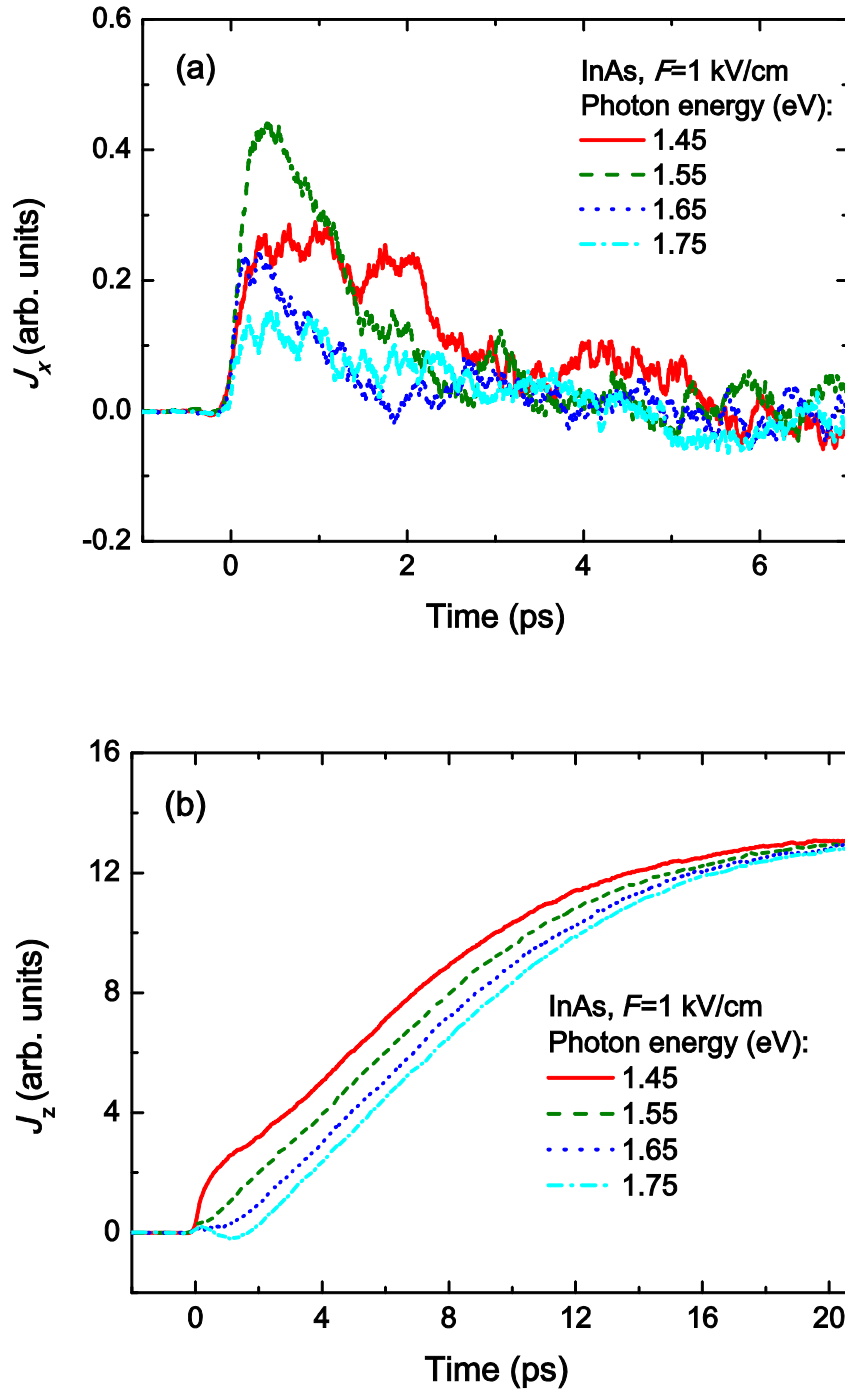
Fig. 4.6. Calculated transversal (a) and longitudinal (b) components of the photocurrent excited in InAs by a 150 fs laser pulses with four photon energies at dc field of 1 kV/cm.

As it follows from Eq. (3.1), in cubic semiconductors the transversal photocurrent component depends on orientation of dc and light-wave electric fields relative to crystallographic axis of semiconductor. In the case of InAs,
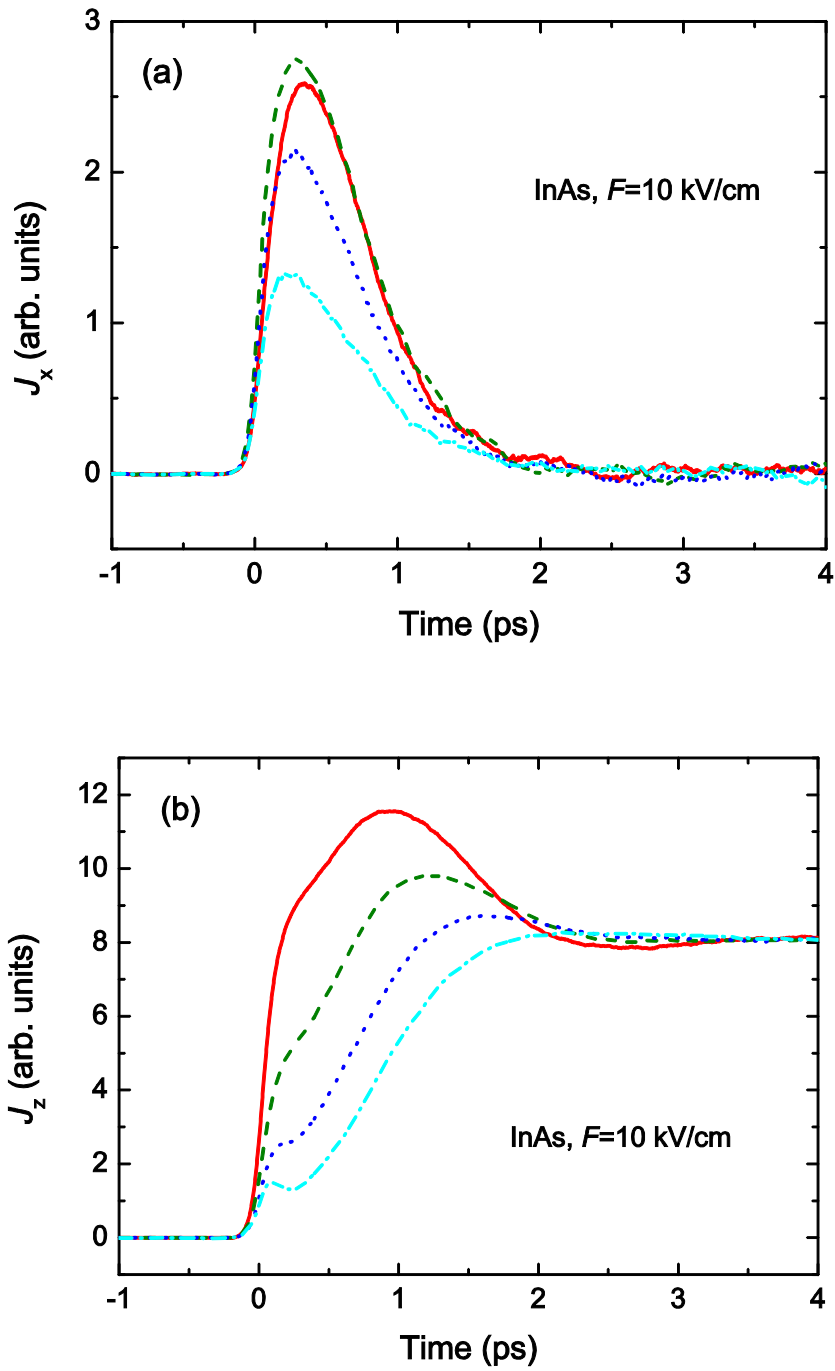
Fig. 4.7. Calculated transversal (a) and longitudinal (b) components of the photocurrent in InAs at dc field of 10 kV/cm. The specifications of the curves are the same as in Fig. 4.6.
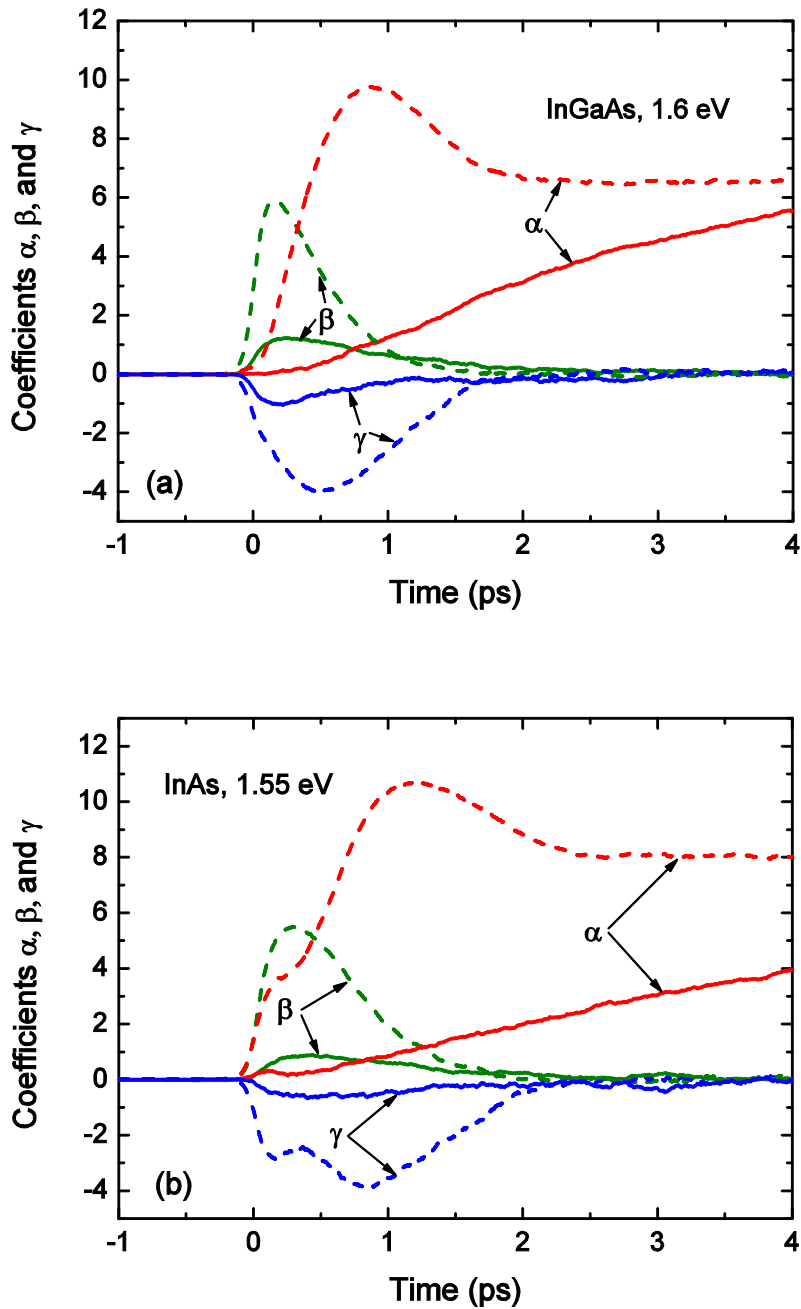
Fig. 4.8. Temporal dependencies of the coefficients α, β, and γ calculated for InGaAs at the 1.6 eV excitation (a), and for InAs at the 1.55 eV excitation (b) for two values of dc electric field of 1 kV/cm (solid lines) and 10 kV/cm (dash lines).

the contribution of this component explains experimental results of both the azimuthal anisotropy of the emitted terahertz pulse amplitude [81, 82, 98-100] and its dependence on the exciting photon energy [125, 85, 108]. For (111) surface the dependence of p-polarized THz field on the rotation angle ϕ of the

sample about the surface normal is given by $1 + a\cos 3\phi$, where the parameter a can be approximated as $a \approx \gamma / \left[3\sqrt{2}\left(\alpha - \beta - \gamma/3\right)\sin\theta_r \right]$, θ_r denotes the angle of refraction for the exciting optical radiation [125]. The calculated temporal dependencies of the coefficients α, β, and γ are given in Fig. 4.8 for both semiconductors excited by radiation with the photon energies corresponding to maximal transverse photocurrents. These coefficients were found from Eq. (3.1) with the use of three calculated photocurrent components: J_x, J_z at $\Theta = 45°$, and J_z at $\Theta = 0°$. It can be seen that the coefficients α, β, and γ are comparable in magnitude in the course of about 1 ps after photoexcitation. The estimations carried out with the use of the calculated coefficients α, β, and γ show that the contribution of the transversal photocurrent into THz emission from (111) InAs excited at $h\nu$=1.55 eV results in azimuthal anisotropy approaching the experimentally observed value ($a \sim 1$).

4.4. Experimental observation of anisotropic transient photoconductivity

The optically induced change ΔT of THz probe pulse amplitude is proportional to $(\mathbf{jF})/F^2$, where $\mathbf{j}$ is the transient photocurrent induced by THz field $\mathbf{F}$. From Eq. (3.1) one can obtain

$$\Delta T \sim \alpha + \left(\beta + \gamma\right)\cos^2\left(\vartheta - \psi\right) - \left(\gamma/2\right)\sin 2\vartheta\sin 2\psi , \qquad (4.1)$$

where ϑ and ψ are the respective azimuthal angles of the optical and THz fields measured from [100] crystallographic axis. If both fields are parallel to each other ($\vartheta = \psi$), the change of THz field amplitude takes the form $\Delta T \sim \alpha + \beta + 3\gamma/4 + \left(\gamma/4\right)\cos 4\psi$. For perpendicular orientation of the fields ($\vartheta - \psi = \pi/2$) we obtain $\Delta T \sim \alpha + \gamma/4 - \left(\gamma/4\right)\cos 4\psi$. The difference between ΔT for THz field polarized in parallel and perpendicular to the

electric field of radiation is given by the expression $\beta + \left(\gamma / 2\right)\left(1 + \cos 4\psi\right)$ and is governed by the anisotropic part of the transient photoconductivity determined by the coefficients β and γ. The measured dependence of the difference in transmission of THz pulses polarized along and perpendicular to the electric field of femtosecond optical radiation is presented in Fig. 4.9 in dependence on delay time between THz and pump pulses. It is apparent that for about 1-2 ps after optical excitation the change in transmission of THz pulses depends on the orientation of THz field relative to the polarization of the optical pump radiation. The fourfold rotational symmetry of THz transmission which follows from Eq. (3.1) is supported by our experimental results shown in Fig. 4.10.
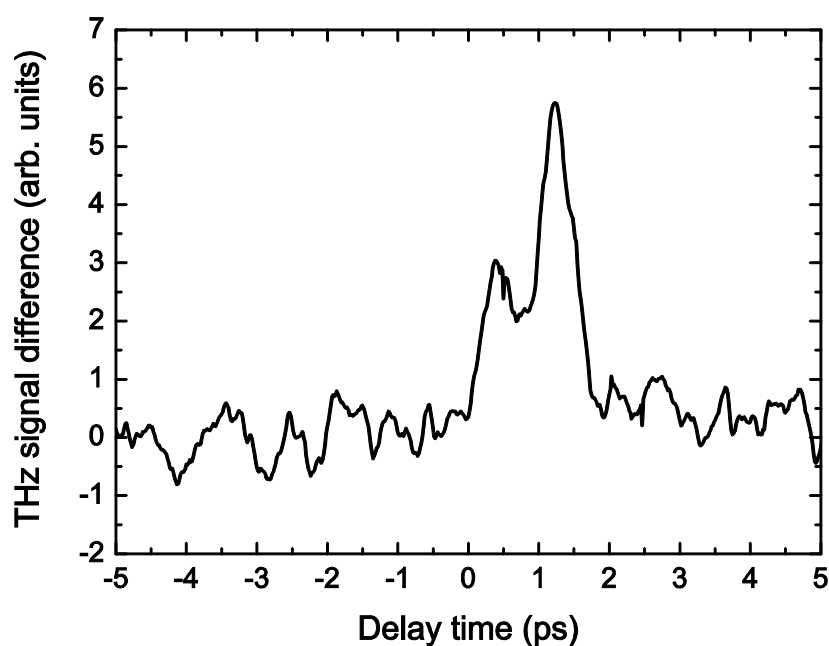

Fig. 4.9. Difference between optically induced changes in transmission of THz probe pulses polarized in parallel and perpendicular to the electric field of radiation as function of delay time between pump and probe pulses.
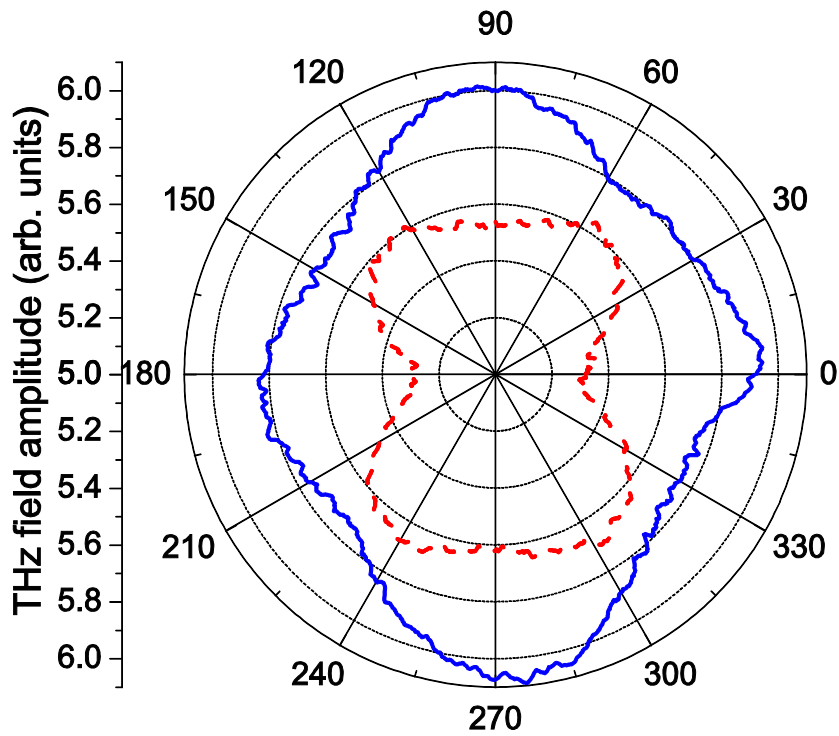
Fig. 4.10. Azimuthal dependencies of the optically induced THz transmissions measured at the delay time of 1.23 ps after photoexcitation for parallel (solid line) and perpendicular polarizations (dash line) of the optical pump and THz-probe pulses.

4.5. Spectral dependence of anisotropy of the photoconductivity in InGaAs excited with femtosecond laser pulses

The photocurrent excited by a femtosecond laser pulse in semiconductors InAs and InGaAs in a static electric field was calculated by the Monte Carlo method in [126]. It was found that, when the photon energy of radiation that excites the semiconductor is close to the threshold for the onset of intervalley transitions of electrons in the conduction band (for InAs and InGaAs, this approximately corresponds to the wavelength of the Ti:sapphire laser), the transverse component of the photocurrent in the first 50–100 fs after excitation can exceed the component along the electric field. Anisotropic photoconductivity can be studied experimentally using the "optical pump–

terahertz probe" technique. This technique is based on measuring the optically induced change in the transmission and/or reflection of probe THz radiation through the sample under study as a function of the delay time between the optical pump pulse and the THz pulse. The main contribution to the change in the transmission of probe THz radiation originates from the Drude absorption by photoexcited electrons and holes, which is determined by the photocurrent induced by the electric field of the THz pulse. Obviously, only the photocurrent component parallel to the THz electric field will contribute to the absorption. The dependence of the photocurrent on the orientation of the THz electric field with respect to the crystallographic axes of the semiconductor and the direction of the polarization of the optical radiation will evidently lead to anisotropy in the absorption of probe THz radiation. This effect was observed experimentally in an InGaAs sample excited by femtosecond laser pulses at a wavelength of 800 nm [126].

Here, using the optical pump–terahertz probe technique [106], we investigate the spectral dependence of anisotropy in the photoconductivity of InGaAs excited with femtosecond laser pulses. We establish experimentally that the degree of photoconductivity anisotropy depends nonmonotonically on the excitation photon energy. The results of Monte Carlo simulation of the interaction of THz pulses with a photoexcited electron–hole plasma are in fairly good agreement with the experimental results.

The sample under study was a 1.08 μm thick n-In$_{0.53}$Ga$_{0.47}$As single crystal film with the (001) orientation grown by molecular-beam epitaxy on an InP substrate. Radiation emitted by a femtosecond laser (Pharos, Light Conversion) with a wavelength of 1.03 μm was split into three beams. Two of them were used for the excitation of a THz emitter and gating of a GaBiAs photoconducting antenna (Teravil) that served to detect the THz radiation. The third and most intense beam was used to pump a parametric converter (Orpheus, Light Conversion) serving as a source of wavelength-tunable femtosecond radiation pulses that excited nonequilibrium electron–hole pairs in the semiconductor. The repetition rate and duration of the femtosecond

excitation pulses were 200 kHz and about 150 fs (FWHM), respectively. A *p*-InAs (111) oriented semiconductor wafer served as the emitter of THz pulses. The use of this type of emitter instead of commonly employed photoconducting antennas provided for a better quality of the THz beam. Wavelength-tunable femtosecond radiation from the parametric converter with an average power of 200 mW was focused onto the sample under study in a 2 mm diameter spot. The polarization direction of the excitation beam with respect to that of the THz radiation pulse was rotated using a half-wave plate. Terahertz radiation incident on and transmitted through the sample was focused by two Teflon lenses placed in front of and behind the sample, respectively. The optically induced change in the amplitude of the THz pulse transmitted by the sample was measured as a function of the time delay between the THz pulse and the femtosecond excitation pulse. The wavelength of the excitation radiation was varied in the range of 0.69–1.0 μm. The measurements were carried out at room temperature for the polarization of the optical excitation oriented parallel and perpendicularly to the electric field of the THz pulse.

The thickness of the layer of the photoexcited electron–hole plasma is determined by the optical radiation absorption length, which is much shorter than the THz radiation wavelength. For this reason, the photoexcited plasma layer may be considered infinitely thin. Then, the optically induced change in the transmitted THz field is $\Delta F = -4\pi I/c(n + 1)$, where c is the speed of light in free space, n is the refractive index of the substrate in the THz spectral range, and I is the component of the surface photocurrent parallel to the electric field of the THz pulse. It should be noted that the surface photocurrent is determined by the effective electric field, which, generally speaking, does not coincide with the incident THz pulse field. However, taking into account that the incident THz field differs from the effective field by a small value proportional to the surface photocurrent, the distinction between them may be disregarded.

The surface photocurrent induced by the THz field was calculated by the Monte Carlo method. The electron spectrum in the L and X valleys of the

conduction band was described using the isotropic Kane model. The scattering of charge carriers by acoustic, optical (polar and deformation), and intervalley (for the case of electrons) phonons was analyzed in the isotropic approximation. The dispersion relations and wave functions of electrons in the central valley of the conduction band and holes in the three valence subbands, as well as the matrix elements of the momentum operator for direct band-to-band transitions, were calculated numerically using an eight-band Hamiltonian matrix in the Luttinger–Kohn representation. This approximation makes it possible to take into account the real cubic symmetry of the crystal, which causes band warping, and the effects of band coupling, which play an important role in narrow gap semiconductors. The computed optical transition probabilities were then used to calculate the initial electron and hole momentum distribution functions. The calculations show that the distribution function of photoelectrons excited to the states of the conduction band with energies comparable to the semiconductor band gap or exceeding it differs considerably from the distribution function of electrons generated near the bottom of the conduction band. In particular, the momenta of electrons excited from the heavy- and light-hole subbands high into the conduction band align predominantly within the plane perpendicular to the radiation polarization vector.

We used a Monte Carlo simulation algorithm in which the number of particles in the ensemble is considered constant. The appearance of real electrons and holes in the bands as a result of optical excitation was taken into account by varying the effective charge of the simulated particles. The electric field F of the THz probe pulse was approximated by the function $F(t) \sim t^2 (1 - 5t/3) exp(-5t)$ (where t is time in picoseconds), which describes the actual pulse shape fairly well.

The calculations demonstrate (see Fig. 4.11) that the component of the surface photocurrent I parallel to the THz electric field depends on the direction of the polarization vector of the optical radiation. Immediately after
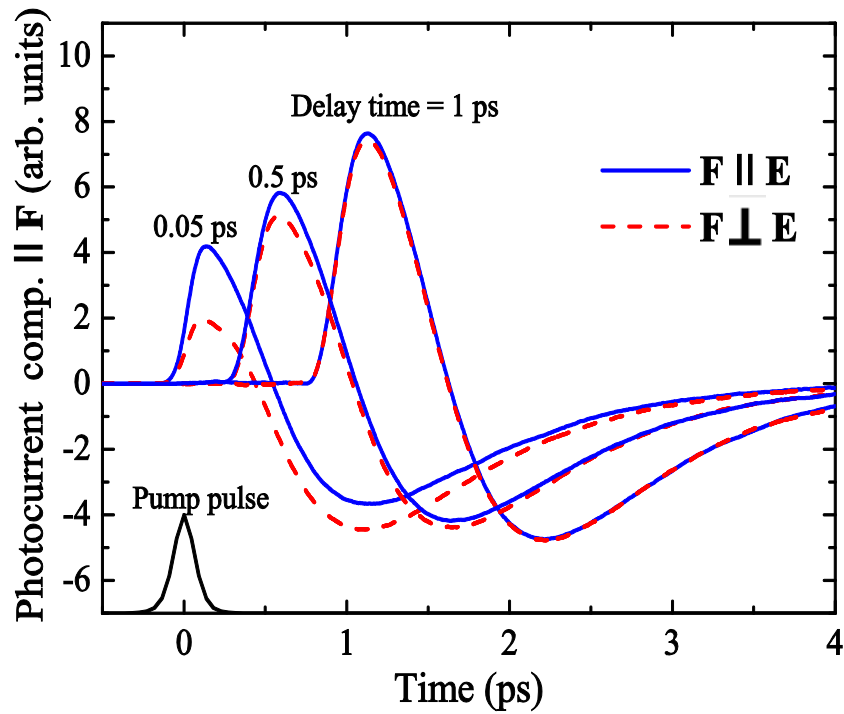
Fig. 4.11. Time dependences of the parallel component of the surface photocurrent *I* induced by the THz electric field in photoexcited InGaAs calculated for different delays of the THz pulse with respect to the optical pulse for two orientations of its polarization. The delay time is determined according to the peak positions of the THz and optical pulses. The optical excitation pulses are polarized along the [110] direction.

the end of the excitation pulse (see curves for a delay time of 0.05 ps, Fig. 4.11), the difference between the photocurrents for the parallel and perpendicular orientations of the polarization vector of the optical radiation with respect to the THz field is comparable to the magnitude of the photocurrent at this moment. As the delay of the THz pulse with respect to the optical pulse increases, the difference between the photocurrents decreases with a characteristic relaxation time of 1 ps. A small, on the order of 100 fs, delay of the photocurrent with respect to the electric field of the THz pulse seen in Fig. 4.11 is related to finite electron relaxation time. The calculations also indicate that the photocurrent amplitude increases with the delay of the THz pulse with respect to the optical pulse. It is reasonable to attribute this

behavior of the photocurrent to an increase in the mobility of photoexcited electrons upon their relaxation toward the bottom of the conduction band.

The physical mechanism of the anisotropy can be most readily understood if we consider the ballistic phase of the transport of photoexcited electrons in a constant electric field in a band with a nonparabolic dispersion relation. Consider a pair of photoelectrons with equal but oppositely directed momenta. Under the action of an electric field **F**, the energy of the photoelectron whose initial momentum component along the field is positive will decrease, while the electron with oppositely directed momentum will accelerate and its energy will increase. Owing to nonparabolicity, the effective mass of the first electron will decrease and that of the second electron will increase. During the ballistic phase of the transport, i.e., in the first few hundred femtoseconds after the excitation, the contribution from this pair of electrons to the photocurrent component parallel to the field **F** will be determined by the expression

$$j = -e\left[\left(p_{\parallel} - eFt\right)\Big/m\left(\varepsilon_{p_{\perp},p_{\parallel}-eFt}\right) - \left(p_{\parallel} + eFt\right)\Big/m\left(\varepsilon_{p_{\perp},p_{\parallel}+eFt}\right)\right]. \qquad (4.2)$$

Here, $m(\varepsilon_{\mathbf{p}})$ is the effective mass of the electron depending on the energy $\varepsilon_{\mathbf{p}}$ and $p_{\parallel}$ and $p_{\perp}$ are the absolute values of the components of the initial electron momentum after photoexcitation parallel and perpendicular to the electric field, respectively. In the approximation linear with respect to the electric field, we obtain from Eq. (4.2)

$$j = \frac{2e^2Ft}{m}\left[1 - p_{\parallel}\frac{d\varepsilon_p}{dp_{\parallel}}\frac{d\ln m}{d\varepsilon_{\mathbf{p}}}\right]. \qquad (4.3)$$

The effective mass and its derivative with respect to energy in Eq. (4.3) are taken at the initial electron energy at the moment of excitation. The first

term in Eq. (4.3) is independent of the initial momentum of photoexcited electrons and describes the ordinary contribution to the photocurrent originating from the asymmetry of their momentum distribution caused by the electric field **F**. The second term depends on the orientation of the initial photoelectron momentum and describes the contribution to the photocurrent owing to nonparabolicity, which results in a nonlinear dependence of the velocity of the electron on its momentum. Evidently, averaging over the momenta of photoexcited electrons with an anisotropic distribution function will lead to the dependence of this term on the orientation of the polarization vector of the excitation radiation with respect to the pulling electric field. During the next phase, in which the transport of photoexcited charge carriers is determined by scattering processes, another contribution to the photocurrent anisotropy will also arise owing to the energy dependence of the electron momentum relaxation rate.
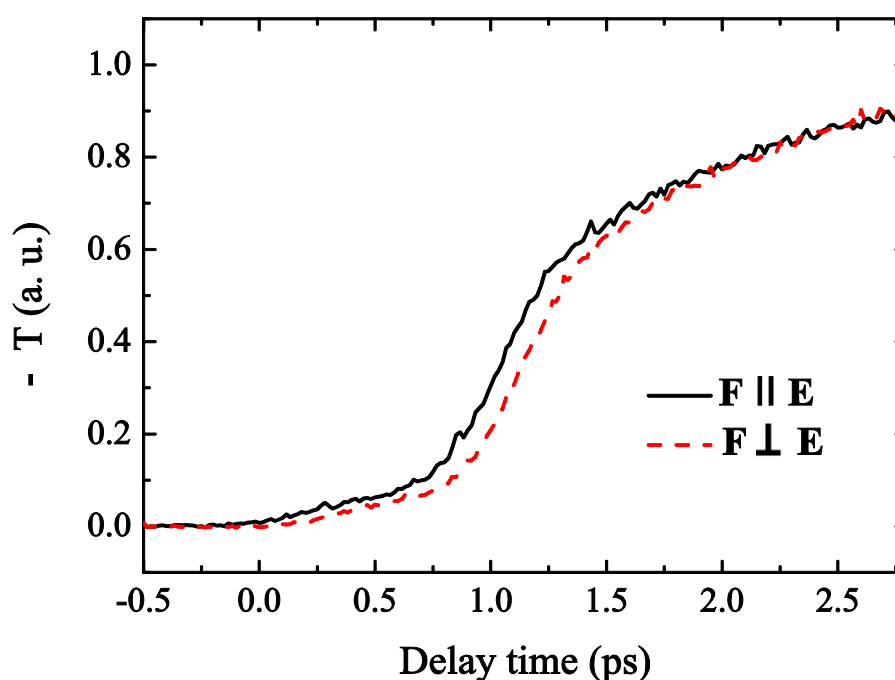

Fig. 4.12. Photoinduced change in the THz transmission ΔT versus the delay time of the THz pulse with respect to the optical pulse measured for two directions of its polarization. The excitation radiation wavelength is 780 nm.

Fig. 4.12 shows the typical experimental dependences of the photoinduced change ΔT in the THz transmission on the time delay between the THz and optical

pulses. The THz transmission decreases with increasing delay. This is explained by the energy relaxation of photoexcited electrons, which leads to an increase in their mobility and, thus, in the photocurrent induced by the THz electric field (see Fig. 4.11). Fig. 4.12 also clearly demonstrates that, in the first two picoseconds after the excitation, the change in the THz transmission depends on the orientation of the polarization vector of the optical radiation with respect to the electric field of the THz pulse. It can be concluded that the observed polarization dependence of the photoinduced change in the THz transmission is caused by the effect of the anisotropic photoconductivity.

According to Eq. (4.3), the anisotropic contribution to the photoconductivity depends on the initial energy of photoexcited electrons. Thus, it should depend on the photon energy of the excitation radiation. This conclusion is illustrated by Fig. 4.13, which shows the dependence of the anisotropy of the photoinduced change in the THz transmission in InGaAs on the wavelength of femtosecond excitation pulses. Both the experimentally determined dependence and the one obtained by the Monte Carlo calculations are plotted. One can see that the degree of anisotropy attains a maximum for an excitation wavelength of 780 nm, which approximately corresponds to a photon energy of 1.6 eV. In InGaAs, radiation with this wavelength generates electrons in the central valley of the conduction band with energies near the threshold for the onset of their transitions to the subsidiary valleys. Thus, it is reasonable to assume that the occurrence of a spectral maximum in the anisotropic photoconductivity is caused by intervalley transfer of photoexcited electrons. Indeed, those photoelectrons whose momentum component along the electric field direction is positive decelerate and remain in the central valley, where the electron mobility is high. In contrast, the energy of electrons with oppositely directed momenta will increase and they will experience rapid scattering to the subsidiary valleys of the conduction band, where the mobility
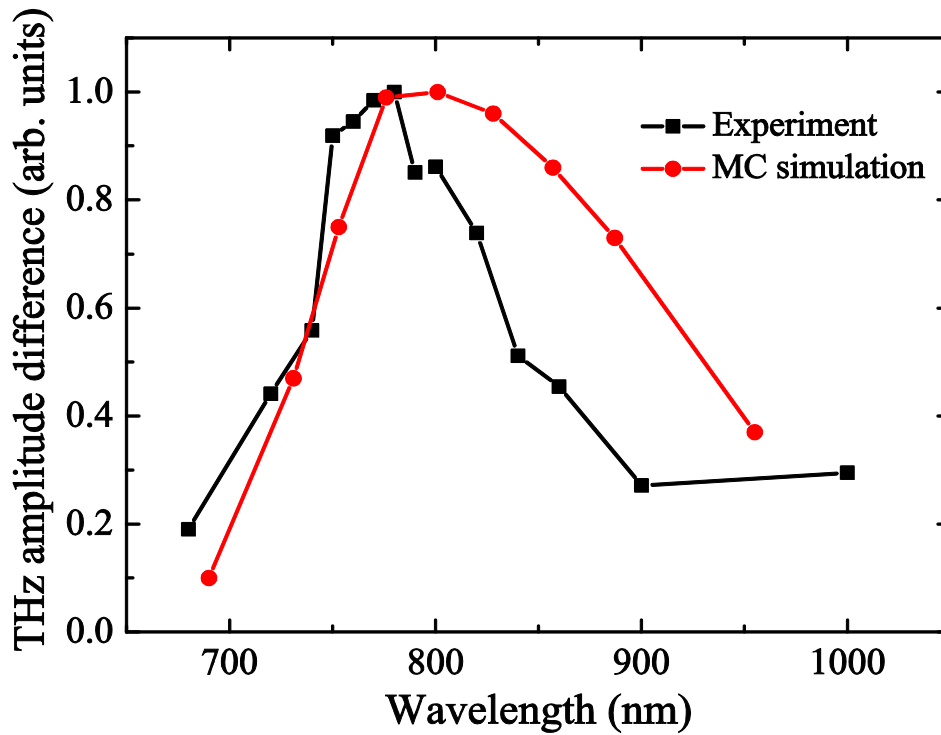
Fig. 4.13. Spectral dependence of the anisotropy in the change of the THz transmission of InGaAs excited by linearly polarized femtosecond pulses. The vertical axis represents the difference in the amplitudes of THz pulses transmitted by the sample that are polarized along and across the excitation optical pulses. The average power of the excitation radiation was normalized to maintain a constant photon flux upon the variation of the wavelength.

is low. Consequently, the main contribution to the anisotropic part of the photocurrent will come from the electrons in the central valley that move at acute angles with respect to the field. The contribution of these electrons to the anisotropic part of the photoconductivity will lead to a reduction in the photocurrent component along the THz field and, thus, to an increase in the THz transmission. This effect will be most prominent for electrons whose momenta are oriented along the THz field $\mathbf{F}$. Since photoelectrons in the case under study are mainly aligned in the plane perpendicular to the vector $\mathbf{E}$, this condition is satisfied for the field orientation $\mathbf{F} \perp \mathbf{E}$ (see Fig. 4.12). It is worth noting that the warping of the energy bands, originating from the cubic symmetry of the semiconductor, will lead to the dependence of the anisotropic

photoconductivity on the orientation of the polarization of the excitation radiation with respect to the crystallographic axes of the semiconductor.

Here it should be mentioned that, according to earlier measurements, the degree of azimuthal anisotropy in the THz signal generated at the surface of InAs excited by femtosecond laser pulses depends nonmonotonically on the excitation wavelength. It attains a maximum for a photon energy of 1.55 eV [85], which approximately corresponds to the threshold energy for the onset of electron transitions to the *L* subsidiary valleys of the conduction band. Apparently, the observed spectral maximum in the degree of azimuthal anisotropy is caused by the contribution to the THz generation from the lateral component of the photocurrent. This component appears owing to the photoconductivity anisotropy, which also attains a maximum for the photon energy corresponding to the threshold for intervalley transitions.

4.6. Chapter summary

The transient photoconductivity in cubic semiconductors InGaAs and InAs excited by linearly polarized femtosecond laser pulses in the presence of a dc uniform electric field has been investigated by Monte Carlo simulation. It has been found that the optical alignment of photoexcited electrons over momenta and the dependence of electron mobility on its energy results in anisotropy of photoconductivity, when except for the customary longitudinal photocurrent along dc field, the transversal photocurrent component directed perpendicular to this field occurs over the course of 1-2 ps after optical excitation. This transient photocurrent depends on orientation of the dc and light wave electrical field relative to crystallographic axes of semiconductor and is a non-monotonic function of the photon energy of the exciting femtosecond radiation.

The transient anisotropic photoconductivity results in the polarization dependence of THz pulse transmission through the semiconductor excited by femtosecond laser radiation. We have used optical pump – THz probe technique for studying this effect in (001) oriented *n*-type InGaAs sample. It

has been found that in the first few picoseconds after excitation the optically induced change of THz transmission depends on the direction of THz field relative to polarization of the optical pump pulse and crystallographic axes of the semiconductor. On rotation of the sample around normal to the excited semiconductor surface the fourfold symmetry of THz transmission is observed. The obtained experimental data correlate with the results of Monte Carlo simulation and is explained in terms of the transient anisotropic photoconductivity.

On the basis of both Monte Carlo simulations and experimental studies, it has been demonstrated that intervalley transitions of photoexcited electrons may affect considerably the anisotropy of the picoseconds photoconductivity in cubic semiconductors excited by ultrashort laser pulses. We have established that the anisotropy of the photoconductivity is maximal when photoelectrons are produced by radiation with a photon energy near the threshold for the onset of electron transitions to the subsidiary valleys in the conduction band. Simulations also show that at the femtosecond excitation with the photon energy near the threshold for intervalley electron transfers the longitudinal photocurrent can become negative in the subpicosecond time domain after optical excitation.

MAIN RESULTS AND CONCLUSIONS

The purpose of work presented in this thesis was to study the transient anisotropic photoconductivity in cubic semiconductors excited by femtosecond laser pulses and to investigate how this effect is manifested in emission of THz radiation from the semiconductor surface. The existing notion of the transient picosecond photoconductivity is far from complete in spite of the intensive study of this phenomenon. Thus, the influence of the optical alignment of photocarriers over momenta on the transient photoconductivity has not been properly investigated. Meanwhile, as shown in this work the anisotropic momentum distribution of photocarriers can have a dramatic effect on the photocarrier dynamics during the first few hundred femtoseconds after photoexcitation.

The following results were obtained in this work.

1. The terahertz power radiated by the femtosecond laser excited semiconductor surfaces was measured by the Golay cell. Intrinsic InSb crystals as well as p-type InAs were investigated by using three different wavelengths: 780 nm, 1030 nm, and 1550 nm, femtosecond lasers. It has been shown that p-type InAs crystal is the most efficient THz emitter for all three laser wavelengths with a nearly constant optical-to-THz power conversion efficiency of approximately 10^{-6}.

2. The photocurrent in InAs excited by femtosecond laser pulse with different photon energy taking into account optical alignment effect has been calculated with use of the transport equation for photoexcited electrons and holes in collisionless approximation. It has been found that the nonparabolicity of the electron dispersion law as well as the optical alignment of the photoexcited carrier momenta result in anisotropic photocurrent with a lateral component perpendicular to the surface dc electric field even in semiconductors with a cubic symmetry.

3. The lateral transient photocurrent component is the strongest during the first few hundreds of femtoseconds after the photoexcitation and causes the emission of terahertz radiation pulses with an amplitude dependent on the angle between the optical field and the crystallographic axes. In the case of InAs the contribution of this component in terahertz emission can be comparable to the contribution of the photocurrent component directed perpendicular to the crystal surface and explains experimental results of both the azimuthal anisotropy of the emitted terahertz pulse amplitude and its dependence on the exciting photon energy.

4. Transient photoconductivity in cubic semiconductors InGaAs and InAs excited by a femtosecond laser pulse in the presence of an uniform dc electric field has been studied with the use of a Monte Carlo simulation by taking into account optical alignment of photoexcited electrons over their momenta. Simulations show that due to the optical alignment effect and energy dependence of the electron mobility, the transient photoconductivity in cubic semiconductors becomes anisotropic during the first few picoseconds after optical excitation. The magnitude of this anisotropy reaches its peak when the excess energy of the optically excited electrons approaches the threshold for the intervalley transfer. It has been also found that when the electrons are excited near the threshold energy for the intervalley transfer, the component of the transient photocurrent directed along dc field for a short time after the end of the femtosecond optical pulse can become negative.

5. The anisotropy of the transient photoconductivity has been investigated experimentally on (001) InGaAs sample by optical pump – terahertz probe technique. It has been found that in the first few picoseconds after excitation the optically induced change of THz transmission depends on the direction of THz field relative to polarization of the optical pump pulse and crystallographic axes of the semiconductor. On rotation of the sample around normal to the excited semiconductor surface the fourfold

symmetry of THz transmission is observed. Experimental data are explained in terms of the transient anisotropic photoconductivity and are correlating with the results of the Monte Carlo simulation.

6. Using the optical pump–terahertz probe technique, the spectral dependence of anisotropy in the photoconductivity of InGaAs excited with femtosecond laser pulses has been investigated. An optical pump–terahertz probe setup using parametric converter as a source of wavelength-tunable femtosecond pump radiation has been assembled. It has been experimentally established that the degree of photoconductivity anisotropy depends nonmonotonically on the exciting photon energy. It grows with increasing the photon energy and reaches the maximum in the vicinity of the threshold for photoelectron transitions to the lateral valleys. The results of performed Monte Carlo simulation of the interaction of THz pulses with photoexcited electron–hole plasma are in fairly good agreement with the experimental data.

Thus, it has been shown in this work that the anisotropic transient photoconductivity in cubic semiconductors excited by femtosecond laser pulses is determined by photocarrier dynamics on a subpicosecond time scale and plays a significant role in THz emission from semiconductors. The study of this phenomenon gives us a better insight into ultrafast electronic processes which are of fundamental importance to the operation of high-speed semiconductor devices having a picosecond response time. In the future it might be desirable to investigate the transient anisotropic photoconductivity in more details. Basing on the results obtained in this work we allow oneself to state some problems relating to the anisotropic transient photoconductivity which are of most interest in our opinion.

a) To extend the study of the transient anisotropic photoconductivity to other semiconductor materials.

b) To investigate anisotropy of the transient photocurrent under high electric field. This experiment can be performed using optical pump–terahertz

probe technique and intense THz pulses obtained for instance by tilted-pulse-front excitation.

c) It would be interesting to carry out experiment at higher level of photoexcitation. It allows to increase the density of electron-hole plasma in semiconductor sample and thus to investigate the influence of carrier-carrier scattering and absorption saturation on the transient anisotropic photoconductivity.

d) It makes sense to perform experiment at low temperature and thus to study the influence of carrier scattering processes on the degree of anisotropy of the transient photoconductivity.

e) The anisotropic transient photoconductivity considered in this work is characterized by a subpicosecond response time. Therefore, it would be interesting to consider utility of this effect in fast semiconductor optoelectronic.

REFERENCES

[1] C. V. Shank, R. L. Fork, B. I. Greene, F. K. Reinhart, and R. A. Logan, "Picosecond nonequilibrium carrier transport in GaAs," *Appl. Phys. Lett.* **38**, 104 (1981).

[2] M. A. Osman and D. K. Ferry, "Electron-hole interaction and high-field transport of photoexcited electrons in GaAs," *J. Appl. Phys.* **61**, 5330 (1987).

[3] M. C. Nuss, D. H. Auston, and F. Capasso, "Direct subpicosecond measurement of carrier mobility of photoexcited electrons in gallium arsenide," *Phys. Rev. Lett.* **58**, 2355 (1987).

[4] A. E. Iverson and D.L. Smith, "Mathematical modeling of photoconductor transient response," *IEEE Trans. Electron Devices* **34**, 2098 (1987).

[5] G. M. Wysin, D. L. Smith, and A. Redondo, "Picosecond response of photoexcited GaAs in a uniform electric field by Monte Carlo dynamics," *Phys. Rev. B* **38**, 12514 (1988).

[6] S. N. Chamoun, R. Joshi, E. N. Arnold, R. O. Grondin, K. E. Meyer, M. Pessot, and G. A. Mourou, "Theoretical and experimental investigations of subpicosecond photoconductivity," *J. Appl. Phys.* **66**, 236 (1989).

[7] A. S. Vengurlekar and S. Jha, "Conductivity response of nonthermal hot carriers photoexcited by subpicosecond pulses in GaAs," *Phys. Rev. B* **38**, 2044 (1988).

[8] M. C. Beard, G. M. Turner, and C. A. Schmuttenmaer, "Transient photoconductivity in GaAs as measured by time-resolved terahertz spectroscopy," *Phys. Rev. B* **62**, 15764 (2000).

[9] A. E. Iverson, G. M. Wysin, D. L. Smith, and A. Redondo, "Overshoot in the response of a photoconductor excited by subpicosecond pulses," *Appl. Phys. Lett.* **52**, 2148 (1988).

[10] W. Sha, J. K. Rhee; T.B. Norris, and W. J. Schaff, "Transient carrier and field dynamics in quantum-well parallel transport: From the ballistic to the quasi-equilibrium regime," *IEEE J. Quant. Electron.* **28,** 2445 (1992).

[11] T. Dekorsy, T. Pfeifer, W. Kütt, and H. Kurz, "Subpicosecond carrier transport in GaAs surface-space-charge fields," *Phys. Rev. B* **47**, 3842 (1993).

[12] Y. Rosenwaks, B.R. Thacker, R. K. Ahrenkiel, A. J. Nozik, and I. Yavneh, "Photogenerated carrier dynamics under the influence of electric fields in III-V semiconductors," *Phys. Rev. B* **50**, 1746 (1994).

[13] V.L. Malevich, "Dynamics of photoinduced field screening; THz-pulse and second harmonic generation from semiconductor surface," *Surf. Sci.* **454-456**, 1074 (2000).

[14] X.-C. Zhang, B. B. Hu, J. T. Darrow, and D. H. Auston, "Generation of femtosecond electromagnetic pulses from semiconductor surfaces," *Appl. Phys. Lett.* **56**, 1011 (1990).

[15] X.-C. Zhang and D. H. Auston, "Optoelectronic measurement of semiconductor surfaces and interfaces with femtosecond optics," *J. Appl. Phys.* **71**, 326 (1992).

[16] A. Leitenstorfer, S. Hunsche, J. Shah, M. C. Nuss, and W. H. Knox, "Femtosecond high-field transport in compound semiconductors," *Phys. Rev. B* **61**, 16642 (2000).

[17] T. Dekorsy, H. Auer, C. Waschke, H. J. Bakker, H. G. Roskos, H. Kurz, V. Wagner, and P. Grosse, "Emission of Submillimeter Electromagnetic Waves by Coherent Phonons," *Phys. Rev. Lett.* **74,** 738 (1995).

[18] M. A. Osman and D. K. Ferry, "Monte Carlo investigation of the electron-hole-interaction effects on the ultrafast relaxation of hot photoexcited carriers in GaAs," *Phys. Rev. B* **36**, 6018 (1987).

[19] C. J. Stanton, D.W. Bailey, and K. Hess, "Femtosecond-pump, continuum-probe nonlinear absorption in GaAs," *Phys. Rev. Lett.* **65**, 231 (1990).

[20] T. Kuhn and F. Rossi, "Analysis of coherent and incoherent phenomena in photoexcited semiconductors: A Monte Carlo approach," *Phys. Rev. Lett.* **69**, 977 (1992).

[21] C. Jacobini and L. Reggiani, "The Monte Carlo method for the solution of charge transport in semiconductors with applications to covalent materials," *Rev. Mod. Phys.* **55**, 645 (1983).

[22] V.L. Bonch-Bruevich, S.G. Kalashnikov, *Semiconductor Physics*, (Moscow: Nauka, 1977).

[23] R. A. Smith, *Semiconductors*, (University Press, 1961).

[24] R. H. Bube, *Photoconductivity of Solids*, (Wiley, 1960).

[25] A. M. Danishevskiĭ, A. A. Kastal'skiĭ, B. S. Ryvkin, S. M. Ryvkin, and I.D. Yaroshetskiĭ, "Intraband photoconductivity in p-Ge," *Pis'ma Zh. Eksp. Teor. Fiz.*, **10**, 470 (1969) [*JETP Lett.* **10**, 302 (1969)].

[26] E. M. Epshtein, "On the heating of conduction electrons by infrared radiation," *Izvestiya Visshikh Uchebnykh Zavedenii, Radiofizika*, **13**, 1398 (1970) [*Radiophys. Quantum Electron.* **13**, 1076, (1970)]

[27] V. I. Puchkov and E. M. Epshtein, "Effect of a powerful electromagnetic wave on the electrical conductivity of a semiconductor," *Izvestiya Visshikh Uchebnykh Zavedenii, Radiofizika*, **16**, 305 (1973) [*Radiophys. Quantum Electron.* **16**, 227, (1973)]

[28] Yu. S. Gal'pern and Sh. M. Kogan, "Anisotropic photoelectric effects," *Zh. Eksp. Teor. Fiz.* **56**, 355 (1969) [*Sov. Phys. JETP* **29**, 196 (1969)].

[29] Y. V. Gulyaev, "Dependence of the photoconductivity of semiconductors on the polarization of the incident radiation," *Pis'ma Zh. Eksp. Teor. Fiz.*, **7**, 171 (1968) [*JETP Lett.* **7**, 132 (1968)].

[30] V. I. Belinicher and V. N. Novikov, *Fiz. Tekh. Poluprov.* **15**, 1957 (1981) [*Sov. Phys. Semicond.* **15**, 1138 (1981)].

[31] B. P. Zakharchenya, D. N. Mirlin, V. I. Perel', I. I. Reshina, "Spectrum and polarization of hot-electron photoluminescence in semiconductors," *Sov. Phys. Usp.* **25,** 143 (1982).

[32] F. Meier, B. P. Zakharchenya, *Optical Orientation,* (North-Holland, 1984)

[33] V.L. Al'perovich, V.I. Belinicher, V.N. Novikov, A.S. Terekhov, "Surface photovoltaic effect in solids. Theory and experiment for interband transitions in gallium arsenide," *Zh. Eksp. Teor. Fiz.* **80**, 2298 (1981) [*Sov. Phys. JETP* **53**, 1201 (1981)].

[34] C. V. Shank, R. L. Fork, R. F. Leheny, and J. Shah, "Dynamics of photoexcited GaAs band-edge absorption with subpicosecond resolution," *Phys. Rev. Lett.* **42**, 112 (1979).

[35] R. W. Schoenlein, W. Z. Lin, E. P. Ippen, and J. G. Fujimoto, "Femtosecond hot-carrier energy relaxation in GaAs," *Appl. Phys. Lett.* 51, 1442 (1987).

[36] A. Leitenstorfer, C. Fürst, A. Laubereau, W. Kaiser, G. Tränkle, and G. Weimann, "Femtosecond carrier dynamics in GaAs far from equilibrium," *Phys. Rev. Lett.* **76**, 1545 (1996).

[37] M. Ulman, D. W. Bailey, L. H. Acioli, F. G. Vallée, C. J. Stanton, E. P. Ippen, and J. G. Fujimoto, "Femtosecond tunable nonlinear absorption spectroscopy in $Al_{0.1}Ga_{0.9}As$," *Phys. Rev. B* **47**, 10267 (1993).

[38] D.N. Mirlin, I.Ja. Karlik, L.P. Nikitin, I.I. Reshina, and V.F. Sapega, "Hot electron photoluminescence in GaAs crystals," *Sol. St. Commun.* **37**, 757 (1981).

[39] A. Leitenstorfer, A. Lohner, T. Elsaesser, S. Haas, F. Rossi, T. Kuhn, W. Klein, G. Boehm, G. Traenkle, and G. Weimann, "Ultrafast coherent

generation of hot electrons studied via band-to-acceptor luminescence in GaAs," *Phys. Rev. Lett.* **73**, 1687 (1994).

[40] J. Shah, B. Deveaud, T. C. Damen, W. T. Tsang, A. C. Gossard and P. Lugli, "Determination of intervalley scattering rates in GaAs by subpicosecond luminescence spectroscopy," *Phys. Rev. Lett.* **59**, 2222 (1987).

[41] P. N. Saeta, J. F. Federici, B. I. Greene, and D. R. Dykaar, "Intervalley scattering in GaAs and InP probed by pulsed far-infrared transmission spectroscopy," *Appl. Phys. Lett.* **60** , 1477 (1992).

[42] M. Lindberg and S. W. Koch, "Effective Bloch equations for semiconductors," *Phys. Rev. B* **38**, 3342 (1988).

[43] A. V. Kuznetsov, "Coherent and non-Markovian effects in ultrafast relaxation of photoexcited hot carriers: A model study," *Phys. Rev. B* **44**, 13381 (1991).

[44] A. V. Kuznetsov, "Interaction of ultrashort light pulses with semiconductors: Effective Bloch equations with relaxation and memory effects," *Phys. Rev. B* **44**, 8721 (1991).

[45] F. Rossi, S. Haas, and T. Kuhn, "Ultrafast relaxation of photoexcited carriers: The role of coherence in the generation process," *Phys. Rev. Lett.* **72**, 152 (1994).

[46] A. L. Smirl, T. F. Boggess, B. S. Wherrett, G. P. Perryman, and A. Miller, "Picosecond optically induced anisotropic state filling in semiconductors," *Phys. Rev. Lett.* **49**, 933 (1982).

[47] J.L. Oudar, A. Migus, D. Hulin, G. Grillon, J. Etchepare, and A. Antonetti, "Femtosecond orientational relaxation of photoexcited carriers in GaAs", *Phys.Rev.Lett.* **53**, 384 (1984).

[48] V. F. Gantmakher and Y. B. Levinson, *Carrier scattering in metals and semiconductors*, (Amsterdam: North-Holland, 1987)

[49] A. S. Vengurlekar and S. S. Jha, "Transient electrical conductivity of nonequilibrium carriers excited by subpicosecond optical pulses in GaAs" *Appl. Phys. Lett.* **51**, 323 (1987).

[50] O. E. Raichev and F. T. Vasko, "Absolute negative conductivity of electrons after ultrafast photoexcitation," *Phys. Rev. B* **73**, 075204 (2006).

[51] V. F. Elesin and E. A. Manykin, "Some features of the photoconductivity spectrum of semiconductors," *Zh. Eksp. Teor. Fiz.* **50**, 1381 (1966) [*Sov. Phys. JETP* **23**, 917 (1966)].

[52] H. J. Stocker, "Total negative photoconductance in solids and possibility of a new type of instability," *Phys. Rev. Lett.* **18**, 1197 (1967).

[53] A. S. Vengurlekar and S. S. Jha, "Terahertz-frequency-resolved transient conductivity of nonthermal electrons photoexcited in GaAs," *Phys. Rev. B* **43**, 12454 (1991).

[54] W. Sha, T. B. Norris, W. J. Schaff, and K. E. Meyer, "Time-resolved ballistic acceleration of electrons in a GaAs quantum-well structure," *Phys. Rev. Lett.* **67**, 2553 (1991).

[55] S. L. Teitel and J. W. Wilkins, "Ballistic transport and velocity overshoot in semiconductors: Part I-Uniform field effects," *IEEE Trans. Electron Dev.* **ED-30**, 150 (1983).

[56] A. Leitenstorfer, S. Hunsche, J. Shah, M. C. Nuss, and W. H. Knox, "Femtosecond charge transport in polar semiconductors," *Phys. Rev. Lett.* **82**, 5140 (1999).

[57] R. B. Hammond, "Electron velocity overshoot observed in an impulse-excited GaAs photoconductor," *Physica B* **134**, 475 (1985).

[58] K. Meyer, M. Pessot, G. Mourou, R. Grondin and S. Chamoun, "Subpicosecond photoconductivity overshoot in gallium arsenide observed by electro-optic sampling," *Appl. Phys. Lett.* **53**, 2254 (1988).

[59] V. N. Genkin and P. M. Mednis, "Contribution to the theory of nonlinear effects in crystals with account taken of partially filled bands," *Zh. Eksp. Teor. Fiz.* **54**, 1137 (1968) [*Sov. Phys. JETP* **27**, 609 (1968)].

[60] D. S. Chemla, D. A. B. Miller, and S. Schmitt-Rink, "Generation of ultrashort electrical pulses through screening by virtual populations in biased quantum wells," *Phys. Rev. Lett.* **59**, 1018 (1987).

[61] M. Yamanishi, "Field-induced optical nonlinearity due to virtual transitions in semiconductor quantum well structures," *Phys. Rev. Lett.* **59**, 1014 (1987).

[62] E. Yablonovitch, J. P. Heritage, D. E. Aspnes, and Y. Yafet, "Virtual photoconductivity," *Phys. Rev. Lett.* **63**, 976 (1989).

[63] Y. Yafet and E. Yablonovitch, "Virtual photoconductivity due to intense optical radiation transmitted through a semiconductor," *Phys. Rev. B* **43**, 12480 (1991).

[64] A. V. Kuznetsov and C. J. Stanton, "Ultrafast optical generation of carriers in a dc electric field: Transient localization and photocurrent," *Phys. Rev. B* **48**, 10828 (1993).

[65] T. Meier, G. von Plessen, P. Thomas, and S. W. Koch, "Coherent Electric-Field Effects in Semiconductors," *Phys. Rev. Lett.* **73**, 902 (1994).

[66] Yun-Shik Lee, *Principles of Terahertz Science and Technology*, (New York: Springer, 2009)

[67] K. Reimann, "Table-top sources of ultrashort THz pulses," *Rep. Prog. Phys.* **70,** 1597 (2007).

[68] P. K. Benicewicz, J. P. Roberts, and A. J. Taylor, "Scaling of terahertz radiation from large-aperture biased photoconductors," *J. Opt. Soc. Am.* **11**, 2533 (1994).

[69] M. Suzuki and M. Tonouchi, "Fe-implanted InGaAs terahertz emitters for 1.56µm wavelength excitation," *Appl. Phys. Lett.* **86**, 051104 (2005)

[70] J. Lloyd-Hughes, E. Castro-Camus, and M.B. Jonston, "Simulation and optimization of terahertz emission from InGaAs and InP photoconductive switches," *Solid State Commun.* **136**, 595 (2005)

[71] K Bertulis, A Krotkus, G Aleksejenko, V Pacebutas, R Adomavicius, G Molis, and S. Marcinkevicius, "GaBiAs: A material for optoelectronic terahertz devices," *Appl. Phys. Lett.* **88,** 201112 (2006)

[72] V. L. Malevich, R. Adomavičius, A. Krotkus, "THz emission from semiconductor surfaces," *Compt. Rend. Physiq.* **9**, 130 (2008).

[73] L.D. Landau and E.M. Lifshitz, *The Classical Theory of Fields*, (Oxford: Butterworth-Heinemann, 1980)

[74] B. B. Hu, A. S. Weling, D. H. Auston, A. V. Kuznetsov, and C. J. Stanton, "dc-electric-field dependence of THz radiation induced by femtosecond optical excitation of bulk GaAs," *Phys. Rev. B* **49**, 2234 (1994).

[75] J. Darmo, G. Strasser, T. Müller, R. Bratschitsch, and K. Unterrainer, "Surface-modified GaAs terahertz plasmon emitter," *Appl. Phys. Lett.* **81**, 871 (2002).

[76] M. B. Johnston, D. M. Whittaker, A. Corchia, A. G. Davies, and E. H. Linfield, "Simulation of terahertz generation at semiconductor surfaces," *Phys. Rev. B* **65**, 165301 (2002).

[77] V. L. Malevich, "Monte Carlo simulation of THz-pulse generation from semiconductor surface," *Semicond. Sci. Technol.* **17**, 551 (2002).

[78] R. Kersting, K. Unterrainer, G. Strasser, H. F. Kauffmann, and E. Gornik, "Few-cycle THz emission from cold plasma oscillations," *Phys. Rev. Lett.* **79**, 3038 (1997).

[79] R. Kersting, J. N. Heyman, G. Strasser, and K. Unterrainer, "Coherent plasmons in n-doped GaAs," *Phys. Rev. B* **58**, 4553 (1998).

[80] P. Gu, M. Tani, S. Kono, K. Sakai, and X.-C. Zhang, "Study of terahertz radiation from InAs and InSb," *J. Appl. Phys.* **91**, 5533 (2002).

[81] S. Kono, P. Gu, M Tani, and K. Sakai, "Temperature dependence of terahertz radiation from n-type InSb and n-type InAs surfaces," *Appl. Phys. B.* **71**, 901 (2000).

[82] K. Liu, J. Xu, T. Yuan, and X.-C. Zhang, "Terahertz radiation from InAs induced by carrier diffusion and drift," *Phys. Rev. B* **73**, 155330 (2006).

[83] V.I. Belinicher, S.M. Ryvkin, "Jetlike photoelectromotive force in semiconductors," *Zh. Eksp. Teor. Fiz.* **81**, 353 (1981) [*Sov. Phys. JETP* **54**, 190 (1981)].

[84] V. L. Malevich, "Monte Carlo simulation of the Dember effect in n-InAs exposed to femtosecond pulse laser excitation," *Semiconductors*, **40**, 155 (2006).

[85] R. Adomavičius, G. Molis, A. Krotkus, V. Sirutkaitis, "Spectral dependencies of terahertz emission from InAs and InSb," *Appl. Phys. Lett.* **87**, 261101 (2005).

[86] M. Suzuki, M. Tonouchi, K. Fujii, H. Ohtake, and T. Hirosumi, "Excitation wavelength dependence of terahertz emission from semiconductor surface," *Appl. Phys. Lett.* 89, 091111 (2006).

[87] H. Takahashi, Y. Suzuki, M. Sakai, S. Ono, N. Sarukura, T. Sugiura, T. Hirosumi, and M. Yoshida, "Significant enhancement of terahertz radiation from InSb by use of a compact fiber laser and an external magnetic field," *Appl. Phys. Lett.* 82, 2005 (2003).

[88] R. McLaughlin, A. Corchia, M. B. Johnston, Q. Chen, C. M. Ciesla, D. D. Arnone, G. A. C. Jones, E. H. Linfield, A. G. Davies, and M. Pepper, "Enhanced coherent terahertz emission from indium arsenide in the presence of a magnetic field," *Appl. Phys. Lett.* 76, 2038 (2000).

[89] J. N. Heyman, P. Neocleous, D. Hebert, P. A. Crowell, T. Müller, and K. Unterrainer, "Terahertz emission from GaAs and InAs in a magnetic field," *Phys. Rev. B* **64**, 085202 (2001).

[90] H. Takahashi, A. Quema, R Yoshioka, S Ono, and N. Sarukura, "Excitation fluence dependence of terahertz radiation mechanism from femtosecond-laser-irradiated InAs under magnetic field," *Appl. Phys. Lett.* 83, 1068 (2003).

[91] S. R. Andrews, A. Armitage, P. G. Huggard, C. J. Shaw, G. P. Moore, and R. Grey, "Magnetic field dependence of terahertz emission from an optically excited GaAs p-i-n diode," *Phys. Rev. B* 66, 085307 (2002).

[92] H. Ohtake, H. Murakami, T. Yano, S. Ono, N. Sarukura, H. Takahashi, Y. Suzuki, G. Nishijima, and K. Watanabe, "Anomalous power and spectrum dependence of terahertz radiation from femtosecond-laser-irradiated indium arsenide in high magnetic fields up to 14 T," *Appl. Phys. Lett.* 82, 1164 (2003).

[93] S. L. Chuang, S. Schmitt-Rink, B. I. Greene, P. N. Saeta, and A. F. J. Levi, "Optical rectification at semiconductor surfaces," *Phys. Rev. Lett.* **68**, 102 (1992).

[94] B. I. Greene, P. N. Saeta, D. R. Dykaar, S. Schmitt-Rink, S. L. Chuang, "Far-infrared light generation at semiconductor surface and its spectroscopic applications," *IEEE J. Quantum Electron.* **28**, 2302 (1992).

[95] X.-C. Zhang, Y. Jin, K. Yang, and L. J. Schowalter, "Resonant nonlinear susceptibility near the GaAs band gap," *Phys. Rev. Lett.* **69**, 2303 (1992).

[96] A. Bonvalet, M. Joffre, J. L. Martin, and A. Migus, "Generation of ultrabroadband femtosecond pulses in the mid-infrared by optical rectification of 15 fs light pulses at 100 MHz repetition rate," *Appl. Phys. Lett.* **67**, 2907 (1995).

[97] A. Rice, Y. Jin, X. F. Ma, X.-C. Zhang, D. Bliss, J. Larkin, and M. Alexander, "Terahertz optical rectification from ⟨110⟩ zinc-blende crystals," *Appl. Phys. Lett.* **64**, 1324 (1994).

[98] R. Adomavičius, A. Urbanowicz, G. Molis, A. Krotkus and E. Šatkovskis, "Terahertz emission from p-lnAs due to the instantaneous polarization," *Appl. Phys. Lett.* **85**, 2463 (2004).

[99] M. Reid, I. V. Cravetchi, and R. Fedosejevs, "Terahertz radiation and second-harmonic generation from InAs: Bulk versus surface electric-field-induced contributions," *Phys. Rev. B* **72**, 035201 (2005).

[100] R. Mendis, M. L. Smith, L. J. Bignell, R. E. M. Vickers, and R. A. Lewis, "Strong terahertz emission from (100) p-type InAs," *J. Appl. Phys.* **98**, 126104 (2005).

[101] X. Mu, Y. J. Ding, and Y. B. Zotova, "Transition from photocurrent surge to resonant optical rectification for terahertz generation in *p*-InAs," *Opt. Lett.* **32**, 3321 (2007).

[102] A. Krotkus, R. Adomavičius, G. Molis, and V. L. Malevich, "TeraHertz Emission from InAs Surfaces Excited by Femtosecond Laser Pulses," *J. Nanoelectron. Optoelectron.* **2**, 108 (2007).

[103] T. Dekorsy, H. Auer, H. J. Bakker, H. G. Roskos, and H. Kurz, "THz electromagnetic emission by coherent infrared-active phonons." *Phys. Rev. B* 53, 4005 (1996).

[104] N. Sarukura, H. Ohtake, S. Izumida, and Z. Liu, "High average-power THz radiation from femtosecond laser-irradiated InAs in a magnetic field and its elliptical polarization characteristics," *J. Appl. Phys.* **84**, 654 (1998).

[105] P. Y. Han, M. Tani, M. Usami, S. Kono, R. Kersting, and X.-C. Zhang, "A direct comparison between terahertz time-domain spectroscopy and far-infrared Fourier transform spectroscopy," *J. Appl. Phys.* 89, 2357 (2001).

[106] J.B. Baxter and C.A. Schmuttenmaer, in *Terahertz Spectroscopy: Principle and Applications*, ed. By S. L. Dexheimer, (Taylor & Francis Group, 2008), p. 73.

[107] A Urbanowicz, R Adomavičius, A Krotkus, and V L Malevich, "Electron dynamics in Ge crystals studied by terahertz emission from photoexcited surfaces," *Semicond. Sci. Technol.* **20,** 1010 (2005).

[108] G. Molis, A. Krotkus, and V. Vaičaitis "Intervalley separation in the conduction band of InGaAs measured by terahertz excitation spectroscopy," *Appl. Phys. Lett.* 94, 091104 (2009).

[109] A. G. Markelz, and E. J. Heilweil, "Temperature-dependent terahertz output from semi-insulating GaAs photoconductive switches," *Appl. Phys. Lett.* 72, 2229 (1998).

[110] N. Sarukura, H. Ohtake, S. Izumida, and Z. Liu, "High average-power THz radiation from femtosecond laser-irradiated InAs in a magnetic field and its elliptical polarization characteristics," *J. Appl. Phys.* 84, 654 (1998).

[111] M. Nakajima, M. Takahashi, and M. Hangyo, "Temperature dependence of THz radiation from semi-insulating InP surface," *J. Lumines.* **94**, 627 (2001).

[112] M. Nakajima, M. Takahashi, and M. Hangyo, "Reversal of subpicosecond carrier transport direction with temperature observed in semi-insulating InP using THz radiation," *Physica B* **314**, 176 (2002).

[113] M. C. Hoffmann, J. Hebling, H. Y. Hwang, K. Yeh, and K. A. Nelson, "THz-pump/THz-probe spectroscopy of semiconductors at high field strengths [Invited]," *J. Opt. Soc. Am. B* **26**, A29 (2009).

[114] M. Reid and R. Fedosejevs, "Terahertz emission from (100) InAs surfaces at high excitation fluencies," *Appl. Phys. Lett.* **86**, 011906 (2005).

[115] Y. R. Shen, *Principles of Nonlinear Optics,* (John Wiley & Sons, NewYork/London, 1984).

[116] J. B. Khurgin, "Optical rectification and terahertz emission in semiconductors excited above the band gap," *J. Opt. Soc. Am. B* **11**, 2492 (1994).

[117] J. E. Sipe and A. I. Shkrebtii, "Second-order optical response in semiconductors," *Phys. Rev. B* **61**, 5337 (2000).

[118] D. Côté, N. Laman and H. M. van Driel, "Rectification and shift currents in GaAs," *Appl. Phys. Lett.* **80**, 905 (2002).

[119] V. I. Zemskii, B. P. Zakharchenya, and D. N. Mirlin, "Polarization of hot photoluminescence in semiconductors of the GaAs type," *Pis'ma Zh. Eksp. Teor. Fiz.* **24**, 96 (1976) [*JETP Lett.* **24**, 82 (1976)].

[120] B. P. Zakharchenya, D. N. Mirlin, V. I. Perel', and I. I. Reshina, "Spectrum and polarization of hot-electron photoluminescence in semiconductors," *Usp. Fiz. Nauk.* **136**, 459 (1982) [*Sov. Phys. Usp.* **25**, 143 (1982)].

[121] I. Vurgaftman, J. R. Meyer, and L. R. Ram-Mohan, "Band parameters for III–V compound semiconductors and their alloys," *J. Appl. Phys.* **89**, 5815 (2001).

[122] G. L. Bir and G. E. Pikus, *Symmetry and Strain-Induced Effects in Semiconductors,* (Wiley, New York, 1974)

[123] See http://www.ioffe.rssi.ru/SVA/NSM/Semicond/ for band-structure parameters of InAs

[124] S. Adachi, *Physical Properties of III–V Semiconductor Compounds: InP, InAs, GaAs, GaP, InGaAs, and InGaAsP,* (Wiley, New York, 1992).

[125] V. L. Malevich, P. A. Ziaziulia, R. Adomavičius, A. Krotkus, and Y. V. Malevich, "Terahertz emission from cubic semiconductor induced by a transient anisotropic photocurrent," *J. Appl. Phys.* **112,** 073115 (2012).

[126] Y. V. Malevich, R. Adomavičius, A. Krotkus, and V. L. Malevich, "Anisotropic picosecond photoconductivity caused by optical alignment of electron momenta in cubic semiconductors," *J. Appl. Phys.* **115**, 073103 (2014).

LIST OF PUBLICATIONS

Publications in peer-reviewed journals:

[1] A. Bičiūnas, Y.V. Malevich, and A. Krotkus, "Excitation wavelength dependences of terahertz emission from surfaces of InSb and InAs," *Electron. Lett.* **47,** 1186 (2011).

[2] V. L. Malevich, P. A. Ziaziulia, R. Adomavičius, A. Krotkus, and Y. V. Malevich, "Terahertz emission from cubic semiconductor induced by a transient anisotropic photocurrent," *J. Appl. Phys.* **112,** 073115 (2012).

[3] Y. V. Malevich, R. Adomavičius, A. Krotkus, and V. L. Malevich, "Anisotropic picosecond photoconductivity caused by optical alignment of electron momenta in cubic semiconductors," *J. Appl. Phys.* **115**, 073103 (2014).

[4] Y. V. Malevich, R. Adomavičius, A. Krotkus, V. Pačebutas, and V. L. Malevich, "Spectral dependence of anisotropic picosecond photoconductivity in cubic semiconductors," *JETP Lett.* **101**, 108 (2015).

International conferences:

[5] Y. Malevich, R. Adomavičius, A. Krotkus, V. Pačebutas, and V. Malevich, "Spectral dependence of a picosecond anisotropic photoconductivity in cubic semiconductor," *16th International Conference "Laser Optics 2014",* June 30 - July 04, 2014, Saint Petersburg, Russia, ThR5-28.

[6] V. L. Malevich, G. V. Sinitsyn, R. Adomavičius, A. Krotkus, and Y. V. Malevich, "Transient anisotropic photocurrent and terahertz emission from narrow-gap semiconductors," *The 2-nd International Conference "Terahertz and Microwave Radiation: Generation, Detection and Applications"*, June 20 -22, 2012, Moscow, Russia, P. 30.

[7] Y. V. Malevich, M. M. Nazarov, D. A. Sapozhnikov, A. V. Shepelev, A. P. Shkurinov, and V. A. Skuratov, "Terahertz wave generation in semiconductors with nanostructures fabricated by high-energy ions," *The 2-nd International Conference "Terahertz and Microwave Radiation: Generation, Detection and Applications"*, June 20 -22, 2012, Moscow, Russia, P. 38.

[8] Y. V. Malevich, M. M. Nazarov, A. P. Shkurinov, V. A. Shepelev, and V. A. Skuratov, "Terahertz wave generation in semiconductors with controlled nanostructures,: *International Conference on Coherent and Nonlinear Optics (ICONO)/International Conference on Lasers, Applications, and Technologies (LAT)*, August 23 – 26, 2010, Kazan, Russia, ITuT5